



**PREPARATION AND CHARACTERISATION OF
SPINEL FERRITES - THEIR INCORPORATION
IN RUBBER MATRIX AND EVALUATION OF
PROPERTIES**

Thesis submitted to

COCHIN UNIVERSITY OF SCIENCE AND TECHNOLOGY

in partial fulfilment of the requirements for the award of the degree of

DOCTOR OF PHILOSOPHY

By

SINDHU S.

**DEPARTMENT OF PHYSICS
COCHIN UNIVERSITY OF SCIENCE AND TECHNOLOGY
COCHIN - 682 022, INDIA**

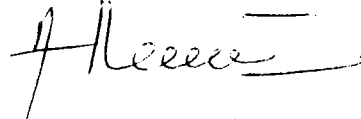
APRIL 2001

Department of Physics
Cochin University of Science and Technology
Cochin – 682 022
India

Certificate

Certified that the work presented in this thesis entitled " Preparation and characterisation of spinel ferrites - Their incorporation in rubber matrix and evaluation of properties " is based on the bonafide research work carried out by Miss. Sindhu S under my guidance, at the Magnetics laboratory of the Physics Department, Cochin University of Science & Technology, Cochin - 682 022, and has not been included in any other thesis submitted previously for the award of any degree.

Cochin - 22
09.04.2001


Dr.M.R.Anantharaman
(Supervising Guide)

CONTENTS

Page No.

Preface

Chapter I Introduction

1.1. History of magnetism.....	1
1.2. Science behind magnetism.....	3
1.3. Kinds of magnetic materials.....	6
1.4. Applications of magnetic materials.....	9
1.5. Ferrimagnetism and ferrites.....	10
1.6. Crystal chemistry of spinel ferrites.....	11
1.7. Magnetic properties of ferrites.....	13
1.8. Electrical properties of ferrites.....	15
1.9. Magnetostriction.....	16
1.10. About Butyl rubber.....	17
1.11. Rubber Ferrite Composites (RFCs).....	19

Chapter II Experimental Methods

2.1. Preparation of ceramic $Ni_{1-x}Zn_xFe_2O_4$	22
2.2. Structural Evaluation of $Ni_{1-x}Zn_xFe_2O_4$	23
2.3. Incorporation of $Ni_{1-x}Zn_xFe_2O_4$ in butyl rubber matrix...	24
2.4. Cure characteristics	25
2.5. Magnetic characterisation.....	25
2.5.1. Principle & Theory involved in VSM.....	26
2.6. Surface studies on $ZnFe_2O_4$	27
2.6.1. Low Energy Ion Scattering (LEIS).....	27
2.7. Mössbauer studies.....	29
2.8. Electrical characterisation.....	32
2.8.1. Dielectric properties.....	32
2.8.2. Ac electrical conductivity.....	35

Chapter III Cure characteristics and magnetic properties of Rubber Ferrite Composites (RFCs)

3.1. Introduction.....	36
3.2. Structural studies on $Ni_{1-x}Zn_xFe_2O_4$	37
3.3. Magnetic properties of ceramic $Ni_{1-x}Zn_xFe_2O_4$	41

3.4. Cure characteristics of RFCs.....	49
3.5. Magnetic properties of RFCs.....	51
3.6. Tailoring magnetic properties of RFCs.....	56
3.7. Low temperature VSM results of $x = 0.2, 120\text{phr}$	59
3.8. Conclusion.....	61

Chapter IV On the magnetic properties of ultrafine zinc ferrites

4.1. Introduction.....	62
4.2. Preparation of zinc ferrite at low temperature.....	64
4.3. Preparation of zinc ferrite at high temperature.....	64
4.4. Structural evaluation of ZnFe_2O_4	64
4.5. Magnetic measurements.....	66
4.6. BET surface area measurements.....	66
4.7. Results and Discussion.....	66
4.8. Conclusion	72

Chapter V Dielectric properties of RFCs containing mixed ferrites

5.1. Introduction.....	73
5.2. Dielectric properties of ceramic $\text{Ni}_{1-x}\text{Zn}_x\text{Fe}_2\text{O}_4$	74
5.2.1. Frequency dependence.....	75
5.2.2. Compositional dependence.....	76
5.2.3. Temperature dependence.....	78
5.3. Dielectric properties of blank butyl rubber.....	80
5.4. Dielectric studies on RFCs.....	81
5.4.1. Frequency dependence.....	81
5.4.2. Compositional dependence.....	83
5.4.3. Loading dependence.....	84
5.4.4. Temperature dependence.....	88
5.5. Conclusion.....	88

Chapter VI Evaluation of AC conductivity of RFCs from dielectric measurements

6.1. Introduction.....	90
6.2. AC electrical conductivity - principle & theory.....	91
6.3. Frequency dependence.....	93
6.4. Compositional dependence.....	96
6.5. Loading dependence.....	99
6.6. Temperature dependence.....	101
6.7. Conclusion.....	104

Chapter VII Evaluation of hysteresis loss for RFCs & The
estimation of magnetostrictive constant λ_s

7.1. Introduction.....	105
7.2. Estimation of λ_s from magnetic measurements.....	106
7.3. Results and discussion.....	109
7.4. Conclusion.....	114

Chapter VIII Summary and Conclusion..... 116

References

Appendix 1: List of publications/communicated articles/papers

Preface

Man's quest for exploring the unknown is as old as Adam and Eve. Almost all the foundations of modern discoveries/inventions are an outcome of this canonical attribute of human kind. This has resulted in major advancements in science and technology and has benefited the mankind to a large extent. The developments made in science and technology from time to time during the past three, four centuries have been a catalyst for social development. The industrial revolution of 19th century and later the world wars witnessed many upheavals in the society and this lead to the polarisation of the civilized world in to two blocks, the East and the West. Though this polarisation has vertically split the Western society, the efforts of scientists and engineers under the banner of these blocks have been to make life more humane.

In the broader realm of science and technology magnetism and magnetic materials have played a dominant role. This has provided to the world a whole new products in the form of passive energy storage devices. The vast ocean of knowledge and experience available in this field provided a major impetus to the development of this science called magnetism. The discovery of ferrimagnetism and ferrites by Louie Neel is one of the major milestones in this area. Today the magnetism industry is big as the semiconductor industry or rather it has started outgrowing the latter. The modern world has benefited a lot from the ' wonder material ' (called ferrite) and it will continue to benefit.

Name any device and there is a piece of magnet or an element of magnetism embedded into it. Such is the spectrum of applications of these materials.

The dawn of 21st century has already started witnessing the fruits of past labour in the form of new gadgets called GMR / CMR devices, MRAMs, high density

storages and ferrofluids. Man's desire to improve upon the existing, removal of obsolescence, value addition and bringing cost effectiveness has produced many devices which have superior performance characteristics and at the same time inexpensive.

This piece of work which is undertaken here may be viewed from this angle to improve upon the existing and adding value to the existing without compromising on the quality. The underlying principle of physics will also be dealt with from a fundamental viewpoint.

Of the different kinds of magnetism ferrimagnetism is the term proposed by Neel to describe the magnetism of ferrites. In these substances magnetic ions occupy two different kinds of lattice sites called tetrahedral (A) and octahedral (B). The number of magnetic ions and also the magnitude of spins of individual ions are different on A and B sites and this gives rise to a net magnetisation. These materials are important because of their high frequency applications due to their high resistivity and low eddy current losses. They are employed in various devices like television sets, transformer cores, loud speakers, telephone receivers and memory devices. They are employed in the form of ceramic materials in devices. An inherent drawback of ceramic materials used in devices is their poor machinability to obtain complex shapes. Plastic magnets or elastomer magnets can fill these voids by reduction of cost and can be moulded in to any shape. Hence plastic magnets or rubber ferrite composites have the potential in replacing the ceramic type of magnetic materials for applications.

Rubber ferrite composites can be prepared by the incorporation of poly crystalline ferrite powders in various elastomer matrixes. The addition of magnetic fillers in an elastomer matrix modifies the physical properties of the matrix considerably. They modify the dielectric properties and impart magnetic properties to the matrix. In applications involving ferrites at high frequencies especially for microwave absorbing devices it is essential that the material possess an appropriate dielectric constant and suitable magnetic permeability. This can be achieved in a single shot by preparing rubber ferrite composites.

In this work nickel zinc ferrite having the general formula $\text{Ni}_{1-x}\text{Zn}_x\text{Fe}_2\text{O}_4$, where x varies from 0 to 1 in steps of 0.2 have been prepared by the conventional ceramic techniques. The system of $\text{Ni}_{1-x}\text{Zn}_x\text{Fe}_2\text{O}_4$ is chosen because of their excellent high frequency characteristics. Their structural, magnetic and dielectric properties were evaluated by employing appropriate analytical techniques. These polycrystalline $\text{Ni}_{1-x}\text{Zn}_x\text{Fe}_2\text{O}_4$ were then incorporated in a synthetic rubber matrix namely Butyl rubber. The incorporation was done according to a specific recipe and for various loadings of magnetic fillers and also for all compositions. The cure characteristics, magnetic properties and dielectric properties of these elastomer blends were carried out. The ac electrical conductivity of both ceramic nickel zinc ferrites and rubber ferrite composites were also calculated using a simple relation from the dielectric data. Attempts are made to estimate the magnetostrictive constant (λ_s) of these samples using the magnetic parameters. The results are correlated.

Chapter 1 gives a brief introduction about the history of magnetism followed by a brief discussion on the physics of magnetism. Different magnetic materials and their uses and applications are also dealt with in this chapter. Spinel ferrites and their crystal chemistry are also discussed with emphasis on Neel's two sub lattice model.

An outline about the experimental techniques including the preparative techniques employed for the preparation and characterisation of samples at various stages are cited in Chapter 2. A detailed description of the preparation of Rubber Ferrite Composites are also provided. A brief description about the various analytical tools employed for characterisation at different levels are also given. This includes ideas about Low Energy Ion Scattering (LEIS) and Mössbauer spectroscopy.

Chapter 3 deals with the Structural and magnetic properties of ceramic fillers. The cure characteristics of RFCs and the magnetic properties of RFCs are also dealt with in this Chapter. The correlation of the properties are carried out with a view to tailor making materials with specific magnetic properties. The variation of coercivity with composition and the variation of magnetisation for different filler loadings are compared and correlated.

During the evaluation of magnetic properties of $\text{Ni}_{1-x}\text{Zn}_x\text{Fe}_2\text{O}_4$ an interesting observation of anomalous magnetisation for fine particle ZnFe_2O_4 was observed. Chapter 4 deals with the studies carried out on the magnetic properties of ultrafine zinc ferrites.

The dielectric properties of ceramic $\text{Ni}_{1-x}\text{Zn}_x\text{Fe}_2\text{O}_4$ and rubber ferrite composites containing $\text{Ni}_{1-x}\text{Zn}_x\text{Fe}_2\text{O}_4$ were evaluated and the results are discussed in Chapter 5. They are studied as a function of frequency, composition, loading and temperature.

The ac electrical conductivity (σ_{ac}) calculation were carried out using the data available from the dielectric measurements by employing a simple relationship for both ceramic $\text{Ni}_{1-x}\text{Zn}_x\text{Fe}_2\text{O}_4$ and also for rubber ferrite composites. The results are discussed in detail in Chapter 6. The effect of temperature on the conductivity of the ceramic sample as well as RFCs are carried out and discussed in this chapter.

Chapter 7 deals with the estimation of magnetostriction constant λ_s which was carried out by utilising the hysteresis loop parameters and employing simple relationships.

Chapter 8 is the concluding chapter of the thesis and in this chapter the salient observations and results are discussed and compared. Commercial importance and possibility for applications of rubber ferrite composites are also discussed in this chapter.

Introduction

1.1. History of magnetism

Magnetism is very common to everything you see. The term magnetism comes from a rock called lodestone. The ancient Greeks, and the Chinese knew about this strange and rare stone with the power to attract iron. This natural form of magnet was then named as lodestone. The name magnet was used by the Greeks for this lodestone, because of its property of attracting other pieces of the same material and iron as well. It was proved later that this naturally occurring lodestone is the magnetic iron oxide or the naturally occurring mineral called magnetite. The Chinese found that when a steel needle stroked with such a lodestone became magnetic and the needle pointed north –south when it is suspended freely. They applied this characteristic feature of the lodestone for navigation, fortune telling and a guide for building. Some of the properties of magnets were discovered earlier than 600 B.C, although it is only in the twentieth century that physicists have begun to understand why substances behave magnetically. Thus magnetism is one of the earliest known physical phenomena of solid materials.

In 1263 Pierre de Maricourt a French soldier mapped the magnetic field of a lodestone with a compass. He discovered that a magnet had two magnetic poles north and south poles. The magnetic compass was first used for navigation in the west sometime after AD 1200. In the 13th century important investigations on magnets were made by the French scholar Petrus Peregrinus. His discoveries stood for nearly 300 years until the English physicist and physician to Queen Elizabeth I of England, William Gilbert published his book on Magnets, Magnetic bodies and the Great Magnet of the Earth, in 1600. William Gilbert was the first to apply scientific methods to a systematic exploration of magnetic phenomena. His greatest contribution was the discovery that the earth itself behaves like a giant

magnet. He distinguished clearly between electricity and magnetism. Quantitative studies of magnetism began in the early eighteenth century. In 1750 the English geologist John Michel (1724 – 1793) invented a balance that he used in the study of magnetic forces. He showed that attraction and repulsion of magnets decreases as the square of the distance from the poles increases. The French physicist Charles Augustine de Coulomb (1736- 1806) had measured the forces between electric charges and established the inverse square law of force between magnetic poles and also between electric charges. Thus he verified John Michel's observation with high precision.

In the late 18th and early 19th centuries the theories of electricity and magnetism were investigated simultaneously. In 1819 an important discovery was made by the Danish physicist Hans Christian Oersted, who found that a magnetic needle could be deflected by an electric current flowing through a wire. This discovery, which showed a connection between electricity and magnetism, was followed up by the French scientist Andre Marie Ampere, who studied the forces between wires carrying electric currents and worked out the mathematical relationship between the current of electricity and the strength of the magnetic field. He also had a theory that the electric current in atoms had a magnetic field. In 1831 the English scientist Michel Faraday discovered that moving a magnet near a wire would induce an electric current in that wire and the inverse effect of that was found by Oersted. Eventually simple devices based on magnetic materials started rolling out. They slowly percolated in to every sphere of human life. They came into being as passive energy devices such as transformers and electric motors.

Subsequent studies of magnetism were increasingly concerned with an understanding of the atomic and molecular origins of the magnetic properties of matter. Pierre Curie discovered that magnets lose their magnetism above a certain temperature which became known as the curie point. In the 1900's Edward M. Purcell and Felix Bloch both American physicists developed a way to measure the magnetic field of the nuclei. This discovery led to Magnetic Resonance Imaging (MRI). In 1905 the French physicist Paul Langevin (1872- 1946) produced a theory regarding the temperature dependence of the magnetic properties of paramagnets, which was based on the atomic structure of matter.

This theory is an early example of the description of large scale properties in terms of the properties of electrons and atoms. Langevin's theory was subsequently expanded by the French physicist Pierre Ernst Weiss (1865 – 1940), who postulated the existence of an internal, molecular magnetic field in materials such as iron. This concept, when combined with Langevin's theory, served to explain the properties of magnetic system such as lodestone.

After Weiss theory, magnetic properties were explored in greater detail by Danish physicist Niel's Bohr. His theory of atomic structure, for example, provided an understanding of the periodic table and showed quantitatively why magnetism occurs in the so called transition elements, such as iron and the rare earths or in compounds containing these elements. The American physicists Samuel Abraham Goudsmit (1902 – 1978) and George E. Uhlenbeck (1900 – 1988) showed that the electron itself has a spin and behaves like a small bar magnet. At the atomic level, magnetism is measured in terms of magnetic moments. A moment being analogous to a unit of angular momentum in mechanics, except that electric charge is substituted for mass. The German physicist Wener Heisenberg gave a detailed explanation for Weiss's molecular field in 1927, on the basis of the newly developed quantum mechanics. In the 1960's and 1970's scientists developed superconducting magnets. Only when the magnet is cooled to absolute zero these magnets can degenerate magnetic fields up to 200,000 gauss [1-2].

1.2. Science behind magnetism

Only one kind of magnetism was known until 1821, which was produced by iron magnets. But later it was proved that the flow of an electric current in a wire moves a compass needle near by it. This new phenomenon was again studied by Ampere and concluded that the nature of magnetism was quite different from what everyone had believed. It was basically a force between electric currents. Two parallel currents in the same direction attract and in opposite direction repel.

Magnetism comprises those physical phenomena involving magnetic fields and their effects upon materials. Magnetic fields may be set up on a macroscopic scale by electric currents or by magnets. On an atomic scale, individual atoms cause

magnetic fields when their electrons have a net magnetic moment as a result of their angular momentum. A magnetic moment arises when a charged particle has an angular momentum. It is the cooperative effect of the atomic magnetic moments which causes the macroscopic magnetic field of a permanent magnet.

Magnetic field is defined as the region around a magnet where the magnetic force is exerted. There are two essential ingredients for generating a magnetic field. These two ingredients are magnetic material and current. A magnetic field is said to occupy a region when the magnetic effect of an electric current or of a magnet upon a small test magnet which is brought to the vicinity is detectable. Because of the magnetic effect, a torque will be exerted on the test magnet until it becomes oriented in a particular direction. The magnitude of this torque is a measure of the **strength of the magnetic field, and the preferred direction of orientation is the direction of the field.** In electro magnetic units, the magnitude of the torque is given by

$$L = -|\mu| \cdot |H| \cdot \sin\theta \dots\dots\dots(1.1)$$

Where μ is the magnetic moment of the test magnet. H is the magnetic field strength and θ is the angle between the direction of μ and H. When a magnetic material is placed in a magnetic field H, it becomes magnetized, that is it becomes itself a magnet. The intensity of the induced magnetism is called the magnetization 'M'. More precisely, M is the magnetic moment per unit volume of the material. In a vector field the magnetic induction B is often defined to describe the magnetic forces anywhere in space. In electromagnetic units the definition of B is given by

$$B = H + 4 \pi M \dots\dots\dots(1.2)$$

The motion of an electric charge also produces a magnetic field. The atoms whose electrons in a bar magnet are in constant motion about atomic nuclei. This moving charge creates a tiny current and produces a magnetic field, so every spinning electron is a tiny magnet. Two electrons spinning in the same direction creates a stronger magnetic field, if a pair of electrons are spinning in opposite direction then they cancel each other out and there is no magnetic field. This occurs in substances such as wood and plastics too. Hence it can be said that materials turn magnetic when they acquire a non zero magnetisation in the presence of an applied magnetic field. Based on this magnetic property upon the application of an external field,

magnetic materials can be divided into temporary and permanent magnets. Temporary magnets will lose all or most of their magnetic properties after the removal of the applied field, but a permanent magnet will retain or keep their magnetic properties for a very long time. Temporary magnets are made of such materials as iron nickel and cobalt. These materials are known as soft magnetic materials because they usually do not retain their magnetism outside a strong magnetic field.

Ferromagnets are characterised by spontaneous magnetisation, that is they attain saturation magnetisation in each of the domains even though no field is applied. But the magnetisation curve on the other hand asserts that an unmagnetised ferromagnetic sample displays no overall magnetisation in zero field. Moreover it takes an appreciable field to produce magnetisation close to the saturation value. This discrepancy between the theory and the observation was explained by Weiss based on domain hypothesis. According to Weiss domain hypothesis a ferromagnet of macroscopic size contains numerous regions called magnetic domains in the demagnetized state. Within each domain all the atomic moments are aligned in one of the easy directions. The direction of the spontaneous magnetisation varies from domain to domain, so as to minimize the magnetostatic energy. If the ferromagnetic grains are subdivided into many domains with walls between them then they are called multi domains. When the grain size is of the order of the wall thickness, it would not support a wall and will be a single domain grain. One clear distinction between multi domain and single domain grain is that the multi domain grains have a net zero magnetic moment due to different directions of the individual domain magnetisation, but the single domain grains will always show the saturation intensity until heated to beyond its Curie temperature. The single domain size range could be from less than 1000\AA down to a diameter equal to a few times the lattice constant of the material and these grains are also referred to as fine particles.

The magnetic energy of a single domain particle of volume V with uniaxial anisotropy, coercive force H_c and spontaneous magnetisation J_s is $VJ_s H_c / 2$ and depending on V this could become comparable to the thermal energy kT at ambient temperature. In such a case and when there is no external field, the particle moment VJ_s will orient along one of the two opposite directions (0° or 180°). These

two minimum energy position would be switched between them due to thermal agitation. Particles undergoing such fluctuations are called superparamagnetic particles. The temperature at which the magnetic energy equal to the thermal energy is called blocking temperature (T_B). The hysteresis behaviour of these particles show reversible magnetisation curves with zero remanence and zero coercive force. Another important point is that multi domain particles require a much larger field than single domain and super paramagnetic particles to get saturated. The hysteresis loop of single domain and super paramagnetic particles are inter changeable through an appropriate temperature change, where as multi domain particles are independent of temperature. A simple experiment based on χ vs T can bring out these features very clearly [3-6].

1.3. Kinds of magnetic materials

The magnetic properties of the materials can be classified in to diamagnetic, paramagnetic and ferromagnetic. This was based on how the material reacted to a magnetic field. Diamagnetic materials, when placed in a magnetic field, have a magnetic moment induced in them, that opposes the direction of the applied magnetic field. This property is a result of electric currents that are induced in individual atoms and molecules. These currents according to Amperes law produce the magnetic moments in opposition to the applied field. Many materials are diamagnetic, the strongest ones are metallic bismuth and organic molecules, such as benzene, that have a cyclic structure, enabling the easy establishment of electric current.

Paramagnetic materials result when the applied magnetic field lines up all the existing magnetic moments of the individual atoms or molecules making up the material. This results in an over all magnetic moment that adds to the magnetic field. Paramagnetic structures usually contain transition metals or rare earth materials that posses unpaired electrons. Paramagnetism in nonmetallic substances is usually characterized by temperature dependence, that is, the size of an induced magnetic moment varies inversely to the temperature. Langeven's theory of paramagnetism is based on this assumption. According to this theory the magnetic atoms or ions whose spins are isolated from their magnetic environment and can

more or less freely change their directions. At finite temperatures the spins are thermally agitated and take random orientations. By applying a magnetic field the average orientation of the spins are slightly changed so as to produce a weak induced magnetisation parallel to the applied magnetic field. The orientation of magnetic moment (μ) with respect to the applied field (H) can be arbitrary and therefore, the angle between μ and H can be continuously varied. If there are N number of atoms then the total magnetic moment is given by $M = N\mu$. Langevin function $L(a)$ is used to represent the average effective component of the angle θ between different magnetic dipoles with the applied field, which is represented by

$L(a) = \frac{\mu \cdot H}{3k_B \cdot T}$. Saturation will occur if $L(a)$ is large enough, that is, large field or

low temperature is necessary to make the spins align in the field direction by overcoming the disordering effect of thermal agitation. The susceptibility in this case is inversely proportional to the absolute temperature.

Paramagnetism of the conduction electrons are called Pauli paramagnetism or weak spin paramagnetism. The conduction electrons, present to the extent of one or more per atom, depending on the valence state will have a spin magnetic moment of one Bohr magneton. One would therefore expect them to make a sizable paramagnetic contribution. This does not happen, however, because the conduction electrons of a metal occupy energy levels in such a way that an applied field can reorient the spins of only a very small fraction of the total number of electrons. The resulting paramagnetism is very weak and does not vary much with temperature and the susceptibility is independent of temperature.

A ferromagnetic substance is one that, like iron, retains a magnetic moment even when the external magnetic field is reduced to zero. This effect is due to the strong interaction between the magnetic moments of the individual atoms or electrons in the magnetic substance that causes them to line up parallel to one another. In ordinary circumstances these ferromagnetic materials are divided into regions called domains, in each of which the atomic moments are aligned parallel to one another. Separate domains have total moments that do not necessarily point in the same direction. Thus although an ordinary piece of iron may not have a magnetic

moment, magnetization can be induced in it by placing the iron in a magnetic field, there by aligning the moments of all the individual domains. The energy expended in reorienting the domains from the magnetized back to the demagnetized state manifests itself in a lag in response, which is known as hysteresis. Ferro magnetic materials when heated eventually lose their magnetic properties. This loss becomes complete above the so called Curie temperature, named after Pierre Curie who discovered it in 1895.

In recent years a greater understanding of the atomic origins of magnetic properties has resulted in the discovery of other types of magnetic ordering. The substances in which the magnetic moments interact in a way, such that it is energetically favorable for them to line up antiparallel are called antiferromagnets. There is a temperature analogous to Curie temperature called the Neel temperature, above which antiferromagnetic order disappears.

Other more complex atomic arrangements of magnetic moments have also been found. They are ferrimagnetic substances, they have atleast two different kinds of atomic magnetic moments, which are oriented antiparallel to one another. Because the moments are of different size a net magnetic moment remains, unlike the situation in an antiferromagnet where all the magnetic moments cancel out. Interestingly lodestone is a ferrimagnet rather than a ferromagnet. There are two types of iron ions, ferrous and ferric in the material. More complex arrangements have been found in which the magnetic moments are arranged in spirals. Studies of these arrangements have provided much information on the interactions between magnetic moments in solids. The details are dealt with in the other sections[7].

1.4. Applications of magnetic materials

Numerous applications of magnetism and of magnetic materials have arisen in the past 100 years. The most important use of magnets is in the electric motors, which is based on the principle of an electromagnet. Hence all electric motors use elctromagnets. These motors run refrigerators, vacuum cleaners, washing machines etc. Audio tape and video tape players have electromagnets called heads that record and read information on tapes covered with tiny magnetic particles.

Magnets in speakers transform the signal into a sound by making the speakers vibrate. An electromagnet called a deflection yoke in TV picture tubes helps to form images on a screen. Magnetic materials are also used as isolators and circulators in microwave devices.

The development of new magnetic materials has also been important in the computer revolution. One of the most important applications of magnetic materials is in memory devices. Apart from audio/video applications, most of the present day storage devices used in computer and related devices are based on magnetic materials. The high density diskettes, the hard disk are a few examples. Recently the area of spintronics is being employed to device Magnetic RAMs and efforts are afoot to utilise this concept in making Giga bit memory devices. This will be used as primary memories in computers. These advancement made in magnetics will completely revolutionize the working of modern day computers. The invention of Magneto Optical devices is another breakthrough in the realm of magnetism and is being used extensively as LASER disks in secondary storages.

The magnets used in the industry and business are mostly electromagnetic powered devices, such as cranes, cutters, fax machines magnetic tapes and disks. In transportation, magnetism is applied to trains, subways, trolleys, monorails, escalators and elevators. Scientists and engineers have combined super conductivity and magnetism to levitate trains based on the principle of levitation. This eliminates friction and so it has an advantage of higher speed over ordinary trains. Bending magnets are very powerful magnets which help control beam lines of atomic particles in synchrotron facilities. Magnetic bottles are created to hold plasmas. Another important application of magnetism in medicine is Magnetic Resonance Imaging (MRI). The patient lies in between two magnets and the magnetic fields which cause some of the domains in the human body to align such as the heart, brain, spine and other internal organs. In general we can say that applications of magnetism and magnetic materials is found everywhere including home, industry, business, transportation, science and medicine. The recent discovery of magnetic fluids has opened up a plethora of engineering applications and is being exploited for making many high tech devices. Ideal and typical applications for ferrofluids are still in the area of high technology, such as space

and vacuum technology, aeronautical, robotics, numerically controlled machines siliconwater handling systems, lens grinding, magnetic disk read/write head actuators, film projectors, other computer peripherals and medical equipments. Since ferrimagnetism has dominated the magnetic industry scenario it would be appropriate to discuss ferrimagnetism and ferrites in particular.

1.5. Ferrimagnetism and ferrites

Ferrites are Ferrimagnetic substances and are mixed metal oxides with iron oxides (Fe^{3+}) as their main component. Ferrimagnetic substances are industrially important because they exhibit a substantial spontaneous magnetization at room temperature. Like ferromagnets, ferrimagnets also consists of self saturated domains and they exhibit the phenomena of magnetic saturation and hysteresis. Ferrimagnetic materials developed into a distinct class of magnetic materials and emerged as basic components in various energy storing devices in the late 1950s. Since then research in this frontier area is an ongoing process, not only because of its commercial importance, but also from the point of understanding the fundamental properties exhibited by them.

Ferrites are classified mainly into three groups with different crystal types. They are spinel, Garnets and Magneto-plumbite. Spinel ferrites have a cubic structure with general formula $\text{MO} \cdot \text{Fe}_2\text{O}_3$, where M is a divalent metal ion like Mn, Ni, Fe, Co, Mg etc. Garnets have a complex cubic structure having a general formula $\text{Ln}_3 \text{Fe}_6 \text{O}_{12}$. The third type, magneto-plumbite is having a hexagonal structure with general formula $\text{MO} \cdot \text{Fe}_{12}\text{O}_{18}$. The most important in the group of magneto plumbite is barium ferrite $\text{BaO} \cdot \text{Fe}_{12}\text{O}_{18}$, which is a hard ferrite. Since the proposed work will be based on spinel ferrites having cubic symmetry the crystal chemistry of spinel ferrites will be dealt with in the next section.

1.6. Crystal chemistry of spinel ferrites

The structure of spinel ferrites is derived from that of the mineral spinel $\text{MgO} \cdot \text{Al}_2\text{O}_3$. The structure is complex, in that there are 8 molecules per unit cell ($8 \times \text{A} \cdot \text{Fe}_2\text{O}_4$) where A is the divalent metal ion. The 32 large Oxygen ions form a face centered cubic lattice in which two kinds of interstitial sites are present. The

smaller metal ions occupy these interstitial spaces. These spaces are of two kinds. One is called tetrahedral 'A' sites because it is located at the center of a tetrahedron whose corners are occupied by oxygen ions. There are 64 tetrahedral sites surrounded by 4 oxygen ions. The other is called an octahedral or B site, because the oxygen ions around it occupy the corners of an octahedron. There are 32 octahedral sites surrounded by 6 oxygen ions. The crystallographic environments of A and B sites are therefore distinctly different. Figure 1.1 explains the tetrahedral A site, octahedral B site and the crystal structure of a cubic ferrite. Only one eighth of the A sites and one half of the B sites are occupied by the metal ions. In the chemical formula of $MO \cdot Fe_2O_3$ if M^{2+} are in A sites and Fe^{3+} in B sites then this structure is normally referred to as the normal spinel structure. When the divalent metallic ion M^{2+} occupies the B site and the Fe^{3+} ions equally divided between A and B sites then this configuration is called inverse spinel. $ZnFe_2O_4$ is a normal spinel, while $NiFe_2O_4$ is an inverse spinel. The normal and inverse structure are to be regarded as extreme cases, because X-ray and neutron diffraction have shown that intermediate structures can exist. The distribution of the divalent ions on A and B sites in some ferrites can be altered by heat treatment, it depends on whether the material is quenched from a high temperature or annealed.

The various factors determining the cation distribution includes the size of the cation, valency of the cation and the oxygen parameter of the anions. Large divalent ions tend to occupy tetrahedral sites as this is favoured by polarization effects.

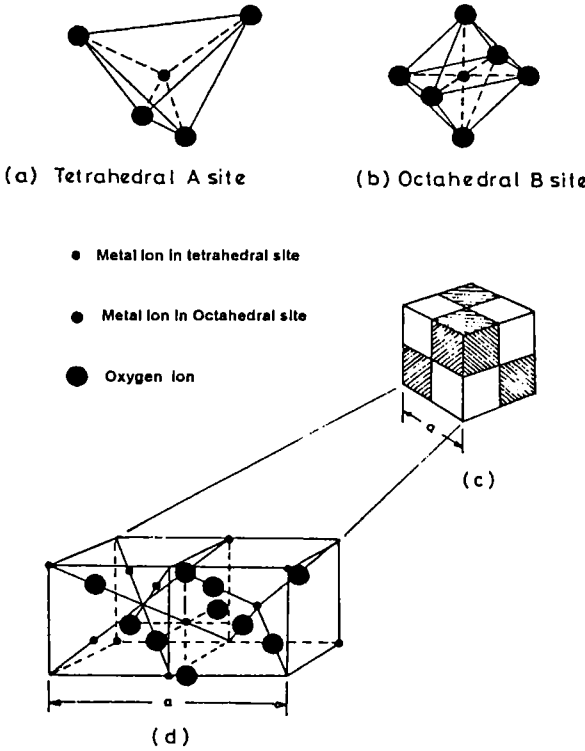


Figure 1.1 Crystal structure of a spinel ferrite

If the A site ions have a lower valency and the B site ions a higher valency then the intermediate O^{2-} ion will become polarized towards B sites. Thus polarization favours normal spinel configuration. It has been proved that the inverse structure has the lowest lattice energy for u parameter ($u < 0.379$), where as the normal structure has the lowest energy when $u > 0.379$. These factors alone can not give consistent picture of the observed cation distribution in spinel ferrites. For instance $CoFe_2O_4$ is an inverse spinel while $ZnFe_2O_4$ crystallizes in normal spinel structure although Zn^{2+} and Co^{2+} have almost the same ionic radii. These discrepancies can be explained by an individual site preference of the various ions as a result of their electronic configuration. In order to explain the site preference of transition metal ions, in oxides, two theories have been proposed, which differ in the concept of chemical bonding in oxides. One is based on crystal field theory, which is purely ionic type of bonding. Second one is a simplified molecular orbital theory, based on the covalent bonding between oxygen and transition metal atoms.

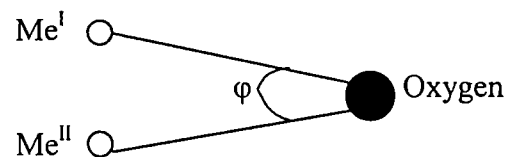
1.7. Magnetic properties of ferrites

It is known that in ferrimagnetic materials the magnitude of the magnetic moments oriented in either way differ, so that there always exists a resultant uncompensated magnetic moment. The various factors that determine the magnetic properties of these ferrites are the nature of cations, heat treatment, preparative methods, site preference energy of cations and madelung energy. According to Neel, ferrites exhibit a magnetic structure distinctly different from any previously recognized structure. Neel explained the spontaneous magnetisation of these ferrites on the basis of Heisenberg's exchange forces. According to this theory the exchange energy between two adjacent atoms having spin angular momentum is given by

$$E_{ex} = -2 J_{ex} S_i \cdot S_j \dots\dots\dots(1.3)$$

Where E_{ex} is the exchange energy, S_i and S_j are the total spins of adjacent atoms and J_{ex} is the exchange integral which represents the probability of exchange of electron. In ferrites three kinds of magnetic interactions are possible, between the magnetic ions, which are occupied in the two crystallographically distinct lattice sites. These interactions are possible through the intermediate O^{2-} ions by

superexchange mechanism. The three possible interactions are A-A interaction, B-B interaction and A-B interaction. The exchange force acting between an ion on A site and an ion on B site is governed by the above equation 1.1. The interaction is ferri, ferro or antiferro and is determined by the value of J_{ex} . It has been established experimentally that these interaction energies are negative for ferrites and hence induce an anti parallel orientation. However the magnitudes of the A and B sublattice magnetisations are not equal and this will produce a resultant net magnetisation in ferrites. In general the magnitude of the interaction energy between two magnetic ions depends upon the distance from these ions to the oxygen ion (through which the interaction occurs) and also the angle ϕ between the magnetic ions ($Me^I - O - Me^{II}$).



An angle of 180° will give rise to the greatest exchange energy and the energy decreases very rapidly with increasing distance. Based on the values of the distance and the angle ϕ it may be concluded that, of the three interactions the A-B interaction is of the greatest magnitude. The A-A interaction is the weakest. Thus with only A-B interaction predominating, the spins of the A and B site ions, in ferrite will be oppositely magnetized in the A and B sublattices, with a resultant magnetic moment equal to the difference between those of A and B site ions. In general the value of saturation magnetic moment for the B lattice (M_B) is greater than that of the A lattice (M_A) so that the resultant saturation magnetization (M_S) may be written as $M_S = M_B - M_A$. Table 1.1 shows the ion distribution and net magnetic moment per molecule of some typical ferrites.

Substance	Structure	Tetrahedral A Sites μ_A	Octahedral B Sites μ_B	Net moment (μ / molecule)		
NiO.Fe ₂ O ₃	Inverse	Fe ³⁺ 5 →	Ni ²⁺ 2 ←	Fe ³⁺ 5 ←	2	
ZnO. Fe ₂ O ₃	Normal	Zn ²⁺ 0	Fe ³⁺ 5 ←	Fe ³⁺ 5 →	0	
MgO. Fe ₂ O ₃	Mostly inverse	Mg ²⁺ 0	Fe ³⁺ 4.5 →	Mg ²⁺ 0 ←	Fe ³⁺ 5.5 ←	1

Table 1.1 Ion distribution and net magnetic moment / molecule of some typical ferrites

1.8. Electrical properties of spinel ferrites

Spinel ferrites are important over conventional magnetic materials because of their wide variety of applications. These materials have low electrical conductivities when compared to other magnetic materials and hence they find wide use at microwave frequencies. Spinel ferrites, in general are semiconductors with their conductivity lying in between 10^2 and 10^{-11} Ohm⁻¹ cm⁻¹. The conductivity is due to the presence of Fe²⁺ and the metal ions (Me³⁺). The presence of Fe²⁺ results in n-type behaviour and of Me³⁺ in p-type behaviour. The conductivity arises due to the mobility of the extra electron or the positive hole through the crystal lattice. The movement is described by a hopping mechanism, in which the charge carriers jump from one ionic site to the other. In short, one can say that the electrostatic interaction between conduction electron(or hole) and nearby ions may result in a displacement of the latter and polarization of the surrounding region, so that the carrier is situated at the centre of a polarisation potential well. The carrier is trapped at a lattice site, if this potential well is deep enough. Its transition to a neighbouring site is determined by thermal activation. This has been described as the hopping mechanism. In such a process the mobility of the jumping electrons or holes are found to be proportional to $e^{-Q/kT}$, where Q is the activation energy, k Boltzman's constant and T the temperature in degree absolute.

1.9. Magnetostriction

Magnetostriction is the phenomena exhibited by both ferro and ferromagnetic materials. When these materials are magnetized they undergo small changes in dimensions. This effect is called magnetostriction. The fractional change in length to the original length ($\Delta l/l$) is simply a strain and is represented as λ . The value of the strain λ measured at magnetic saturation is called the saturation magnetostriction (λ_s).

Magnetostriction occurs in all pure substances. However even in strong magnetic substances the effect is small and λ_s is typically of the order of 10^{-5} . In weak magnetic substances the effect is even smaller, by about two orders of magnitude and can be observed only in very strong fields. The strain due to magnetostriction changes with increase of magnetic field intensity and reaches the saturation value. The process of magnetisation occurs by two mechanisms, domain wall motion and domain rotation. Most of the magnetostrictive change in length usually occurs during domain rotation. This is because each domain is spontaneously deformed in the direction of domain magnetisation and its strain axis rotates with a rotation of the domain magnetisation, thus resulting in a deformation of the specimen.

Magnetostriction is mainly due to spin-orbit coupling. There are two basic kinds of magnetostriction, one is the spontaneous magnetostriction and the other is forced magnetostriction. Spontaneous magnetostriction occurs in each domain when a specimen is cooled below the curie point. Forced magnetostriction occurs when a saturated specimen is exposed to fields large enough to increase the magnetisation of the domain of the spin order. The magnetostrictive strain produced in a domain or a crystal when its direction of magnetisation is changed, is usually very small. This means that the reorientation of the electron clouds take place only to a very small extent. This conclusion supports the assumption that the orbital magnetic moments are not susceptible to rotation by an applied field. The amount of magnetostrictive strain exhibited by a crystal in a particular direction depends on the direction of the magnetisation. The direction of magnetisation is controlled by anisotropy constant K and the stress σ present. The measurement of magnetostriction is not accompanied by the determination of the kind and degree

of preferred orientation. The sign of λ as well as its value depends on the crystallographic direction of magnetisation. For isotropic magnetostriction the spontaneous strain is independent of the crystallographic direction of magnetisation.

The saturation magnetostriction of a polycrystalline specimen parallel to the magnetisation is characterised by a single constant λ_p . Its value depends on the magnetostrictive properties of the individual crystals and the way in which they are arranged, that is the presence or absence of preferred domain or grain orientation. If the grain orientations are completely random, the saturation magnetostriction of polycrystals should be given by some sort of average over these orientations. When a polycrystal is saturated by an applied field, each grain tries to strain magnetostrictively, in the direction of the field, by a different amount than its neighbours.

1.10. About butyl rubber

Since Butyl rubber is chosen as the base matrix for the preparation of rubber ferrite composites, a brief description about the origin, nature, structure and the advantages of butyl rubber is provided below for the sake of clarity and completeness.

The development of Butyl rubber owed its origin to the pioneering research work carried out by Gorianov and Butlerov (1870) and Otto (1927). They found that oily homopolymers of isobutylene could be produced in the presence of boron trifluoride. Subsequent research in the 1930's led W.J.Sparks and R.M.Thomas of Exxon research and engineering company to advance the state of the art of isobutylene polymerization and in 1937, the first vulcanizable isobutylene based elastomer was produced by incorporating small amounts of a diolefin and particularly isoprene, into the polymer molecule. This introduced the first concept of limited olefinic functionality for vulcanization in an otherwise saturated copolymer. Corresponding vulcanizates of these new copolymers (now known as butyl rubber) were found to possess a set of unique and desirable properties, like

low gas permeability, high hysteresis, outstanding resistance to heat, ozone, chemical attack and tearing.

The most widely used commercially available butyl rubbers are copolymers of isobutylene and isoprene. The grades are distinguished by molecular weight (Mooney viscosity) and mole % unsaturation. The mole % unsaturation is the number of moles of isoprene per 100 moles of isobutylene. Figure 1.2 illustrates the physical nature of butyl rubber, where n represents the mole of isobutylene that are combined with m moles of isoprene.

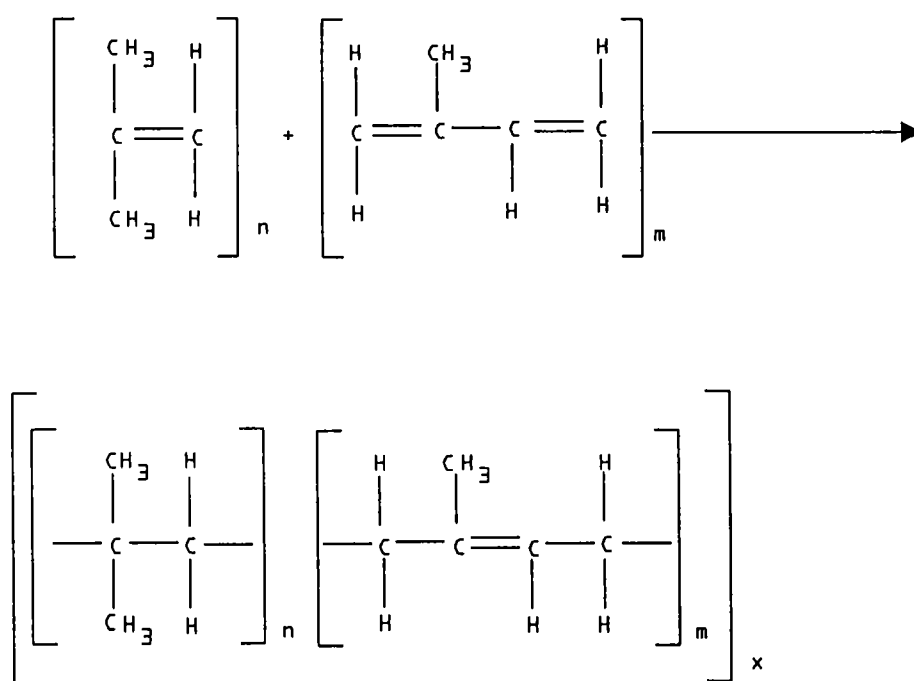


Figure 1.2: Physical nature of butyl rubber

The discovery and development of butyl rubber not only furnished rubber technology with a new elastomer, but, as mentioned earlier, it also provided a new principle, the concept of low functionality. A low functionality elastomer has sufficient chemical unsaturation so that flexible low modulus vulcanized networks can be produced, but the larger inert portions of the chain contribute towards oxidation and ozone resistance. The molecular characteristics of low levels of

unsaturation between long segments of polyisobutylene produce unique elastomeric qualities that find wide variety of applications. The special properties include low rates of gas permeability, thermal stability, ozone and weathering resistance vibration damping and higher coefficients of friction and chemical and moisture resistance. These butyl rubbers were used as the base matrix for the preparation of rubber ferrite composites. The incorporation of magnetic fillers gives rise to rubber ferrite composites.

1.11. Rubber ferrite composites (RFCs)

Nickel zinc ferrites have been found to be one of the most versatile ferrites for general use, because they exhibit a wide range of permeability, coercive force and magnetic and electric loss. Cations like Ni and Zn gives rise to mixed ferrites which exhibits interesting magnetic and electric properties depending on the composition[8-11]. They are important mixed ferrites because of their relatively high resistivity at carrier frequencies and sufficiently low loss for microwave applications. Non-stoichiometric NiZn ferrites are used in many types of electronic devices, such as transformers and inductors in high frequency circuits, because of the low eddy current loss attributable to it's high resistivity. In this work it is proposed to synthesize mixed ferrites belonging to the series $Ni_{1-x}Zn_xFe_2O_4$. Here x varies from 0 to 1 in steps of 0.2. The incorporation of these cations in the spinel lattice is expected to effect changes in cation distribution on A and B sites and thus it is possible to alter its various properties. So it is also envisaged to study the variations in magnetic, dielectric and conducting properties with respect to the change in composition. The structural properties of these ceramic materials will also be evaluated.

Composite magnetic materials or rubber ferrite composites are possible with commercially important polymer matrixes along with different magnetic fillers. Synthesis of these rubber ferrite composites (RFCs) will be carried out by the incorporation of ferrite powders in synthetic rubber like butyl rubber. This could lead to making devices meant for flexible elastomeric magnetic devices [12]. While preparing these composites with tailored properties care should be taken to choose the suitable magnetic filler with optimal size and shape of the particles. A judicious choice of the magnetic filler with the appropriate recipe can give a

combination of dielectric and magnetic properties suited for various applications. Also factors like percolation limit or nature of the matrix, like saturated/unsaturated / polar rubber all influences the final properties of the composites. In principle the macroscopic parameters of the composites would be influenced by the interaction between the filler and the matrix. The effect of fillers in modifying the properties is to be understood properly in explaining the dielectric and magnetic properties of the composites. For plastic magnets it is easy to see that the properties of the polymer matrices, especially viscoelasticity may affect the processability as well as magnetic property. Further more, because identical poles in magnetic particles are oriented repulsively in the anisotropic plastic magnets, it will be interesting to study the effect of polymer matrix as well as the shape and concentration of the magnetic powder on the magnetic properties and also change in the magnetic properties during thermal treatment. It has also been reported that incorporation of nano crystals of these types in polymer bases have potential applications in color imaging, magnetic memories for computers, magnetic fluids, microwave and radar technology and magnetic refrigeration [13-16]. These composite materials are useful as microwave absorber materials due to their advantages in respect to lightweight, low cost, design flexibility and microwave properties. The addition of reinforcing fillers like carbon black increases the bandwidth of absorption there by suppressing the reflected waves. The absorption properties vary with the amount of added ferrites to the matrix. A number of investigations has been reported for studying the effect of composition on their microwave properties. Also there are reports where in the effect of ferrite materials and their volume percentage in the composites for absorption have been studied [17-38].

The proposed work includes the preparation of nickel zinc ferrites belonging to the series $Ni_{1-x}Zn_xFe_2O_4$ with x varying from 0 to 1 in steps of 0.2 by using ceramic methods. Structural evaluation of these $Ni_{1-x}Zn_xFe_2O_4$ by using X-ray diffraction will be carried out to confirm the single phasic nature of these magnetic powders. The magnetic powders will then be incorporated in to a butyl rubber matrix for the preparation of rubber ferrite composites. The impregnation is to be carried out for various volume fractions (loading) of the filler. The cure characteristics will be evaluated by employing Gottfert elastograph. Then the evaluation of magnetic

properties for both ceramic $\text{Ni}_{1-x}\text{Zn}_x\text{Fe}_2\text{O}_4$ and rubber ferrite composites will be carried out by using vibrating sample magnetometer. The structural and magnetic properties with respect to composition and loading will be correlated. The evaluation of dielectric properties for ceramic nickel zinc ferrites and rubber ferrite composites in the frequency range 5Hz to 13MHz at different temperature, from 30°C to 200°C will also be carried out by using an impedance analyzer and a dielectric cell. The dependence of dielectric constant on various factors like frequency, composition, loading and temperature will be studied for both ceramic and rubber ferrite composites. The evaluation of ac electrical conductivity and its dependence on various factors will also be investigated by using the data available from dielectric measurements. The magnetostriction constant for RFCs will be estimated using the hysteresis loop parameters. Thus the objectives of the proposed work could be summarised as follows

- Preparation of ceramic nickel zinc ferrite belonging to the series $\text{Ni}_{1-x}\text{Zn}_x\text{Fe}_2\text{O}_4$ with x varying from 0 to 1 in steps of 0.2.
- Structural, Magnetic and Electrical characterization of $\text{Ni}_{1-x}\text{Zn}_x\text{Fe}_2\text{O}_4$.
- Preparation of Rubber Ferrite Composites (RFCs).
- Evaluation of Cure characteristics of RFCs.
- Magnetic characterization of RFCs using vibrating sample magnetometer (VSM).
- Electrical characterization of RFCs (Dielectric and ac electrical conductivity studies).
- Estimation of magnetostriction constant from HL parameters.

Experimental Methods

In this chapter the techniques employed for the synthesis of spinel like ferrites belonging to the series $\text{Ni}_{1-x}\text{Zn}_x\text{Fe}_2\text{O}_4$, where x varies from 0 to 1 in steps of 0.2 is presented. The incorporation of mixed nickel zinc ferrites in butyl rubber to obtain rubber ferrite composites is explained. Various analytical tools employed for the characterization of these samples at different stages are also discussed in the ensuing sections.

2.1. Preparation of $\text{Ni}_{1-x}\text{Zn}_x\text{Fe}_2\text{O}_4$

Nickel zinc ferrites having the general formula $\text{Ni}_{1-x}\text{Zn}_x\text{Fe}_2\text{O}_4$ for various x values (where x varies from 0 to 1 in steps of 0.2) were synthesized by the ceramic technique[39-41]. Appropriate amount of precursors, necessary for the synthesis of the mixed ferrites were weighed according to molecular weight considerations. AR grade precursors namely iron oxide, nickel oxide and zinc oxide were employed for the preparation of nickel zinc ferrites. It is to be noted that ferric oxide in turn was prepared by decomposing freshly precipitated ferrous oxalate dihydrate (FOD). FOD in turn was prepared by the co-precipitation technique. Nickel oxide, zinc oxide together with the required amount of ferric oxide were mixed thoroughly in an agate mortar to produce a homogeneous mixture of fine particles. The process of mixing was carried out in slurry of acetone to ensure uniformity. This homogeneous mixture was pre-fired at around 500°C for five hours in a furnace in an ambient atmosphere. The pre sintering was repeated twice for ensuring homogeneity. The pre-sintered samples were then crushed into powder form. The pre-sintered powders were pressed in the form of cylindrical pellets having a diameter of 10mm and then they were finally sintered at around 1000°C by keeping the pellets inside the furnace for several hours. They were then allowed to cool naturally under ambient conditions and now these pellets are ready for

characterization. $\text{Ni}_{1-x}\text{Zn}_x\text{Fe}_2\text{O}_4$ for various x values (x varies from 0 to 1 in steps of 0.2) were synthesized using this technique.

2.2. Structural Evaluation of $\text{Ni}_{1-x}\text{Zn}_x\text{Fe}_2\text{O}_4$

The method of X ray powder diffraction was used to evaluate the various structural parameters namely inter atomic spacing (d), relative intensity (I/I_0) and lattice parameter. The identification of the phase was carried out by comparing the observed structural parameters with that of the standard values reported in the literature. The powder diffractograms of the samples were recorded on a Philips PW 1710 model X ray diffractometer using $\text{Cu K}\alpha$ radiation ($\lambda = 1.5414 \text{ \AA}$). From the XRD pattern obtained the 'd' values are calculated using the relation $2d \sin\theta = n \lambda$. Then the lattice parameter (a) was calculated assuming cubic symmetry by using the relation

$$d = \frac{a}{\sqrt{h^2 + k^2 + l^2}} \dots\dots\dots(2.1)$$

The particle size was also calculated from the XRD data using Scherer formula, which is given by

$$D = \frac{0.9 \lambda}{\beta \cos\theta} \dots\dots\dots(2.2)$$

This method is used to estimate the particle size from the measured width of their diffraction curves. D is the particle size, β is the angular width which is equal to the full width at half maximum and λ is the wavelength of X-ray radiation which is equal to 1.5414 \AA . Porosity of the samples were also calculated using the X-ray density and apparent density. The X-ray density was calculated using the equation

$\frac{n.M}{a^3.N_a}$. Where 'a' is the lattice parameter, N_a is the avagadro number, M the

molecular weight of the compound, and n is the number of molecules per unit cell. Apparent densities of these samples were also calculated by taking the pellet samples. Porosity is given by $(\text{X-ray density} - \text{Apparent density}) / \text{X-ray density}$.

2.3. Incorporation of $\text{Ni}_{1-x}\text{Zn}_x\text{Fe}_2\text{O}_4$ in butyl rubber matrix

Mixed ferrites containing Ni and Zn prepared by ceramic techniques were incorporated in a butyl rubber matrix at various loadings to obtain rubber ferrite composites (RFCs). The loading was done at 20phr, 40phr, 80phr and 120phr (phr is the parts per hundred grams of rubber by weight). The mixing was carried out in a brabender plasticorder. The brabender plasticorder is a device for measuring processability of polymers and blending of polymers and similar materials under the influence of temperature and shear. It consists of different measuring mixers like MB 30, W30, W50 and N 50. MB 30 measuring mixer is used for determining the flow and curing behaviour of thermosetting materials. Measuring mixers W30 and W50 are used to test thermoplastics especially to determine fusion time, heat and shear stability, melt viscosity and the start of cross linking polymers. The mixer measuring head N 50 is used especially for the analysis of elastomers like natural and synthetic rubber types. It consists of a jacketed mixing chamber whose volume is approximately 50cc. The mixing was done by two horizontal rotors. The resistance put up by the test material against the rotating rotors in the mixing chamber is made visible with the help of a dynamometer balance. A dc thyristor controlled drive is used for speed control of rotors (0 to 150 rpm range). The temperature of the mixing chamber is controlled by circulating oil and can be varied up to 300°C. The ingredients cited in the recipe were used as base formula for compounding (cf Table 2.1).

Ingredients	Blank	20phr	40phr	80phr	120phr
Butyl rubber	100.0	100.0	100.0	100.0	100.0
Zinc Oxide	5.0	5.0	5.0	5.0	5.0
Stearic acid	2.0	2.0	2.0	2.0	2.0
Sulphur	1.25	1.25	1.25	1.25	1.25
MBTS	1.5	1.5	1.5	1.5	1.5
TMTD	1.25	1.25	1.25	1.25	1.25
$\text{Ni}_{1-x}\text{Zn}_x\text{Fe}_2\text{O}_4$	0.0	20.0	40.0	80.0	120.0

Table 2.1 Formulation details of mixing

Here sulphur plays the role of a cross linking agent, while zinc oxide is added for activation. Stearic acid, MBTS and TMTD act as accelerators. The mixing was performed at around 50°C and the mixing operation went on for around 7 minutes. A constant torque of 450Nm and a frequency of rotation of 50rpm was maintained through out the course of mixing.

2.4. Cure characteristics

After the physical blending of the elastomer with the magnetic filler according to the recipe, the resulting blend has to be cured. For this the knowledge of cure characteristics is very much essential. Cure characteristics also throws light on the processability of these polymers. Parameters like maximum and minimum torque, cure time, cure temperature were evaluated by determining the cure characteristics of compounds on a Gottfert Elastograph (model: 67.85). Gottfert Elastograph is a rotor less curometer. This instrument gives the time of cure which would be expected to produce 90%, 95% or 100% optimum cross links in a sheet of rubber of 2.5mm in thickness. The accuracy of this measuring system depends on certain design factors, like the temperature of the specimen, the amount of work done on the rubber during the course of measurements and the nature of the cured product. Vulcanized rubber with relatively large amounts of filler at high frequency must result in a substantial rise in the interior temperature of the material. Hence measurements at low frequency are preferred. Also care must be taken to ensure that the frequency is sufficient enough to give an adequate curve for quick curing compounds at high temperatures. After curing, the compounds were then vulcanized at 170°C on an electrically heated laboratory hydraulic press up to their respective cure times to make sheets of the sample.

2.5. Magnetic characterisation

The magnetic characterization of both ceramic $\text{Ni}_{1-x}\text{Zn}_x\text{Fe}_2\text{O}_4$ and rubber ferrite composites were carried out by using Vibrating Sample Magnetometer (VSM) (model: EG & G PARC 4500). Parameters like Saturation magnetization (M_s), Retentivity (M_r), Coercivity (H_c) and energy loss were obtained from the hysteresis loop obtained from VSM measurements.

2.5.1. Principle & Theory involved in VSM:

When a sample material is placed in a uniform magnetic field, a dipole moment proportional to the product of the sample susceptibility times the applied field is induced in the sample. If the sample is made to undergo sinusoidal motion, an electrical signal can as well be induced in suitably located stationary pick up coils. This signal which is at the vibration frequency is proportional to the magnetic moment, vibration amplitude and vibration frequency. This means of producing an electrical signal related to the magnetic properties of a sample material is used in the model 4500 VSM. The material under study is contained in a sample holder, which is centered in the region between the pole pieces of an electromagnet. A slender vertical sample rod connects the sample holder with a transducer assembly located above the magnet, which in turn supports the transducer assembly by means of sturdy adjustable support rods.

The transducer converts a sinusoidal ac drive signal provided by a circuit located in the console into a sinusoidal vertical vibration of the sample rod and the sample is thus made to undergo a sinusoidal motion in a uniform magnetic field. Coils mounted on the pole pieces of the magnet pick up the signal resulting from the sample motion. This ac signal at the vibrating frequency is proportional to the magnitude of the moment induced in the sample. However, it is also proportional to the vibration amplitude and frequency. A servo system maintains constancy in the drive amplitude and frequency so that the output accurately tracks the moment level without degradation due to variation in the amplitude and frequency of vibration.

This technique depends on the ability of a vibrating capacitor located beneath the transducer to generate an ac control signal, which varies solely with the vibration amplitude and frequency. This signal, which is at the vibration frequency, is fed back to the oscillator where it is compared with the drive signal so as to maintain a constant drive output. It is also phase adjusted and routed to the signal demodulator where it functions as the reference drive signal. The signal originating from the sample in the pick up coils is then buffered, amplified and applied to the demodulator. Then it is synchronously demodulated with respect to the reference signal derived from the moving capacitor assembly. The resulting dc output is an

analog of the moment magnitude alone, uninfluenced by vibration amplitude changes and frequency drifts [42-44].

2.6. Surface studies on ZnFe_2O_4

Low energy ion scattering spectroscopy (LEIS) is a powerful tool to probe the outermost layer of atoms on a material, it gives information about the surface composition of samples. The experiment was performed with LEIS instrument NODUS on two samples of zinc ferrite at the Technical University of Eindhoven, The Netherlands. The basic design of the instrument NODUS is illustrated elsewhere [45]. In this apparatus it is possible to compensate for surface charging by impinging thermal electron over the surface from all sides. The base pressure in the UHV system was about 10^{-9} mbar and during operation it increases to 10^{-8} mbar. The polycrystalline powders used for the LEIS experiments were pressed into pellets in lead holders. A 3keV $^4\text{He}^+$ ion beam was used for the measurements. The scattering conditions were kept constant during the measurements in order to facilitate comparison of data on an absolute level on different powder samples having different surface areas.

2.6.1 Low Energy Ion Scattering (LEIS) - Principle & Theory:

The technique of Low Energy Ion Scattering (LEIS) is increasingly being used for the identification of surface stains and corrosion products, compositional depth profiling, surface study of oxides etc. It enables to probe clean surfaces. Its extreme surface sensitivity enables the selective analysis of the outermost atomic layer. It is this layer that is largely responsible for many chemical and physical properties of oxides. In contrast to other commonly used surface analytical methods such as Auger Electron Spectroscopy (AES), X-ray Photoelectron Spectroscopy (XPS) or Electron Spectroscopy for Chemical Analysis (ESCA) and Secondary Ion Mass Spectroscopy (SIMS) that probe several atomic layers, it was shown by Brongersma and Mul [46-47] that LEIS can be used to selectively study the outermost atomic layer of a surface. The extreme surface sensitivity of LEIS is because of using inert gas ions. They have high neutralization probability and scattering cross sections at energies of few keV. Because of its high neutralization probability all most all ions, which penetrate beyond the first atomic layer, get

neutralized. With energy analyzers it is possible to detect only ionized particles by eliminating scattered particles from the deeper layers. The data thus gathered yields information on atomic and electronic structures, surface composition of alloys and oxides. Figure 2.1 shows a schematic picture of the LEIS process and defines the scattering angle.

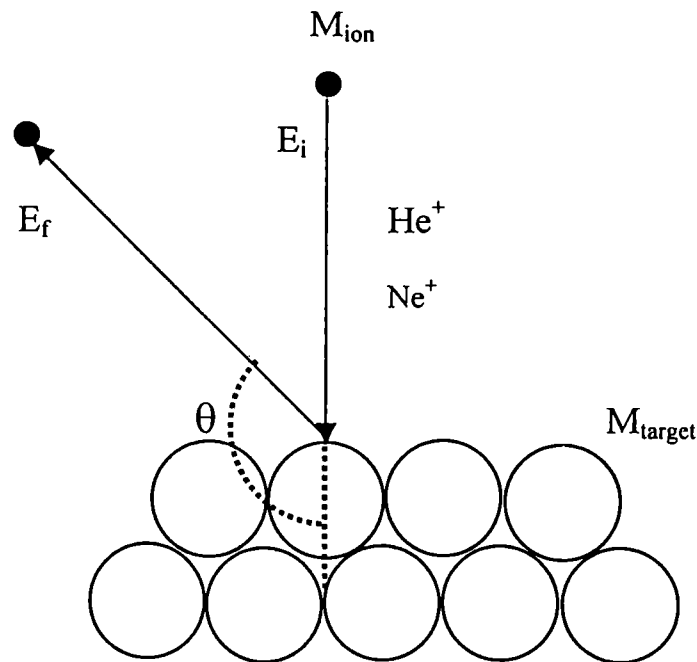


Figure 2.1 Schematic representation of the binary collision in the LEIS process

Here M_{ion} is the mass of the incident ion and M_{target} is the mass of the target atom at the surface. The initial energy E_i is directed on to the surface of a material and the final energy E_f of the backscattered ions is determined using an electrostatic analyzer.

Here for each collisions the incident ions losses kinetic energy. The loss depends on the energy of the ion before collision (E_i) and the masses of the ion (M_i) and the target atom (M_2) and the scattering angle (θ). The energy of the scattered ion (E_f) can be calculated from the classical laws of conservation of momentum and energy and is given as

$$E_f = E_i K^2(\theta, A) \dots\dots\dots(2.3)$$

Kinematic factor K depends on the scattering angle θ and the mass ratio $A = M_2/M_1$, and is found out from the relation

$$K = \frac{\cos\theta + \sqrt{A^2 - \sin^2\theta}}{1 + A} \dots\dots\dots(2.4)$$

provided the mass of the projectile ion is lower than the mass of the surface atom.

Segregation of impurities or dopants may dominate surface properties, especially with single crystals and sintered ceramics, which have a low specific surface area. Since thermodynamics often restricts the enrichment to the outermost atomic layer, LEIS is the ideal technique to detect and quantify segregation. In most applications the main reason for using LEIS is its monolayer sensitivity. In general, the ability of LEIS to perform compositional analysis is related to the following features, like selectivity for first atomic layer, straightforward quantification, very rough surfaces can be studied, detection of isotopes, samples can be conductors as well as insulators and in-situ studies are also possible at high temperatures.

2.7. Mössbauer studies

The phenomenon of the emission or absorption of a γ -ray photon without loss of energy due to recoil of the nucleus and without thermal broadening is known as the Mössbauer effect. In other words one can say that the Mössbauer effect is the recoil free emission of gamma radiation from a solid radioactive material. Since the gamma emission is recoil free it can be resonantly absorbed by stationary atoms. It enables the study of minute energy changes and hyperfine interactions which are otherwise undetectable. The nuclear transitions are very sensitive to the local environment of the atom and Mössbauer spectroscopy is a sensitive probe of the different environments an atom occupies in a solid material [48-51].

To observe this effect a source and an absorber of gamma rays are required. Both should have a recoilless fraction at the operating temperature. A gamma ray detection system can monitor the process. Usually the transmission mode is followed where the intensity of the gamma rays after passing through the absorber decreases during resonance. In the off resonance regions, the intensity does not change sufficiently. To create resonance and off resonance conditions, the energy

of gamma rays is modulated by imparting Doppler velocity between the source and the absorber. They are in the range of 0-16mm/sec for ^{57}Fe . In a typical Mössbauer experiment the material under study contains ^{57}Fe or any Mössbauer nucleus. The emitted gamma rays of energy 14.4 KeV were used in the present Mössbauer studies. A block diagram of the instrumental setup is shown in Figure 2.2

Nuclei are positively charged and may possess various kinds of nuclear moments. They generally interact with the electric and magnetic field in the nuclear region and perturb the nuclear energy levels. The perturbation is called nuclear hyperfine interactions. These interactions shift the nuclear energy levels, as is the case in electric monopole interaction. It splits degenerate nuclear levels into sublevels without shifting the centroid of the multiplet, as is observed in electric quadrupole interaction and magnetic dipole interaction.

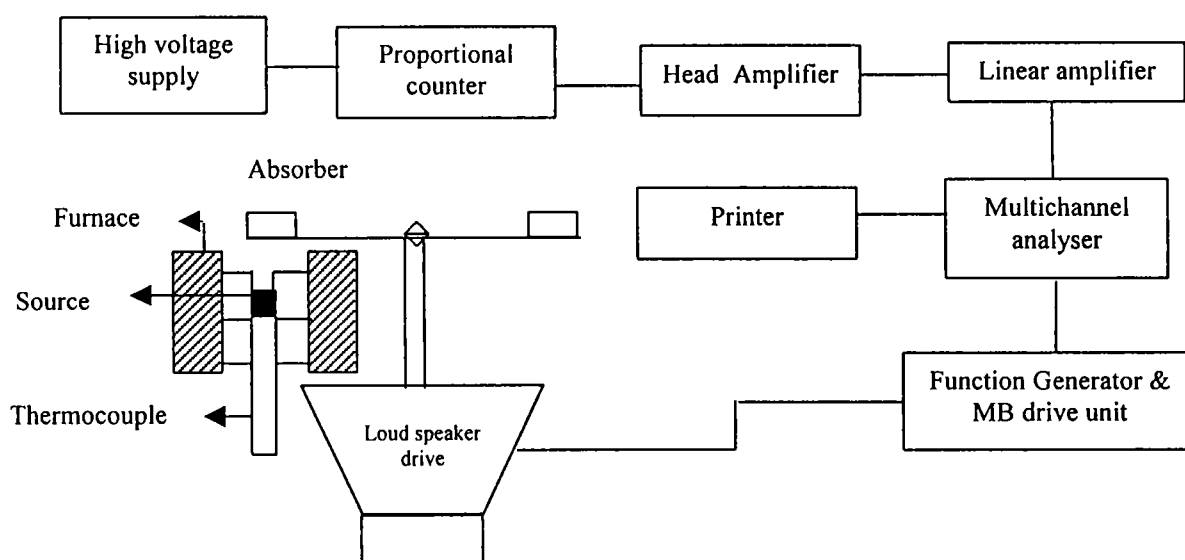


Figure 2.2 Schematic diagram of the Mössbauer spectrometer

The hyperfine field H_{eff} at the nucleus was calculated using the formula $H_{\text{eff}} = \text{total split in mm/sec} / 31.25 \text{KOe}$. The total split here corresponds to the split between the extreme lines. The factor 31.25KOe was deduced from the total split (in channels) of the iron foil spectrum for calibration. The three kinds of interactions considered in Mössbauer spectroscopy are electric monopole interaction, electric quadrupole interaction and magnetic dipole interaction. Interactions of higher order are

negligible, their energy effects are so small that they can not be resolved in a Mössbauer spectrum.

A Mössbauer spectrum in general reflects the nature and strength of the hyperfine interactions. Electric monopole interactions affects the position of the resonance lines on the Doppler velocity scale and gives rise to the so-called isomer shift (chemical shift 'δ'). Isomer shift values must always be reported with respect to a given reference material, because the Mössbauer spectra of a particular compound **are measured with different sources**. By electric monopole interaction, we simply mean the electrostatic coulomb interaction between the nuclear charge and electron inside the nuclear region. But the electric quadrupole and magnetic dipole interactions split the resonance lines originating from transition between degenerate nuclear levels. Most valuable chemical information can be extracted from these Mössbauer parameters like Electric quadrupole splitting (ΔE_Q), Magnetic dipole splitting (ΔE_M), and chemical shift or isomer shift (δ). The isomer shift and the quadrupole splitting can be calculated using the following formula

$$\text{Isomer shift } (\delta) = \frac{V_1 + V_6 + V_2 + V_5}{4} \dots\dots\dots(2.5)$$

$$\text{and Quadrupole splitting } (E_q) = \frac{(V_6 - V_5) - (V_2 - V_1)}{4} \dots\dots\dots(2.6)$$

where V_1 , V_2 etc are the velocities. Electric quadrupole interaction only occurs if there is an observable nuclear quadrupole moment and simultaneously a non zero electric field gradient at the nucleus. An atomic nucleus in the energy state E with spin quantum number $I > 0$ possesses a non zero magnetic dipole moment μ and may interact with a magnetic field H at the nucleus. The interaction is called magnetic dipole interaction or nuclear Zeeman effect. The nuclear Zeeman effect splits the nuclear state with spin quantum number I in to $2I+1$ equally spaced and non degenerate substates.

Because of the recoil free resonance absorption of nuclear gamma rays, Mössbauer spectroscopy has been known to be a powerful tool for investigating the properties of internal fields acting on nuclei in solids. The 14.4 keV γ - rays of ^{57}Fe have been employed to study the internal fields at iron nuclei in several ferro and antiferromagnetic materials. If the iron atoms occupy the two non-equivalent sites

of position as in the case of ferrites, one would expect to obtain a superposition of two patterns. Mössbauer studies on ferrites provides valuable information on the ratio of the Fe^{3+} ion in tetrahedral and octahedral sites, the type of ordering (Neel type or Yafet Kittel type) and any deviation from stoichiometry leading to mixed valence states such as Fe^{2+} and Fe^{3+} .

In the present study the ^{57}Fe Mössbauer spectrum of ZnFe_2O_4 was recorded at room temperature and also at 16 K using constant acceleration Mössbauer Spectrometer. A closed cycle He -refrigerator (CTI cryogenics model 226) was used to cool the absorber at 16 K.

2.8. Electrical characterization

2.8.1: Dielectric properties:

Every material has a unique set of electrical characteristics that are dependent on its dielectric properties. Accurate measurements of these properties will provide scientists and engineers with valuable information. This information when properly incorporated and correlated can pave way for intended applications or monitor a manufacturing process for improved quality control.

A measurement of dielectric parameters can provide initial design parameters for many electronic applications. With this, one can relate the loss of a cable insulator, the impedance of a substrate or the frequency of a dielectric resonator with the dielectric properties. Dielectric information is also useful for improving ferrite absorbers. Recent applications in the area of industrial microwave processing of food, rubber, plastic and ceramics have also been found to benefit from knowledge of dielectric properties.

The utmost dielectric property of importance to physicists and engineers is the permittivity. These properties are not constant; they can change with frequency, temperature, orientation, mixture, pressure and molecule structure of the material. A material is said to be dielectric if it has the ability to store energy when an external electric field is applied. If a dc voltage source is placed across a parallel plate capacitor, more charge is stored when the separation between the plates is

occupied by a dielectric material. The dielectric material increases the storage capacity of the capacitor by neutralizing charges at the electrodes, which ordinarily would contribute to the external field.

If an ac sinusoidal voltage source is placed across the same capacitor, the resulting current will be made up of a charging current and a loss current that is related to the dielectric constant. Here we are interested only in the permittivity (ϵ_r) of the material and the loss ($\tan\delta$). Permittivity describes the interaction of a material with an electric field. The relative permittivity $\epsilon_r = \epsilon / \epsilon_0$. The complex relative permittivity is given by

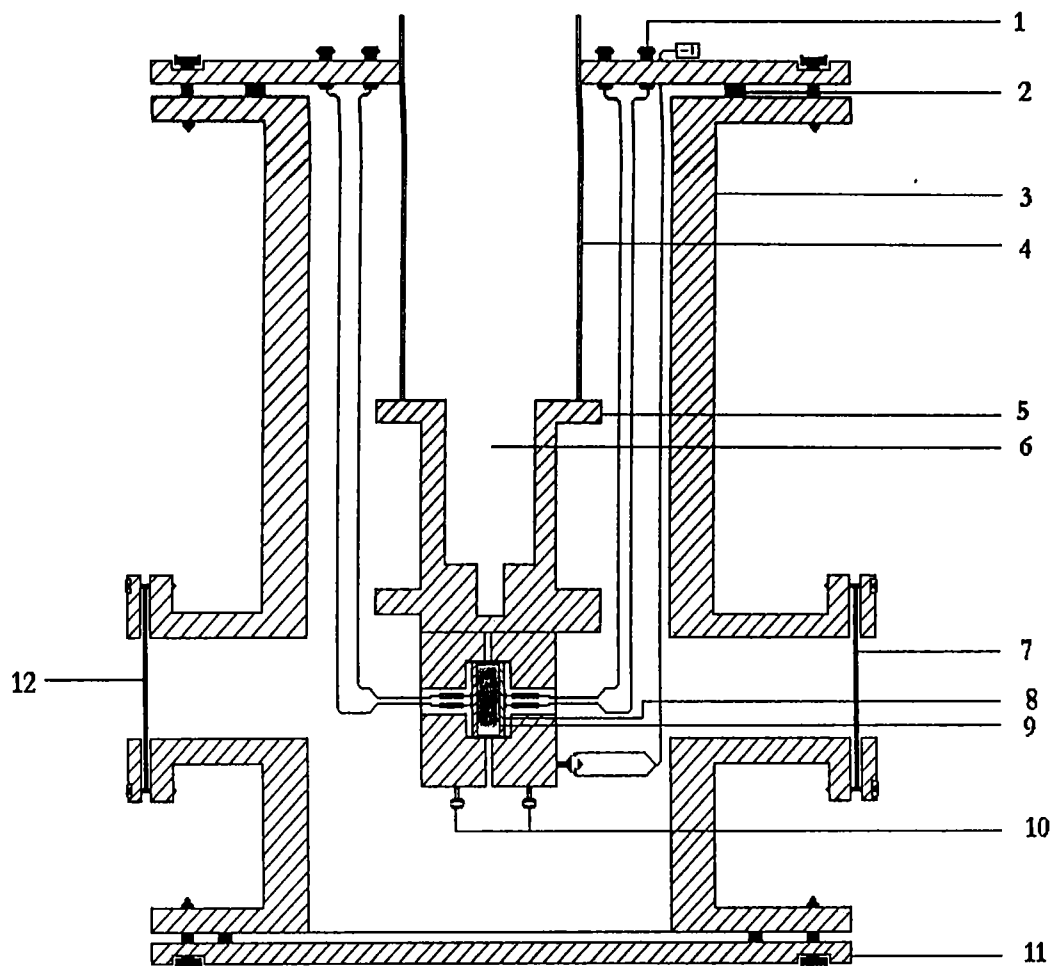
$$\epsilon_r^* = \frac{\epsilon^*}{\epsilon_0} = \frac{\epsilon - j\epsilon''}{\epsilon_0} \dots\dots\dots(2.7)$$

Where ϵ_0 is the permittivity of free space, which is equal to 8.854×10^{-12} F/m. The real part of permittivity (ϵ_r) is a measure of how much energy from an external electric field is stored in a material. The imaginary part of the permittivity (ϵ_r'') is called the loss factor. The loss factor includes the effects of both dielectric loss and conductivity. The dielectric properties of $\text{Ni}_{1-x}\text{Zn}_x\text{Fe}_2\text{O}_4$ was studied using a dielectric cell and an impedance analyzer (Model: HP 4192A) in the frequency range 5Hz to 13 MHz. Schematic of the dielectric cell is shown in Figure. 2.3.

$\text{Ni}_{1-x}\text{Zn}_x\text{Fe}_2\text{O}_4$ samples which was prepared by ceramic techniques were then made in the form of pellets of 10mm diameter and is loaded in to the dielectric cell. The capacitance values at different frequencies ranging from 5Hz to 13MHz was noted. The dielectric constant was calculated using the formula

$$C = \frac{\epsilon_0 \cdot \epsilon_r \cdot A}{d} \dots\dots\dots(2.8)$$

Where A is the area of the sample piece used and d its thickness. ϵ_0 and ϵ_r are the dielectric constant of the air and medium respectively and C is the capacitance value. The measurement was carried out at different temperature in the temperature range 303K to 473K. The sample temperature is controlled by a temperature controller and the temperature on the surface of the sample is sensed by a Fe-K thermocouple kept on the sample.



- | | |
|-------------------------|----------------------|
| 1. BNC | 7. Glass Window |
| 2. Neoprine O Ring | 8. Copper Electrodes |
| 3. MS Chamber | 9. Sample |
| 4. SS Pipe | 10. Fixing Screws |
| 5. Sample Holder | 11. MS Flange |
| 6. Liq. Nitrogen Cavity | 12. To Vacuum pump |

Figure 2.3 Schematic representation of dielectric cell

2.8.2 Ac conductivity.

The ac electrical conductivity of both the ceramic and rubber ferrite composites were evaluated by calculating the ac conductivity values using dielectric parameters. The dielectric studies of both ceramic and rubber ferrite composites were carried out by using a dielectric cell and an impedance analyzer (Model: HP 4192A). Disc shaped samples were used to find out the dielectric constant. The capacitance and dielectric loss in the frequency range 100KHz – 5MHz were found out. Dielectric constant or relative permittivity was calculated using the formula

$$\epsilon_r = \frac{C.d}{\epsilon_0.A} \dots\dots\dots(2.9)$$

where d is the thickness of the sample, C the capacitance and A the area of cross section of the sample. ϵ_r is the relative permittivity of the material which is a dimensionless quantity. The ac conductivity of these samples were then evaluated using the relation

$$\sigma_{ac} = 2\pi f \tan\delta \epsilon_0 \epsilon_r \dots\dots\dots(2.10)$$

f is the frequency of the applied field and $\tan\delta$ is the loss factor. The principle and the theory underlying the evaluation of σ_{ac} from dielectric measurements are based on a treatment dealt by Goswamy [52]. It may be noted that ϵ_r and $\tan\delta$ for both ceramic and RFCs were made available from the dielectric measurements of these samples. The theory and principle involved in the determination of ac conductivity from the dielectric measurements is dealt in detail in chapter 6.

Cure characteristics and magnetic properties of rubber ferrite composites

3.1. Introduction

It is known that magnetic polycrystalline ceramic powders can be incorporated in various elastomer matrixes to produce flexible magnets or rubber ferrite composites (RFC). These plastic magnets can in turn be useful for various applications in different devices. The addition of magnetic fillers in an elastomer matrix modifies the physical properties of the matrix considerably in that they modify the dielectric properties and impart magnetic properties to the matrix [53-54]. In applications involving ferrites at high frequencies it is essential that the material possess an appropriate dielectric constant and suitable magnetic permeability. This can be achieved by synthesizing rubber ferrite composites (RFC) [55-57].

It has also been reported that the chemical incorporation of ferrite particles in polymer matrix can lead to the development of magnetic nanocomposites with excellent performance characteristics [13-15]. The preparation of RFCs and evaluation of various properties such as magnetic, dielectric and mechanical assumes significance not only in tailor making compounds but also in understanding the fundamental aspects that govern these properties. The results of investigations conducted on ceramic nickel zinc mixed ferrites and their incorporation in a butyl rubber matrix are discussed in this chapter.

Mixed ferrites belonging to the series $Ni_{1-x}Zn_xFe_2O_4$ have been prepared with x varying from 0 to 1 in steps of 0.2 using ceramic processing techniques. The details are described in chapter 2. The structural and magnetic properties were evaluated. These NiZn ferrites were then incorporated in a butyl rubber matrix at different loadings according to a specific recipe cited in chapter 2. Their cure

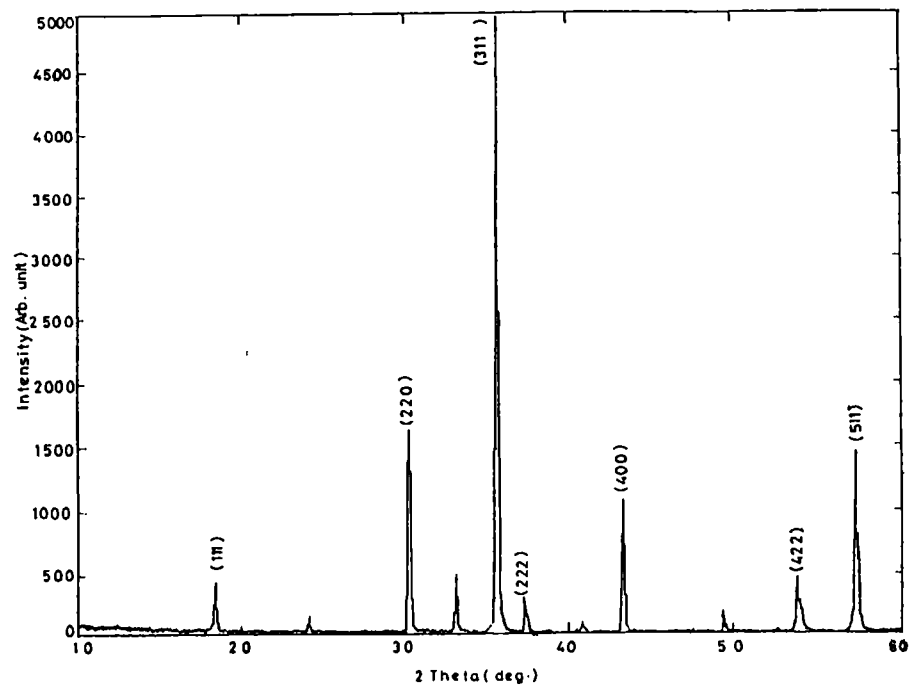
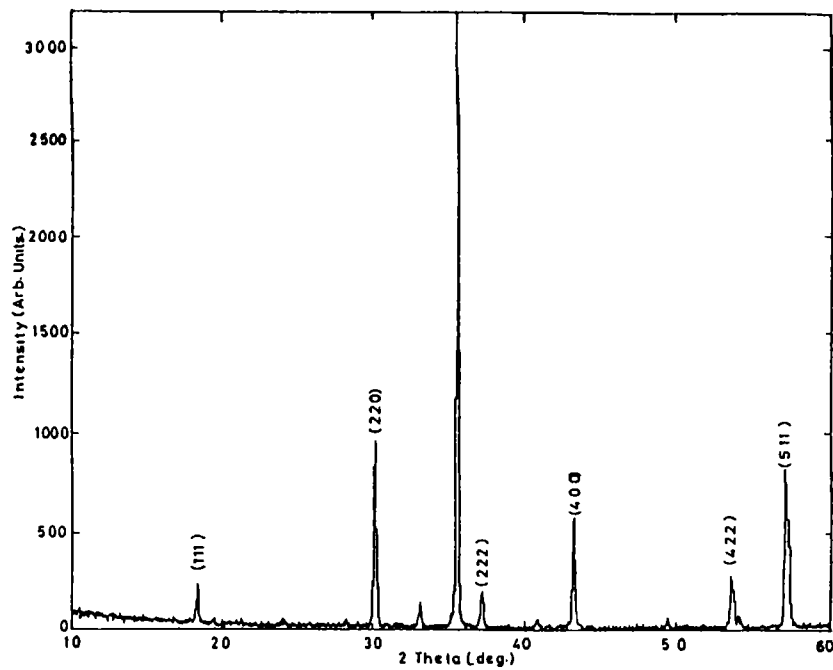
characteristics were evaluated and the magnetic properties of the composites were determined and are presented. Here in this chapter the magnetic data obtained on the ceramic fillers and RFCs are correlated. A general relationship, which connects the M_s of the ceramic component in the RFC and the M_s of RFCs, is brought out. The validity of the equation is then checked with observed data and the calculated values of magnetisation.

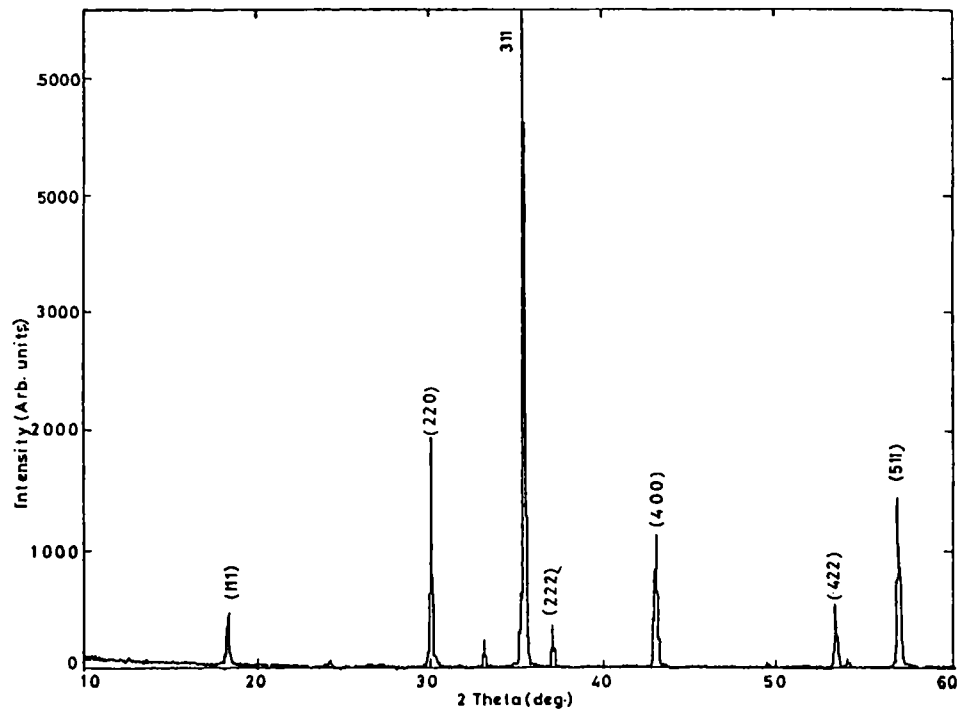
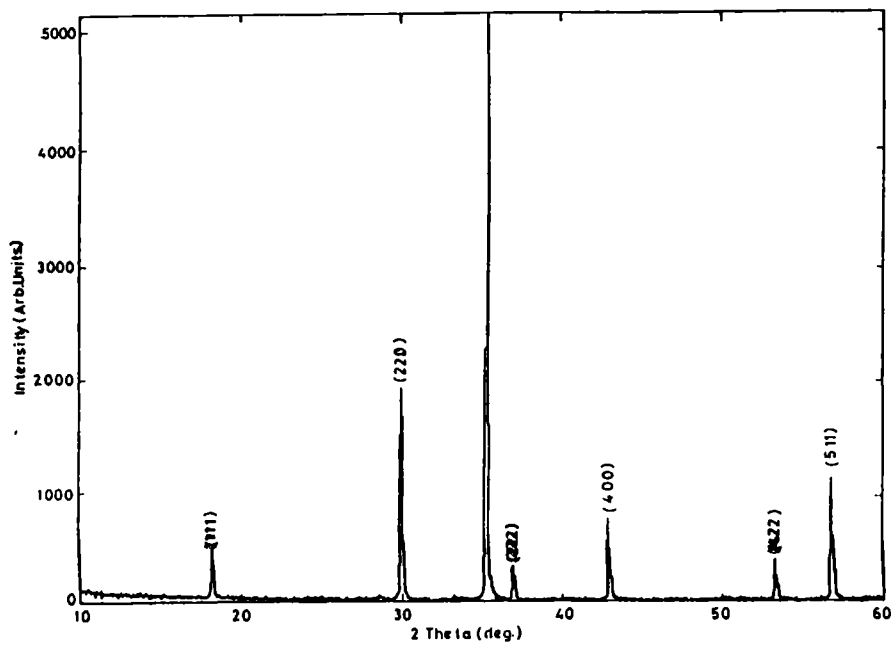
3.2. Structural studies of $Ni_{1-x}Zn_xFe_2O_4$

Nickel zinc ferrites with varying percentage of Ni/Zn were prepared by utilizing the conventional ceramic technique [58]. Six samples with different compositions of Zinc(x) with x varying from 0 to 1 in steps of 0.2 were prepared. It is very much essential that the structure of these samples is identified and also the presence of any other impurities in the prepared compounds is detected. With these objectives, the X – Ray diffractograms of all the samples were recorded. These diffractograms are depicted in Figure .3.1. to 3.5. It can be seen that all the compounds thus prepared show very high crystallinity and the diffraction pattern is characteristic of a spinel structure. The inter atomic spacing (d) were compared with the standard values reported in literature [59]. These values are in good conformity with that of the reported values. Moreover no other impurity lines corresponding to possible oxides of precursors used for synthesis were noticed. The possibility of occurrence of any other phase in the compound is thus ruled out. Thus it was ensured that the prepared compounds are single phasic in nature and they exhibit an inverse/ normal spinel structure. Being cubic spinel, the lattice parameter (a) for all compounds were calculated using the formula

$$d = \frac{a}{\sqrt{h^2 + k^2 + l^2}}$$

Where the inter planar spacing d_{hkl} for different planes were calculated using Bragg's law $2d\sin\theta = n\lambda$. The lattice parameter is found to lie between 0.834 nm to 0.845nm. The variation of lattice parameter with composition is plotted and is depicted in Figure. 3.6. It was found that the variation of lattice parameter with composition is linear. The variation of 'a' with composition is in conformity with reported literature [60]. This linear variation is in accordance with Vegard's law [61].

Figure 3.1 XRD Spectrum of NiFe₂O₄Figure 3.2 XRD Spectrum of Ni_{0.8}Zn_{0.2}Fe₂O₄

Figure. 3.3 XRD Spectrum of $\text{Ni}_{0.6}\text{Zn}_{0.4}\text{Fe}_2\text{O}_4$ Figure. 3.4 XRD Spectrum of $\text{Ni}_{0.4}\text{Zn}_{0.8}\text{Fe}_2\text{O}_4$

$\text{Ni}_{0.4}\text{Zn}_{0.8}\text{Fe}_2\text{O}_4$
0.4 0.8

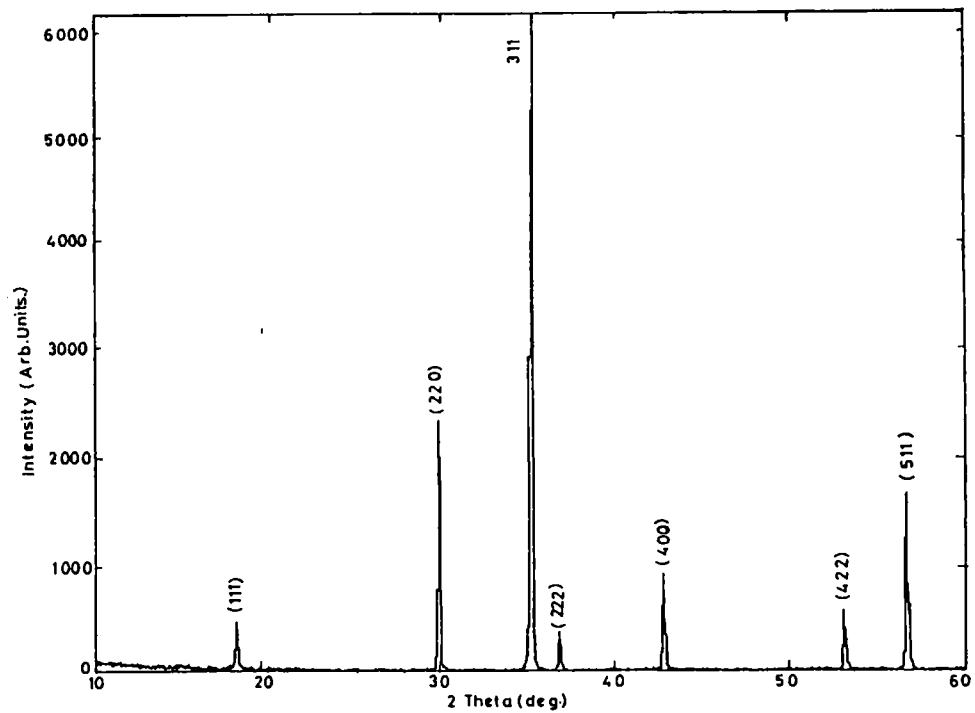


Figure 3.5. XRD Spectrum of $\text{Ni}_{0.2}\text{Zn}_{0.8}\text{Fe}_2\text{O}_4$

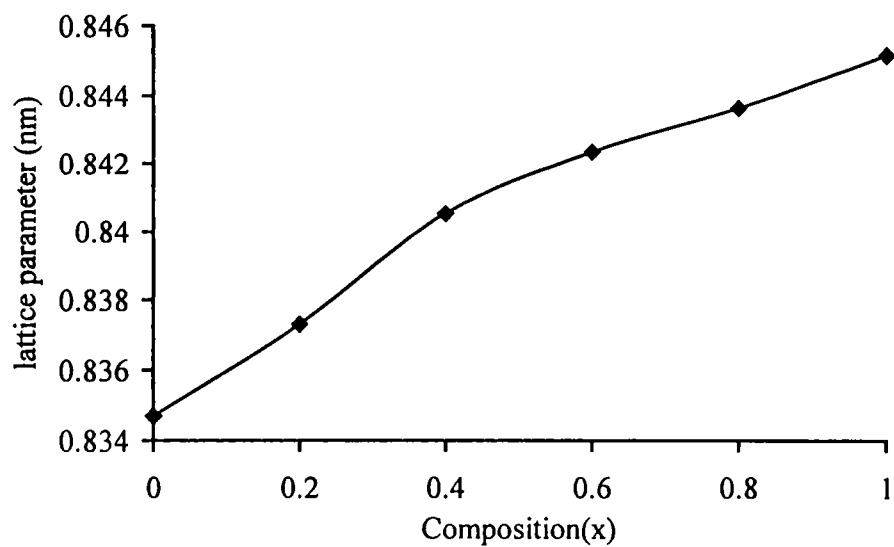


Figure 3.6. Composition Vs Lattice parameter for $\text{Ni}_{1-x}\text{Zn}_x\text{Fe}_2\text{O}_4$

According to Vegard's law the lattice parameter of a solid solution is directly proportional to the atomic percent of the solute present in that compound. From the XRD data the particle size of all the samples were estimated by employing Debye Scherrer's formula $D = \frac{0.9 \lambda}{\beta \cos \theta}$. It was found that the particle size lies in the range 88 – 97nm. The porosity of these samples were also determined by evaluating the X –ray density and apparent density of these samples. The X – ray density was calculated from lattice parameter using the relation $\frac{n.M}{a^3 N_a}$. Where 'a' is the lattice parameter, N_a is the avagadro number, M the molecular weight of the compound, and n is the number of molecules per unit cell. The apparent density of various compositions were also evaluated and the porosity of the samples were determined. The details can be found in Table.3. 1.

Composition	Lattice Parameter(nm)	Particle size (nm)	X–ray density (gm/cm ³)	Apparent density (gm/cm ³)	Porosity (%)
X = 0.0	0.8347	89.2	5.354	4.851	9.39
X = 0.2	0.8373	88.6	5.323	5.023	5.64
X = 0.4	0.8405	88.3	5.303	5.155	2.80
X = 0.8	0.8436	94.26	5.304	5.184	2.26
X = 1.0	0.8451	96.44	5.305	5.057	4.68

$x=0.6^n$

Table 3.1: Structural parameters of $Ni_{1-x}Zn_xFe_2O_4$

3.3. Magnetic properties of ceramic $Ni_{1-x}Zn_xFe_2O_4$

Ferrites possess substantial spontaneous magnetization at room temperature due to the unequal and opposing magnetic moments of the atoms on different sublattices [62]. Ferrites are ionic compounds and their magnetic properties are due to the presence of the magnetic ions in the lattice. The various factors that determine the magnetic properties of these ferrites are nature of

cations, heat treatment, preparation method, site preference energy of cations and Madelung energy [63-69]

According to Neel, ferrites exhibit a magnetic structure distinctly different from any previously recognized structure [70]. The metal ions in a ferrite crystal occupy two crystallographically different kinds of position called tetrahedral (A) sites and octahedral (B) sites. Since cation-cation distances are generally large, direct interactions are negligible. Because of the geometry of orbitals involved the strongest super exchange interaction is expected to occur between octahedral and tetrahedral cation or A-O-B interaction. Another possible interaction is B-O-B interaction. The dominant A-O-B interaction in inverse spinels leads to a saturation magnetisation at 0K, which depends only on the magnetic moment of the divalent cation. Antiparallel order cancels Fe^{3+} moments in octahedral and tetrahedral sites, the divalent cation moment which is parallel to Fe in octahedral sites then accounts for the net resultant magnetisation. Thus the magnetic properties of these ferrites can be modified suitably by a judicious choice of cations.

Magnetic measurements for sintered nickel zinc ferrite samples belonging to the series $\text{Ni}_{1-x}\text{Zn}_x\text{Fe}_2\text{O}_4$ were carried out by using Vibrating Sample Magnetometer (VSM) model:4500 from EG&G PARC by applying a field of 4kAm^{-1} . The details are elaborated in chapter 2. Parameters like saturation magnetization (M_s), retentivity (M_r), coercivity (H_C) were obtained from these measurements for all samples at room temperature. Table.3.2 describes the details of HLT parameters. Figure .3.7 and 3.8 shows a representative hysteresis loop for nickel zinc ferrite. The variation of magnetization with composition (x) are depicted graphically and is shown in Figure 3.9. From the graphs it can be seen that M_s attains a maximum at around $x = 0.4$ and then decreases. The variation of magnetization with composition is in accordance with the results obtained by various researchers [71].

Composition	Magnetization(M_s) Am^2/Kg	Retentivity (M_r) Am^2/Kg	Coercivity(H_c) A/m	M_r/M_s
X = 0	44.12	7.83	8159	0.177
X = 0.2	67.53	3.767	5970	0.056
X = 0.4	69.94	7.044	4593	0.100
X = 0.6	46.82	4.77	3767	0.102
X = 0.8	7.589	0.3759	4975	0.049
X = 1	3.118	0.2419	4975	0.077

Table3. 2. Hysterisis loop Parameters for $\text{Ni}_{1-x}\text{Zn}_x\text{Fe}_2\text{O}_4$

The variation pattern of saturation magnetization (M_s) as a function of Zn content shows an increase for small substitutions, goes through a maximum value of $69.94\text{Am}^2/\text{Kg}$ at $x = 0.4$ and then decreases. Similarly the magnetic moment μ_B for various compositions were calculated by assuming Neel's two sub lattice model and compared with that of observed values. For this a probable cation distribution based on site preference energy, radius ratio rules is necessary. The cation distribution can be written as $\text{Zn}_x\text{Fe}_{1-x} [\text{Ni}_{1-x} \text{Fe}_{1+x}] \text{O}_4$, where Zn^{2+} is diamagnetic and its main effect is to break linkages between magnetic cations. Another effect is to increase interaction distance by expanding the unit cell, since it has an ionic radius larger than the Ni and Fe radii. From Table: 3.3 it can be seen that Nickel has a strong preference for B site while Zinc occupies only tetrahedral sites. Based on octahedral site preference energies and radius ratio rules, a probable cation distribution was arrived at, and the magnetic moment (μ_B) was calculated for all composition. They are cited in Table.3.4. Also, from the measured data μ_B for all compositions were calculated using the formula $\mu_B = \frac{M_s \cdot \text{Mol.wt}}{5585}$ where M_s is the measured magnetisation per atom. Details are shown in Table. 3.5.

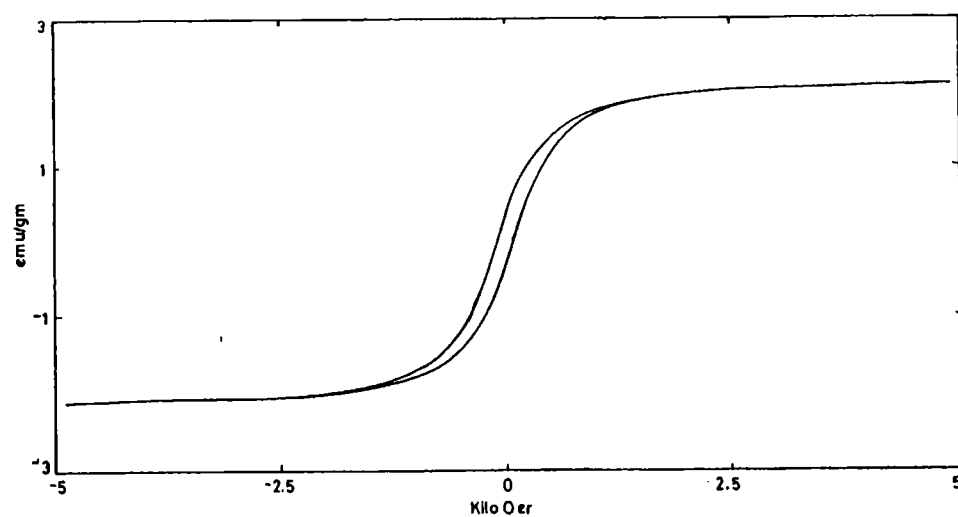


Figure 3.7. Hysteresis loop for NiFe_2O_4

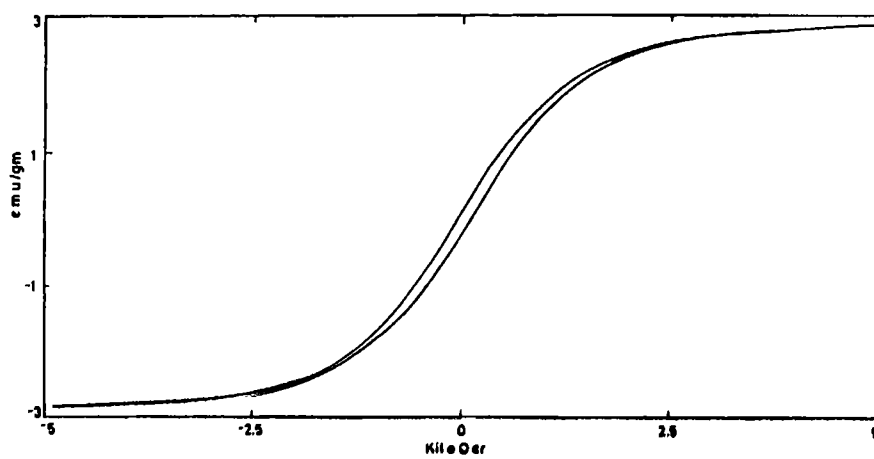


Figure 3.8. Hysteresis loop for $\text{Ni}_{0.4}\text{Zn}_{0.6}\text{Fe}_2\text{O}_4$

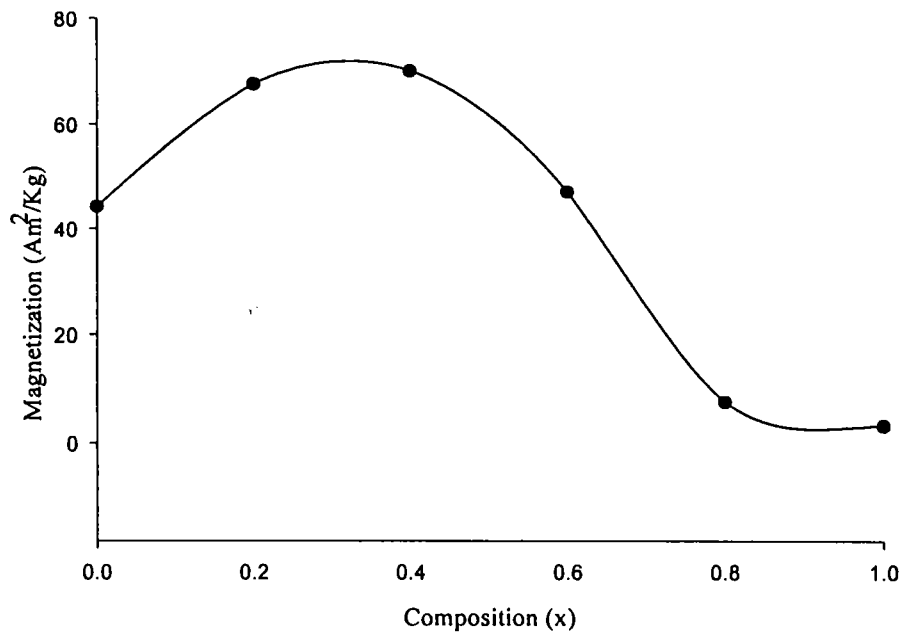


Figure.3.9.Variation of magnetization with composition for $\text{Ni}_{1-x}\text{Zn}_x\text{Fe}_2\text{O}_4$

Cations	Ionic radii (A°)	Octahedral Site preference energy Kcal/g atom
Zn^{2+}	0.74	-31.6
Ni^{2+}	0.69	9
Fe^{3+}	0.64	-13.3
Fe^{2+}	0.74	-9.9

Table. 3.3. Ionic radii and site preference energies of some selected cations

Composition	Compounds	A- Site	B- Site	M_B	M_A	μ_B
X = 0	Ni Fe ₂ O ₄	Fe ³⁺	Ni ²⁺ Fe ³⁺	2 + 5 = 7	5	2
X = 0.2	Ni _{0.8} Zn _{0.2} Fe ₂ O ₄	Zn ²⁺ _{0.2} Fe ³⁺	Ni ²⁺ _{0.8} Fe ³⁺	1.6 + 5 = 6.6	5	1.6
X = 0.4	Ni _{0.6} Zn _{0.4} Fe ₂ O ₄	Zn ²⁺ _{0.4} Fe ³⁺	Ni ²⁺ _{0.6} Fe ³⁺	1.2 + 5 = 6.2	5	1.2
X = 0.6	Ni _{0.4} Zn _{0.6} Fe ₂ O ₄	Zn ²⁺ _{0.6} Fe ³⁺	Ni ²⁺ _{0.4} Fe ³⁺	0.8 + 5 = 5.8	5	0.8
X = 0.8	Ni _{0.2} Zn _{0.8} Fe ₂ O ₄	Zn ²⁺ _{0.8} Fe ³⁺	Ni ²⁺ _{0.2} Fe ³⁺	0.4 + 5 = 5.4	5	0.4
X = 1	Zn Fe ₂ O ₄	Zn ²⁺ Fe ³⁺	Fe ³⁺	0 + 5 = 5	5	0

Table 3. 4: Theoretically calculated μ_B (Neel's model) for various compositions of Ni_{1-x} Zn_x Fe₂O₄

Composition	Magnetization (measured) (M_s) Am ² /kg	Molecular weight	μ_B
X = 0	44.12	234.41	1.852
X = 0.2	67.53	235.242	2.844
X = 0.4	69.94	237.074	2.969
X = 0.6	46.82	238.408	1.999
X = 0.8	7.589	239.738	0.326
X = 1	3.118	241.070	0.1346

Table: 3.5. Calculated values of μ_B for Ni_{1-x} Zn_x Fe₂O₄ using the observed values of magnetisation

The magnetisation variation shows an increases in M_s with increase of zinc content up to $x = 0.4$, there after it decreases with increase of zinc concentration. The variation up to $x = 0.4$ is due to the antiparallel alignment of the spins. As the zinc concentration increases magnetic moment decreases in sublattice B. Further

increase of zinc concentration makes A-O-B interaction is too weak and B-O-B interactions begin to dominate. At this stage instead of a collinear, antiparallel alignment a canted structure appears, where the spins in B-sites are no longer parallel thus resulting in a reduced magnetisation. The average canting angle among the B site spins were found out by various researchers by neutron diffraction studies [72-75]. The strength and sign of the B-B exchange interactions relative to the A-B exchange interactions determine the canting angle. It was also mentioned that the canting angles of the Ni^{2+} and Fe^{3+} ions are expected to be different because the exchange interaction J_{AB} and J_{BB} are known to be different. According to this when $x = 1$ that is for ZnFe_2O_4 , is to have a zero net magnetisation. Instead a net magnetisation of $3.118\text{Am}^2/\text{Kg}$ was observed for ZnFe_2O_4 . This anomalous magnetic behaviour of zinc ferrite is dealt with in detail in chapter 4.

It is also possible that the particle size effect is also a factor in determining the cation distribution. This needs further investigations based on the cation distribution found in fine particle systems of $\text{Ni}_{1-x}\text{Zn}_x\text{Fe}_2\text{O}_4$ ferrites. To extract evidence on the cation distribution of these mixed ferrites in the fine particle regime, a detailed study on these samples using tools like Mössbauer spectroscopy is needed.

The variation of coercivity with composition is shown in Figure.3.10. It was observed that the coercivity first decreases with increase of composition reaches a minimum at $x = 0.6$, and there after increases with increase of composition. The contribution to coercivity are mainly due to shape anisotropy, stress anisotropy and crystal anisotropy. The expression relating coercivity to saturation magnetisation for these three cases can be written as follows ,

$$\text{shape anisotropy } H = h(N_a - N_c) M_s \dots \dots \dots (3.1)$$

$$\text{stress anisotropy } H = h (3\lambda_s \sigma / M_s) \dots \dots \dots (3.2)$$

$$\text{crystal anisotropy } H = h (2K_1 / M_s) \dots \dots \dots (3.3)$$

Where 'h' is a constant for all these cases. λ_s is the magnetostriction constant, σ the stress, N_a and N_c are the demagnetizing coefficients parallel to the a and c axes.

From the magnetic parameters it can be seen that the variation of coercivity is inversely proportional to saturation magnetisation.

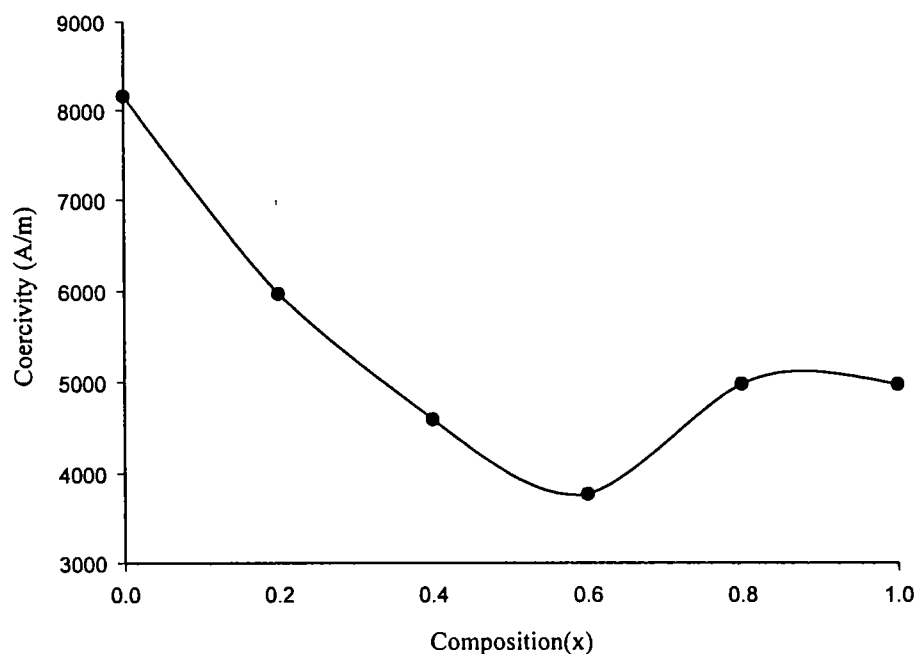


Figure 3.10. Variation of coercivity with composition for $\text{Ni}_{1-x}\text{Zn}_x\text{Fe}_2\text{O}_4$

This indicates that in this nickel zinc ferrite system the contribution is not due to shape anisotropy but it is either due to stress anisotropy or crystal anisotropy. In the case of polycrystalline nickel zinc ferrite samples, the existence of an easy axis of magnetisation is not known. Hence we can only say that the contribution from the stress anisotropy term is predominant in the coercivity mechanism. It is also known that factors like size of domains, nature of domains and grain size have a profound influence in determining the coercivity of the particle. The porosity calculations show a linear dependence with coercivity. The Figure.3.11 shows the composition dependence of both coercivity and porosity. It can be seen that the coercivity increases as porosity increases. The variation of coercivity with porosity is in agreement with the reported literature [76]. Since the porosity is the measure of voids it could be said that it is the stress anisotropy which is the predominant factor responsible for the coercivity of these samples.

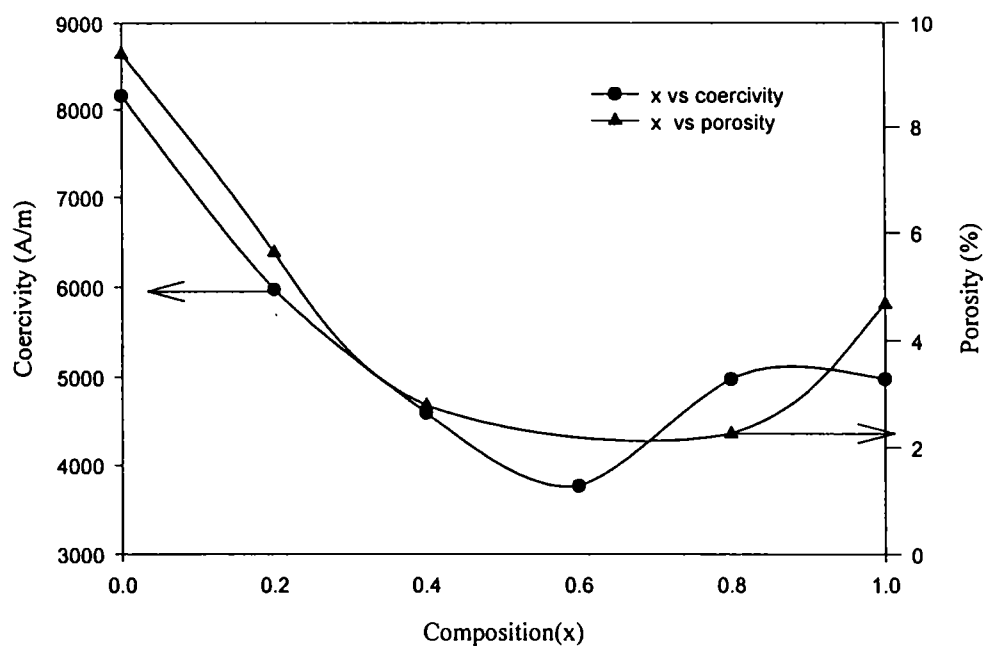


Figure 3.11 Variation of coercivity and porosity with composition

3.4. Cure Characteristics of rubber ferrite composites

Rubber ferrite composites containing various loadings of $\text{Ni}_{1-x}\text{Zn}_x\text{Fe}_2\text{O}_4$ were prepared according to a standard recipe. Details of preparation are described in chapter 2. The processability of these rubber ferrite composites were determined by evaluating the cure parameters of the compounds. After the physical blending of the elastomer with the magnetic fillers, the resulting blend must be cured for making rubber ferrite composites. The important cure parameters like maximum and minimum torque, scorch time (t_{10}), cure rate (t_{50}) and optimum cure (t_{90}) were evaluated by determining the cure characteristics on a Gottfert Elastograph (model: 67.85). The compounds were then vulcanized at 170°C on an electrically heated hydraulic press at 10Mpa pressure up to the respective cure time. Minimum torque gives information about the viscosity of the compound, which is a valuable input as far as processability of the polymer is concerned. From the cure characteristics of the composites it can be observed that minimum torque which is

implicitly known as viscosity of compounds increases with loading and then levels off at a higher loading of 120phr. The decrease of minimum torque at 120phr may be due to the dilution effects, which is general to all fillers, as a result of diminishing volume fraction of the polymer in the composite, some amount of the filler remains unreacted. In other words it can be said that it doesn't find enough counterparts in the rubber for miscibility. The cure parameters for composite containing $\text{Ni}_{0.4}\text{Zn}_{0.6}\text{Fe}_2\text{O}_4$ are given in table. 3.6.

Parameters	Blank	20phr	40phr	80phr	120phr
M_L Nm	0.02393	0.02490	0.02490	0.02295	0.02026
M_H Nm	0.08350	0.09180	0.07910	0.07642	0.08276
$t_{10}(\text{min.})$	9.1	9.3	9.7	7.2	5.4
$t_{50}(\text{min.})$	13.9	14.6	15.6	19.4	19.5
$t_{90}(\text{min.})$	24.8	22.6	19.6	25.6	25.9

Table .3. 6. Cure parameters for composites containing $\text{Ni}_{0.4}\text{Zn}_{0.6}\text{Fe}_2\text{O}_4$

The physical meaning of the maximum torque is that it throws light on the mechanical property of the compound after incorporation. It shows a gradual increase with various loadings of the filler. This is to be expected, since the incorporation results in the increase of hardness and modulus. The scorch time (t_{10}), is defined as an indirect measure of heat generated during mixing. It can be seen that the scorch time initially increases with loading and then decreases. The time for 50% cure, that is t_{50} , which is a measure of cure rate increases for all loadings. The optimum cure time t_{90} remains approximately the same. It can be concluded that the processability of the polymer is not significantly affected because of loading. After having evaluated the cure parameters the compounds were cured at 150°C for optimum cure time (t_{90}) and made in to the form of rubber sheets.

3.5. Magnetic properties of rubber ferrite composites

Further, the magnetic parameters of these Rubber ferrite composites were evaluated by using vibrating sample magnetometer (VSM) and they are shown in Table.3.7. Representative hysteresis loops for rubber ferrite composites are shown in Figure.3.12 to 3.15. The measured values of M_s of the ceramic sample was utilized for the calculation of the M_s of the composite. While calculating the M_s of the rubber ferrite composites it was assumed that only single magnetic component is contributing to the magnetic properties of the matrix. The details of the results are shown in Table.3.7. It was also observed that the magnetization increases with loading for each composition. The variations of magnetization with loading for different compositions are shown in Figure.3.16. But it may be noted that the coercivity remains more or less the same for different loadings of each composition, this value of coercivity tallies well with the value of coercivity obtained for the corresponding ceramic magnetic component in the matrix. From this observation it can be concluded that loading has no effect on coercivity or there is no interaction between the filler and the matrix. Like ceramic samples, for rubber ferrite composites too, the variation of magnetization and coercivity with composition is the same. In the case of composites also the magnetization first increases with increase of composition and reaches a maximum value at $x=0.4$ and thereafter the magnetization decreases with increase of composition. The variation of magnetization with composition for different loadings is shown in Figure.3.17.

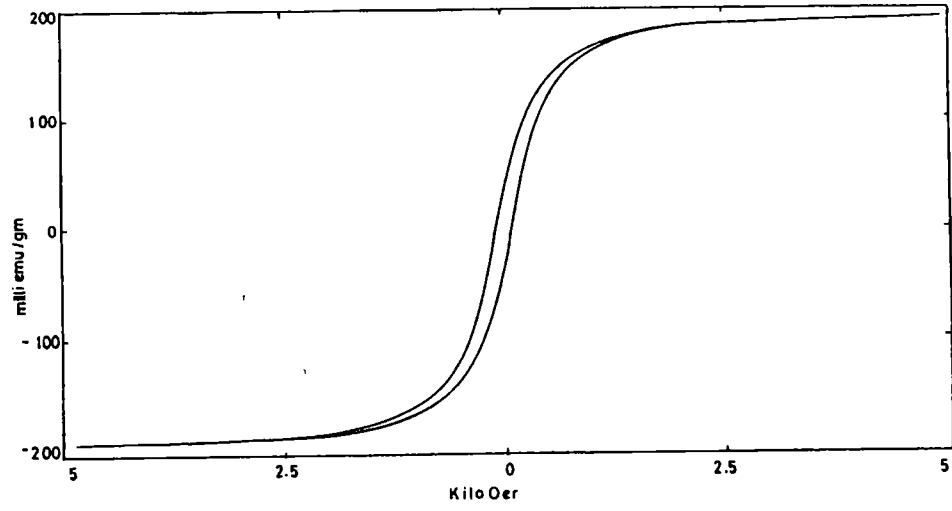


Figure 3.12. Hysteresis loop for RFC (X = 0, 20phr)

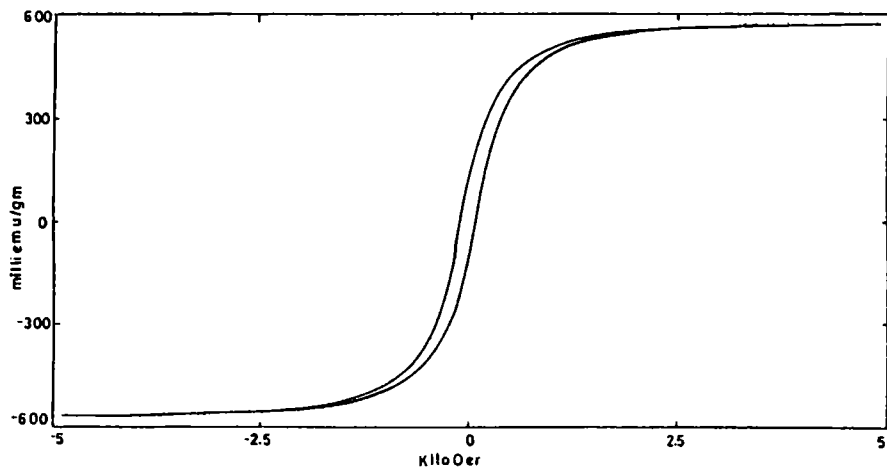


Figure 3.13. Hysteresis loop for RFC (X = 0, 120phr)

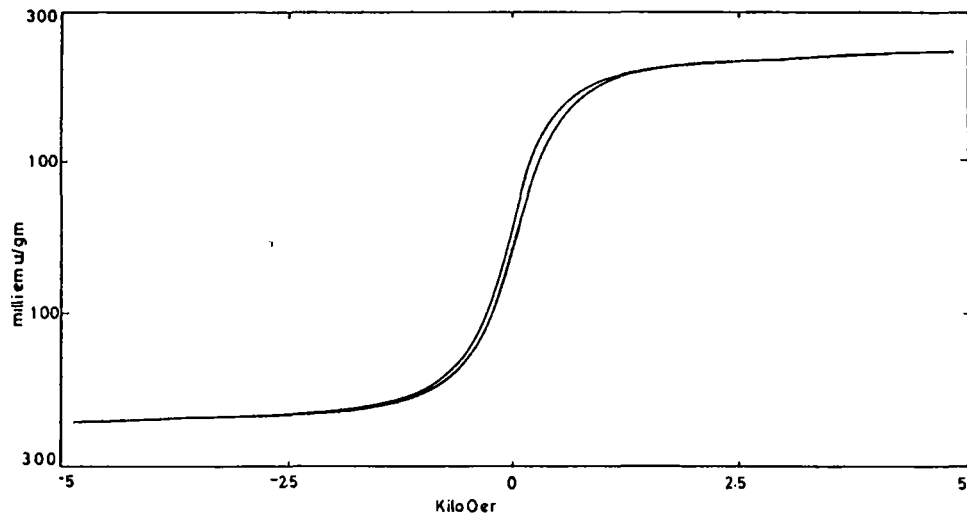


Figure 3.14. Hysteresis loop for RFC (X = 0.6, 20phr)

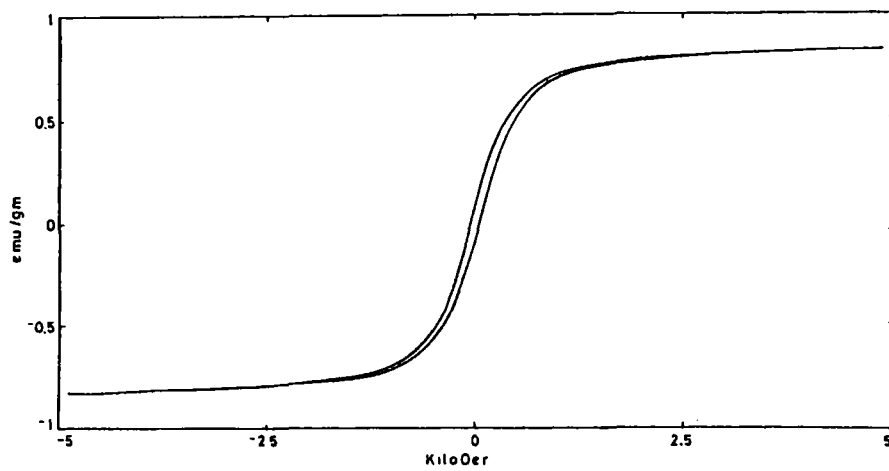


Figure 3.15. Hysteresis loop for RFC (X = 0.6, 120phr)

Composition (x)	Magnetisation Cal. Am ² /Kg	Magnetisation Meas. Am ² /Kg	Retentivity (M _r) Am ² /Kg	M _r /M _s	Coercivity Am ⁻¹
X=0,20phr	6.72	6.587	1.285	0.195	7698.1
X=0,40phr	11.67	9.924	1.974	0.198	7678.2
X=0,80phr	18.45	17.66	3.569	0.202	7567.6
X=0,120phr	22.89	21.62	4.441	0.205	7651.2
X=0.2,20phr	10.29	10.55	1.223	0.115	6112.5
X=0.2,40phr	17.86	18.97	2.238	0.117	5989.9
X=0.2,80phr	28.25	27.15	3.335	0.122	6018.6
X=0.2,120phr	35.04	35.32	4.28	0.121	5930.99
X=0.4,20phr	10.65	10.64	0.8579	0.080	4656.6
X=0.4,40phr	18.49	18.28	1.51	0.082	4455.2
X=0.4,80phr	29.25	28.65	2.515	0.087	4442.5
X=0.4,120phr	36.29	36.29	3.324	0.091	4466.4
X=0.6,20phr	7.13	7.286	0.6945	0.095	4040.5
X=0.6,40phr	12.38	12.04	1.128	0.093	3908.4
X=0.6,80phr	19.58	19.51	1.782	0.091	3827.2
X=0.6,120phr	24.29	23.49	2.263	0.096	3838.3
X=0.8,20phr	1.16	1.508	0.105	0.069	6965
X=0.8,40phr	2.007	2.389	0.160	0.066	6200.8
X=0.8,80phr	3.174	3.142	0.1702	0.054	6609.9
X=0.8,120phr	3.94	3.974	0.2157	0.054	6458.7
X=1,20phr	0.475	0.4545	0.04108	0.090	8955
X=1,40phr	0.825	0.4558	0.0315	0.069	8955
X=1,80phr	1.304	0.625	0.03865	0.062	8955
X=1,120phr	1.618	0.60	0.02938	0.0489	8955

Table 3.7. VSM results of rubber ferrite composites

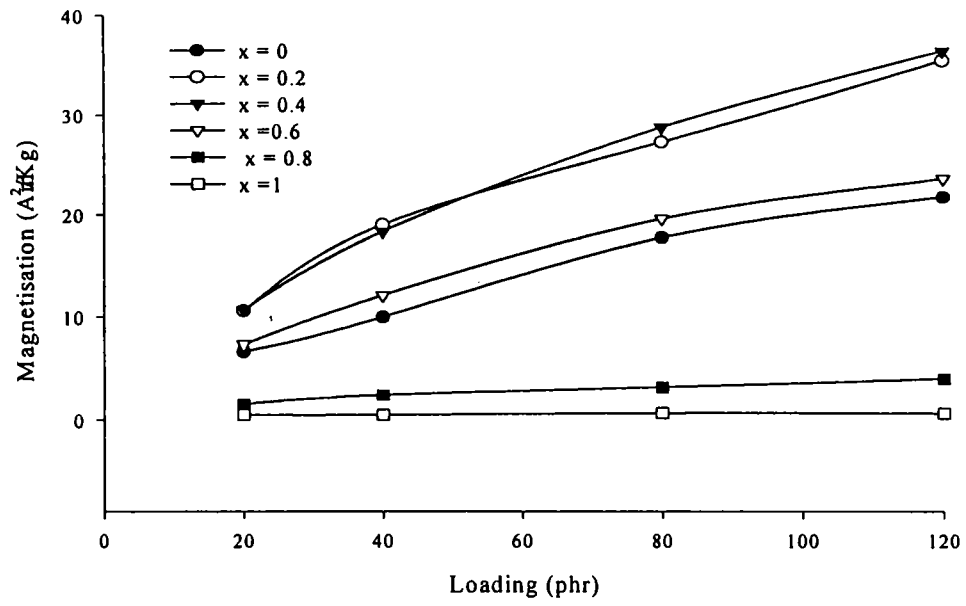


Figure.3.16. Variation of magnetisation with loading for different composition

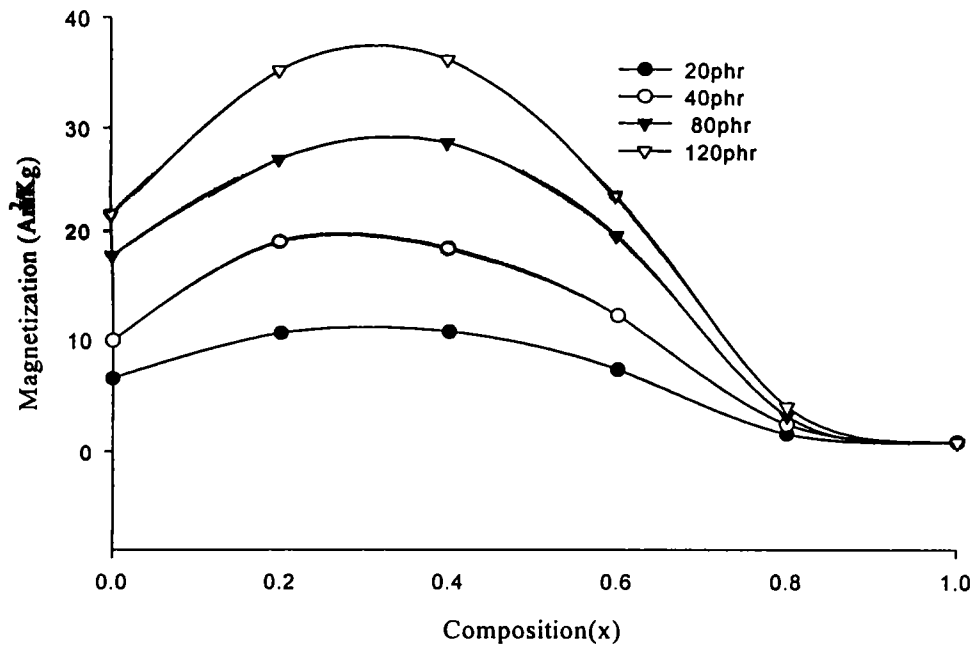


Figure.3.17. Variation of magnetization with composition for RFCs

3.6. Tailoring magnetic properties of RFCs

Synthesis of RFCs with predetermined properties are mandatory when RFCs for applications are required. A simple mixture equation of the general form

$$M_{rfc} = W_1 M_1 + W_2 M_2 \quad \dots\dots\dots(3.6.1)$$

can be applied to evaluate the saturation magnetisation of the composites, where W_1 is the weight fraction of the filler, M_1 is the magnetisation of the filler, W_2 is the weight fraction of the matrix M_2 is the magnetisation of the matrix. Since the matrix butyl rubber is nonmagnetic this equation can be reduced to the following form

$$M_{rfc} = W_1 M_1 \quad \dots\dots\dots(3.6.2)$$

The M_s of RFCs for different volume fractions have been calculated by employing equation 3.6.2 and they are compared with the observed values. The details are shown in Figure .3.18. From the graph it is clear that the measured and calculated values using equation 3.6.2. are in good agreement. This mixture equation requires the magnetisation corresponding to all x values of the filler in order to predetermine the saturation magnetisation (M_s) of the corresponding composites.

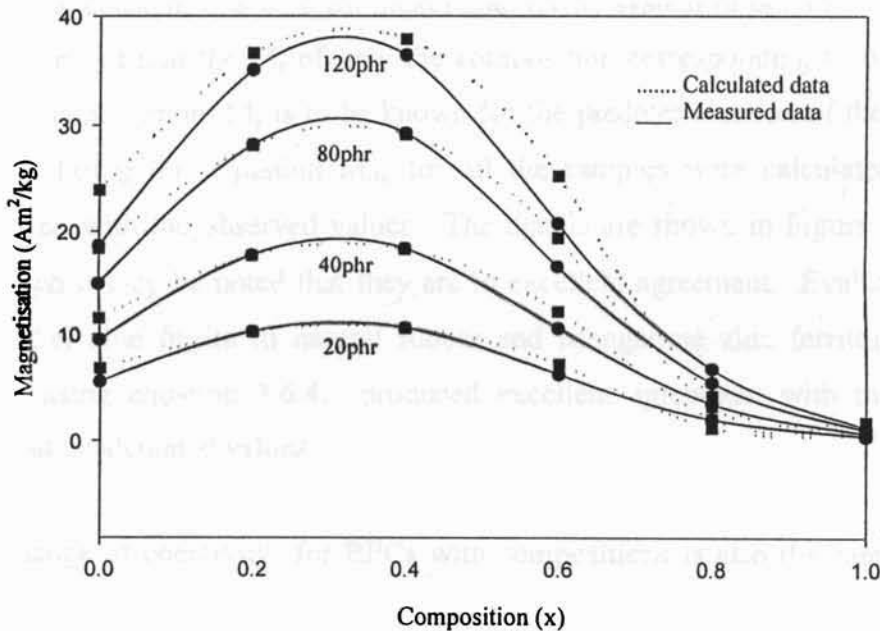


Figure 3.18 Magnetisation Vs composition for measured and calculated data

A close examination of the M_s versus composition for mixed ferrite system (nickel zinc ferrite series in this case) and the rubber ferrite composites containing mixed ferrites indicate that they follow a Gaussian profile. These were then fitted in to a general equation which was first formulated by fitting the experimental data of M_s for different x and for different loading. The equation is of the general form

$$M_s = A \cdot \text{Exp}\left[-0.5\left(\frac{x-x_0}{b}\right)^2\right] \dots\dots\dots(3.6.3)$$

Where A and b are constants. Appropriate meanings were assigned to the coefficients from the observations on the experimental values and a modified equation was formulated to relate the magnetisation (M_s) of RFCs to the magnetisation M_s of the ceramic fillers. The final fit after giving appropriate meanings to the coefficients and constants of equation 3.6.3 assume the following form

$$M_{rfc} = (1 + 0.2x) \cdot M_{cer. max.} \cdot W_2 \cdot \text{Exp}\left[-0.5\left(\frac{x-x_0}{b}\right)^2\right] \dots\dots\dots(3.6.4)$$

Here $M_{cer. max.}$ is the magnetisation corresponding to the maximum M_s of the ceramic filler, x_0 is the composition corresponding to the maximum M_s of the filler, x is the composition (0, 0.2, 0.4, 0.6, 0.8, 1) and W_2 is the weight fraction of the filler. The constant b is 0.26 for nickel zinc ferrite system in butyl rubber. Here it is to be noted that the M_s of only the composition corresponding to that x which shows the maximum M_s is to be known for the predetermination of the M_s of the RFCs. Using this equation M_{rfc} for all the samples were calculated and then compared with the observed values. The details are shown in Figure 3.19. From the graph it may be noted that they are in excellent agreement. Evaluation of M_s for nickel zinc ferrite in natural rubber and Manganese zinc ferrites in natural rubber using equation 3.6.4. produced excellent agreement with the observed values and calculated values.

The change of coercivity for RFCs with compositions is also the same as in the case of ceramic samples. That is, the coercivity first decreases with increase of composition and reaches a minimum at $x=0.6$ and thereafter it increases with increase of composition. The evaluation of coercivity for composites containing nickel zinc ferrites shows that the H_c of the rubber ferrite composites equals the H_c

of the respective ceramic component. The variation of coercivity with composition for different loading is shown in Figure.3.20.

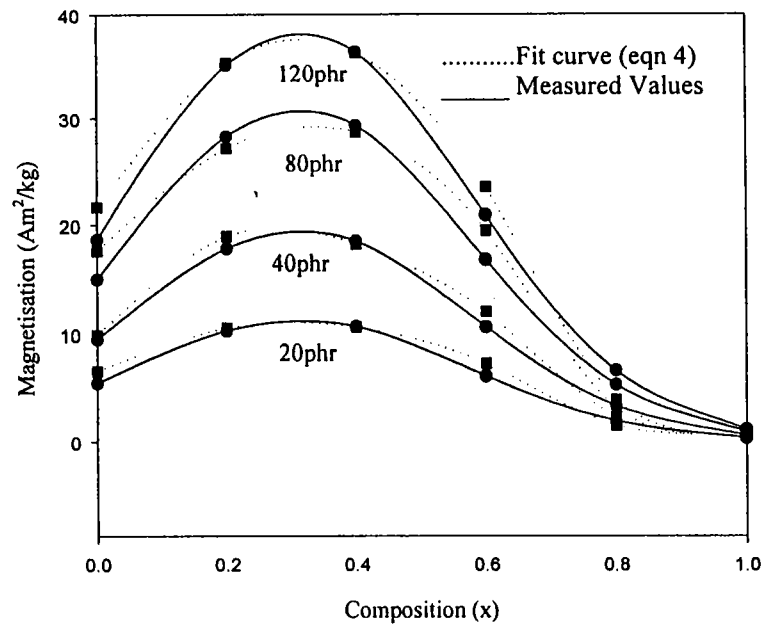


Figure 3.19 Magnetisation Vs composition for measured and calculated data(eqn. 4)

This means that rubber ferrite composites can be tailor made with appropriate M_s and H_c by a judicious choice of the filler belonging to a particular series. The weight fraction can be increased to acquire the required M_s . Precaution should be taken so as not to load beyond the percolation threshold. The employment of RFCs thus enables to mould complex shapes with appropriate magnetisation without compromising on the coercivity. This simple relation of the form of equation 3.6.4 can be conveniently utilized to predict the magnetic properties of RFCs.

From the results available on RFC's loaded with Nickel zinc ferrite, it is evident that the magnetic property of RFC's can be tailored to suit different applications. That is, the required M_s can be attained by estimating the corresponding loading of fillers in RFC's whereas the required H_c can be fixed as per the composition namely 'x' in the ceramic samples. However it must be mentioned that the H_c is greatly influenced by the preparation technique, the firing temperature and the

particle size. Addition of reinforcing fillers to increase the mechanical strength of the RFC's is another added advantage for choosing these RFC's for applications.

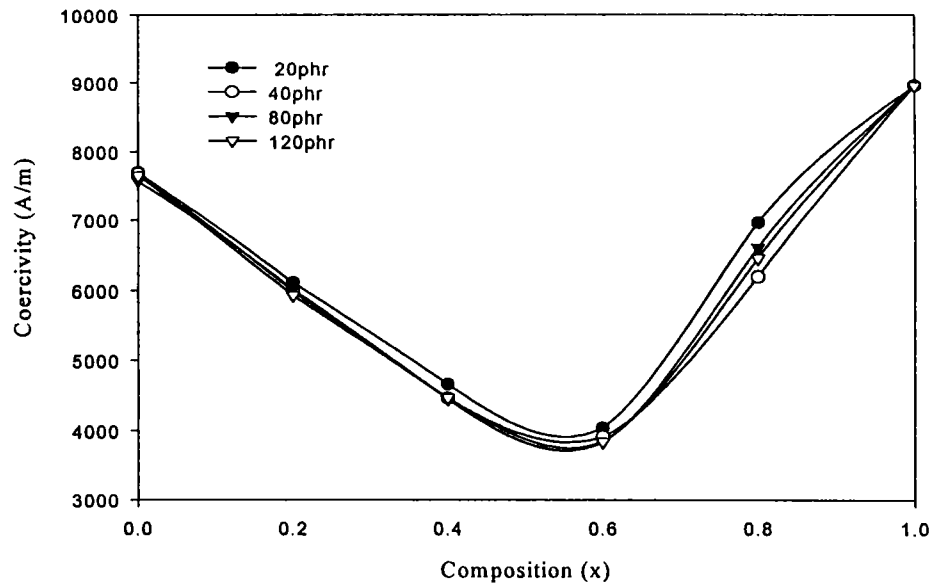


Figure 3.20. Variation of coercivity with composition for RFCs

3.7. Low temperature VSM result of X = 0.2, 120phr

Low temperature magnetisation studies of a representative rubber ferrite composite was carried out. The temperature of the measurements were varied from 80K to room temperature. It was found that the magnetisation increases with decrease of temperature. Coercivity also increases. Details of these results are shown in table 3.8. It can be seen that a magnetisation value of $10 \text{ Am}^2/\text{Kg}$ is increased as the temperature is lowered to 78K. This magnetisation value is very near to the magnetisation value obtained for its ceramic component with $x = 0.2$ concentration of zinc. The variation is represented graphically and is shown in Figure.3.21. The temperature dependence of magnetisation in spinels is also due to the difference in sub lattice magnetisations since each sublattice has its own temperature dependence. This temperature effect also can produce the canted structure but it is to be noted that there is only one transition temperature from an ordered to the paramagnetic phase [77].

Temperature in K	Magnetisation (M_s) Am^2/Kg	Retentivity (M_r) Am^2/Kg	Coercivity (H_c) A/m
78	45.88	5.162	7327
150	44.59	4.522	6539
200	42.81	4.031	5899
240	40.87	3.468	5169
280	38.77	3.378	5100
293	37.80	3.295	4929

Table 3.8. Low temperature VSM results on X = 0.2, 120phr

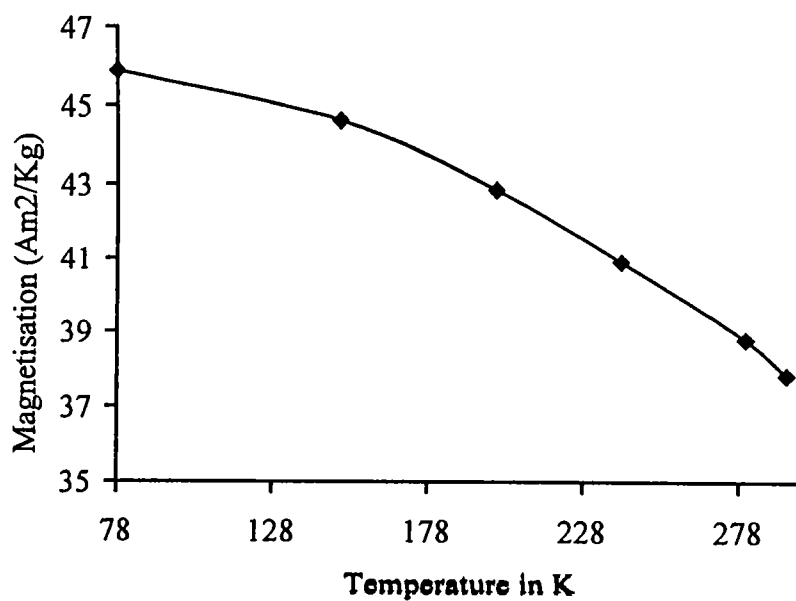


Figure.3.21. Variation of magnetisation with temperature for X =0.2, 120phr

3.8 Conclusion

Polycrystalline nickel zinc ferrite samples were synthesized and characterised by XRD and vibrating sample magnetometry. The X-ray diffraction studies show that these polycrystalline have crystallized in the spinel phase without any detectable impurity phases. These compounds exhibit an increase in lattice parameter with increase in Zn content. The magnetic measurements indicate that the saturation magnetisation increases with increase in x , reaches a maximum at $x = 0.4$, and then decreases. Coercivity decreases with x attains a minimum at $x = 0.6$ and then increases with x . Nickel zinc ferrites were then incorporated in a butyl rubber matrix to produce rubber ferrite composites (RFCs). Before making thin sheets, the processability of these polymers was studied by evaluating the cure characteristics. The results show that the processability is not affected by loading. It was also found that the cure characteristics, particularly the minimum and maximum torque do not vary with increase of composition.

Magnetisation measurements on RFCs suggests that their saturation magnetisation can be modified by a judicious selection of composition, that is x and its loadings. Based on the present study it can be concluded that the magnetic field strength remains as that of the original magnetic component in the matrix. Fundamentally these results indicate that there is no possible interaction between the between the matrix and the filler because , if there were an interaction it would have affected the nature of the domain and hence would have disturbed the coercivity.

A general equation of the form $M_{rfc} = (1 + 0.2x) \cdot M_{cer. max} \cdot W_2 \cdot \exp[-0.5(\frac{x - x_0}{b})^2]$

was also formulated to predict the saturation magnetisation of RFCs. It is to be noted that the calculation requires only the maximum magnetisation value corresponding to the composition x_0 . Calculations and comparisons have shown that this fits well for the present system as well as for other systems and it is to be assumed that a general equation of the above form can be employed to predetermine the saturation magnetisation of RFCs containing any mixed ferrites series.

On the magnetic properties of Ultra fine zinc ferrites

4.1 Introduction

Investigations carried out in evaluating the magnetic properties of $\text{Ni}_{1-x}\text{Zn}_x\text{Fe}_2\text{O}_4$ samples for various compositions have revealed that for the composition corresponding to $x = 1$, that is ZnFe_2O_4 , the magnetisation values obtained are not in conformity with that of the reported literature [78]. These results were difficult to explain by applying conventional understanding of magnetism of micron-sized particles. Hence a detailed study was undertaken to explain the anomalous behaviour exhibited by zinc ferrite samples. The details are discussed in this chapter.

Spinel ferrites are commercially important materials because of their excellent electrical and magnetic properties [79]. These class of materials have been the subject of extensive studies by physicists and chemists alike. A whole range of distribution of cations is possible in spinels which can be represented generally by the formula $(\text{Me}^{\text{II}})_\delta(\text{Fe}^{\text{III}})_{1-\delta}[(\text{Me}^{\text{II}})_{1-\delta}(\text{Fe}^{\text{III}})_{1+\delta}]\text{O}_4$ where the ions inside the square brackets are said to be occupying octahedral sites (B) and the ions outside the bracket occupy the tetrahedral sites (A) [80]. In the above formula when $\delta = 1$, then it is called a normal spinel. When $\delta = 0$ it is called an inverse spinel. When $\delta = 1/3$ it is called a random spinel. The structure can be described as a close packed assemblage of oxygen atoms with metal atoms occupying positions in some of the interstices. The metal position are of two types, those in which the oxygen atoms are tetrahedrally coordinated to the metal atoms, and those in which the surrounding oxygen atoms have octahedral symmetry of the twenty four positions available to the metal atoms in the unit cell, eight are of the tetrahedral type and sixteen belong to the octahedral category. From the fundamental point of view,

these materials serve as ideal candidates for studying ferrimagnetism and ferrimagnetic properties.

The crystal structure of ferrites has been the subject of several investigations in the past [81]. Ferrites are technologically important because of their interesting magnetic properties, which is explained by Neel [82]. The saturation moment according to the theory of Neel is related in a simple and elegant manner to the distribution of magnetic ions among the available lattice sites. According to the Neel model of ferrimagnetism, the exchange integrals between an arbitrary pair of metal ions is such as to produce an antiparallel alignment of the two. The A-B coupling however is taken to be considerably stronger than that between ions located on the same type of crystallographic site. Thus the spin of ions in the octahedral positions are antiparallel to those of the tetrahedral ions. In an inverted spinel the saturation moment is then determined solely by the atomic moment of the divalent cation.

Zinc ferrite belongs to the category of normal spinels [78]. The structural and magnetic properties of zinc ferrites have been the subject of study by various researchers over the last two decades [83-98]. It has been established that structurally $Zn Fe_2 O_4$ is a normal spinel where it can be written as $(Zn^{2+})_A ((Fe^{3+})_2)_B O_4$ and its net magnetisation is zero. Investigations on zinc ferrite indicated that zinc ferrite is antiferromagnetic because of B-B interactions with a Neel temperature of about 10K. Above Neel temperature, it behaves as a paramagnet [99]. There have been reports indicating anomalies in the magnetic properties of zinc ferrites saying that zinc ferrite samples are not completely the normal spinel [100-102]. The Occupancy of Fe^{3+} ions at the A site is larger in smaller crystallite samples and the cation substitution increases with decreasing particle size. This is explained on the basis that a Fe^{3+} ion located at the A-site forms a cluster with its twelve nearest Fe^{3+} neighbours at B-sites through coupling by the A-B interaction, which is much stronger than the B-B interaction. The number of these clusters would increase with decreasing particle size because cation substitution is more pronounced in smaller particles. Thus the magnetisation increases with decreasing particle size. This A-B interaction is short range in

nature. For instance, Lotgering et.al.[100] detected anomalous behaviour in the paramagnetic susceptibility in the zinc ferrite. Brock-house and others [103] found the presence of short-range order of parallel spins separated by 0.29nm in their neutron diffraction studies at 89K.

Investigations on the structural and magnetic properties on zinc ferrite samples prepared by two techniques were under taken. Zinc ferrite samples were prepared by two different routes and have been analyzed by using Low Energy Ion Scattering, Mössbauer Spectroscopy and vibrating sample magnetometry. Low Energy Ion Scattering (LEIS) was used to find out the surface composition of the samples prepared by these two different techniques. Mössbauer spectroscopy was employed as an analytical tool to discern more information on the nature of ordering on these samples.

4.2. Preparation of zinc ferrite at Low temperature

Zinc Ferrite was prepared by low temperature preparative techniques as described by T.Sato et.al.[104] 0.1 m aqueous solution of zinc nitrate and 0.2m aqueous solution of ferric nitrate were prepared separately. 100 ml. of each solution was mixed together, while stirring this mixture, 25% ammonia was added until the pH was between 9 - 11 at 320K. The precipitate was dried at 373K and calcined in air at 773K which yielded zinc ferrite.

4.3. Preparation of Zinc ferrite at high temperature

Zinc ferrite was also prepared by conventional ceramic technique [105]. Appropriate amounts of Zinc oxide were mixed with freshly prepared alpha iron oxide, which in turn was prepared by using oxalate precursors. All the reagents used were AR grade. They were pre-fired at 773K. The pre sintering was repeated twice for ensuring homogeneity. They were finally sintered at around 1223 K for several hours. They were then allowed to cool naturally under ambient conditions.

4.4. Structural evaluation of $ZnFe_2O_4$

The crystal structure of $ZnFe_2O_4$ prepared by two different routes was determined by using X-Ray powder Diffraction techniques. The powder diffractograms were

recorded on a PW1140 model x-ray diffractometer using Cu K α radiation ($\lambda = 1.5418 \text{ \AA}$). The structural parameters thus obtained are shown in Table 4.1 and Table 4.2. The 'd' values (inter atomic spacing) were compared with the standard values reported in literature and found to be in good conformity. The lattice parameter was calculated and is found to be 8.451 \AA .

d[\AA]	Intensity (I/ I $_0$ ×100)	hkl
4.8478	17.1	111
2.9785	74.3	220
2.5391	100.0	311
2.4327	14.3	222
2.1081	40.00	400
1.7187	17.1	422
1.6234	57.10	511
1.4881	80.00	440
1.3357	8.6	620
1.2869	11.4	533

Table: 4.1. X-ray diffraction data for Zinc ferrite prepared by low temperature technique

d[\AA]	Intensity(I/I $_0$ ×100)	hkl
4.8663	6.4	111
2.9824	36.4	220
2.5453	100.0	311
2.4359	7.1	222
2.1104	17.10	400
1.7232	12.1	422
1.6248	34.7	511
1.4929	42.1	440

Table: 4.2. X-ray diffraction data of the Zinc ferrite prepared by ceramic technique

4.5. Magnetic measurements

Room temperature magnetic measurements were carried out by using a VSM (model 4500) and parameters like saturation magnetisation (M_s), coercive force (H_c) and remanence (M_r/M_s) were evaluated.

4.6. BET surface area

BET surface area of the samples were obtained on a micrometric ASAP 2400 adsorption system and subsequently the surface area of the samples were evaluated. The details of measurements are described elsewhere [106].

4.7. Results and discussion

The surface area and surface composition of zinc ferrite sample prepared by two different routes are shown in table. 4.3. It shows that sample prepared by ceramic technique has a surface area of $0.92 \text{ m}^2/\text{gm}$ while the sample prepared by co-precipitation technique has a very large surface area of $29.6 \text{ m}^2/\text{gm}$.

Sample	Method of preparation	Surface composition			BET surface area (m^2/gm)
		from LEIS Experiments($10^3\%$).			
		O	Fe	Zn	
ZnFe_2O_4	Ceramic	4.8	26.5	1.7	0.92
ZnFe_2O_4	Co-precipitation	4.8	27.0	2.4	29.6

Table: 4.3. Results of LEIS Experiments and BET surface area

The XRD analysis of these two samples are shown in table 4.1 and table 4.2. The diffractogram is shown in Figure 4.1. The XRD pattern are indicative of the fact that the compounds are monophasic with no detectable impurities. The lattice parameter for these two compounds have been evaluated and found to be 0.843nm and 0.842nm for ceramic and co-precipitation techniques respectively. Magnetization measurements carried out on these samples showed a magnetization

of $3.12 \text{ Am}^2/\text{kg}$ and coercivity of 4976 A/m . Figure 4.2 shows the hysteresis loop obtained for the ZnFe_2O_4 from VSM measurements. This is an anomalous result in the sense that ZnFe_2O_4 crystallises in the normal spinel structure, where Zn^{2+} is found exclusively on the tetrahedral sites (A). Since Zinc ferrite exhibits a net magnetisation of $3.12 \text{ Am}^2/\text{kg}$ it is to be assumed that some amount of Zn is occupying B site. From LEIS measurements (cf table 4.3) it can be seen that some amount of Zn is detected at the surface. The amount of Zn detected on the ceramic sample is less than that of the zinc ferrite sample prepared by co-precipitation method (cf table 4.3). It must be mentioned in this context that low concentration of Zn on the surface cannot be attributed to a low sensitivity of LEIS for Zn because this is not the case for pure Zn where no matrix effects are expected [107].

Usually, only low index planes are taken in to consideration when discussing the surface of spinels. Following the suggestion by Knozinger and Ratnasamy [108] and using their notation, one can distinguish 6 different low index surface planes, which are shown in Figure 4.3. In the figure the open spheres represents oxygen anions, the solid spheres are octahedrally coordinated cations and cross-hatched spheres are the tetrahedrally coordinated cations. From the figure, it follows that the A(111), C(110), E(100) and F(100) planes have both tetrahedral and octahedral sites on the surface while B(111) and D(110) only expose octahedral coordinated cations. Thus it is possible to construct a spinel surface where tetrahedral sites are not exposed. Ziolkowski and Barbaux [109] have predicted through semi-empirical calculations that in the case of spinels like Co_3O_4 it is the A(111) and D(110) planes which are energetically preferred on the surface, but these predictions do not form a final conclusion. Where as Shelef et.al [110] with the aid of LEIS concluded that tetrahedral sites are not on the surface. These findings were again supported by Beaufile and Barbaux by using differential neutron diffraction [111]. Jacob's et.al [112] and Anantharaman et.al [113] through independent experiments conducted on spinel aluminates and spinel ferrites respectively have established that it is the octahedral sites which are preferentially getting exposed on the surface of spinel compounds. They have predicted that D(110) or B(111) are the preferentially exposed planes on spinel ferrites surfaces which gives scope for selecting catalytically active cations in spinel type compounds.

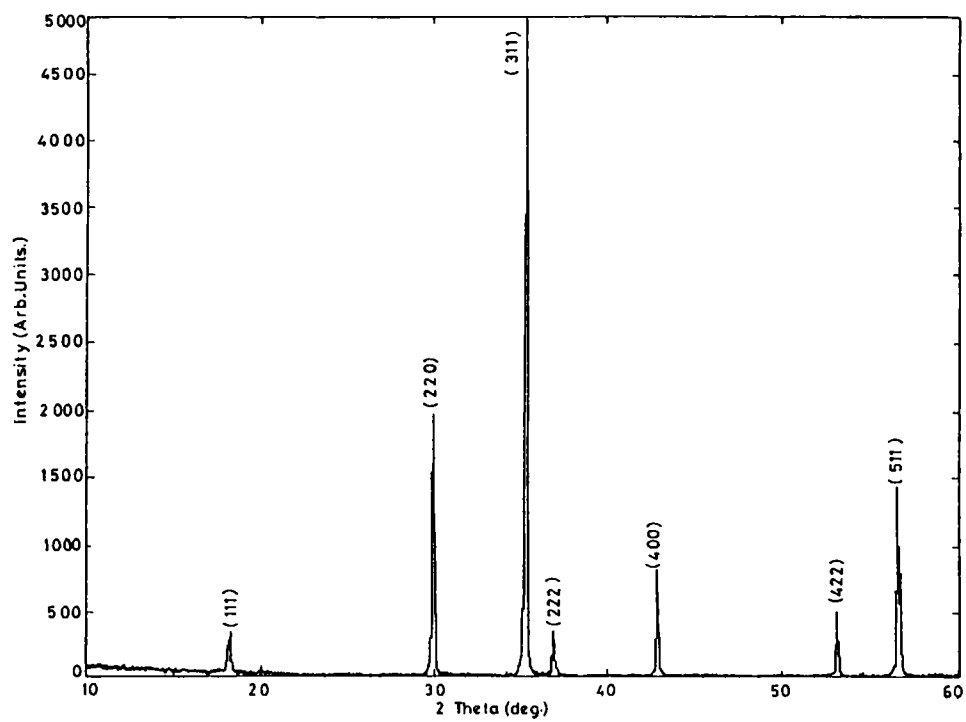


Figure. 4.1 XRD Spectrum of ZnFe_2O_4

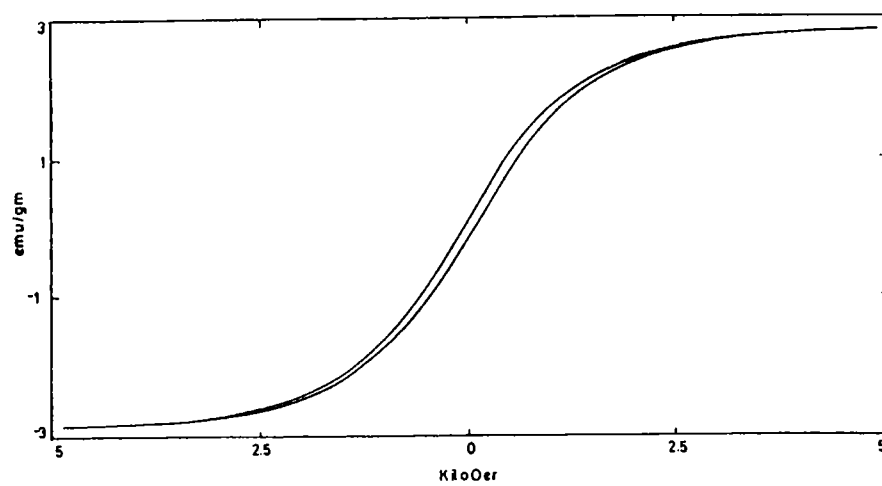


Figure 4.2. Hysteresis loop for ZnFe_2O_4

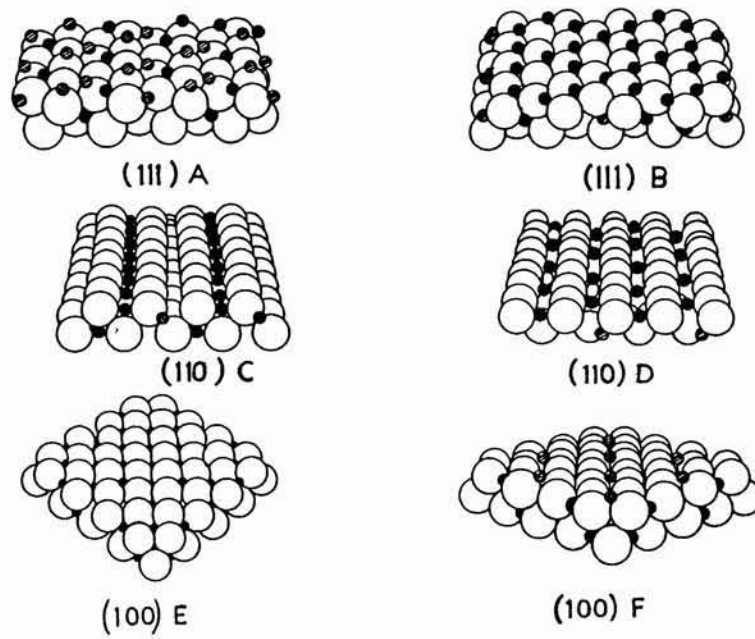


Figure 4.3. Various planes possible on a spinel ferrite surface

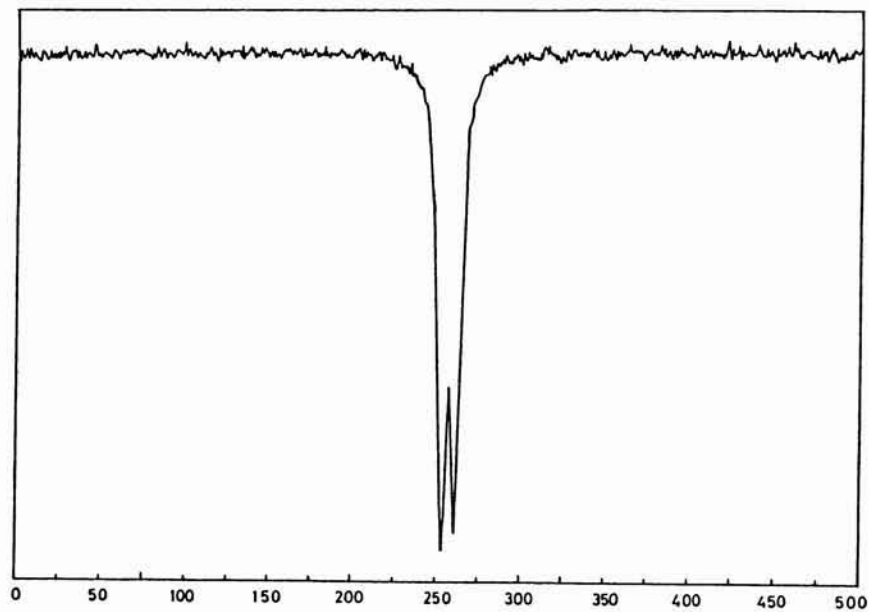


Figure 4.4. Fe^{57} Mössbauer spectrum of ZnFe_2O_4 at room temperature

LEIS results indicate that the amount of Zinc detected on the high surface area sample prepared by coprecipitation method is much more than that detected on the sample prepared by ceramic technique (table 4.3). It has been proven by various researchers that it is the octahedral sites which are preferentially exposed on the spinel surfaces. Thus the detection of Zn on the surface of Zinc ferrite leads to the conclusion that some amount of Zn is occupying the Octahedral sites, and the amount of Zinc occupation is dependent on particle size. The finer the particles, the more is the zinc on the B site. This observation using LEIS receives further evidence in the magnetic measurements conducted by Kamiyame et al.[102]. Kamiyame et al in their experiments have found that finer the particle, the more is the saturation magnetisation. They assumed a cation distribution of $Zn_{1-x}Fe_x[Zn_xFe_{2-x}]O_4$, where $x = 0.04$ or more.

The Mössbauer spectrum at room temperature is shown in figure 4.4. The spectrum was satisfactorily fitted with a single doublet having a quadrupole splitting of 0.37 mm/s and center shift of 0.33mm/s. Since the fitted line width was only 0.30mm/s the presence of another doublet is ruled out. The Fe^{57} Mössbauer spectrum of $ZnFe_2O_4$ recorded at 16K is shown in figure 4.5. The spectrum shows clearly that $ZnFe_2O_4$ is magnetically ordered at 16 K . The data was analysed by means of a procedure developed by Window [114]. In this method it is assumed that the observed line shapes arise from the probability distribution $P(H)$ of hyperfine fields. In figure.4.5 the dots represent the experimental data and the solid line is a result of the fitting of the data using the Window approach. The resultant probability distributions are shown in figure.4.6. The most probable field is found to be 63 kOe and the mean field of the distribution is 80 kOe. The magnetic ordering in $ZnFe_2O_4$ is possible only if there is an inversion that is, some of the Zn^{2+} ions occupy the octahedral sites and some of the Fe^{3+} ions occupy the tetrahedral sites which give rise to a strong coupling between Fe^{3+} ions at A- and B- sites due to the A-B interaction. This experimental observations receives further support from the studies conducted on ultrafine zinc ferrite particles by Sato et al. [104]. In their experiments, they found that the saturation magnetization of ultra fine zinc ferrite particles increases with a decrease in particle size at room temperature. They observed the same trend at low temperature also.

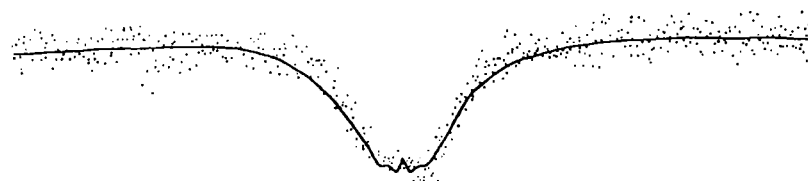


Figure 4.5 Mössbauer spectrum of ultrafine zinc ferrite at 16K

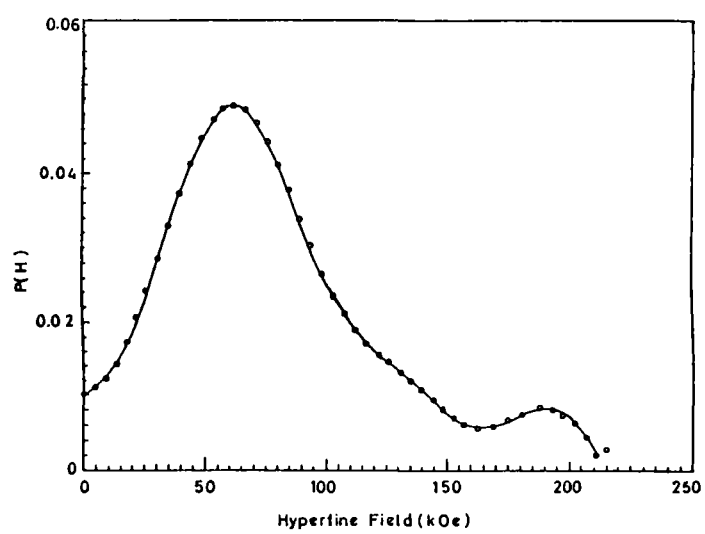


Figure 4.6 Hyperfine field distribution in ultrafine ZnFe₂O₄ at 16 K

Further more , EXAFS studies conducted on zinc ferrites by Jayadevan et al. [115] also support the presence of Zn^{2+} on the B site. Thus it is reasonable to conclude that the Fe^{3+} situated on A sites , according to cation distribution $Zn_{1-x}Fe_x [Zn_x Fe_{2-x}]O_4$ forms a cluster with its 12 nearest Fe^{3+} neighbours at B sites through coupling . Probably the number of clusters increases with decreasing particle size. So anomalous magnetisation may be due to the short range ordering of the samples as reported by Schiessel et al [116] and Kamiyame et al [102]. However it must be mentioned that the surface spins may also contribute to the observed magnetization as they are expected to be considerably high in number due to small size of particles.

4.8. Conclusion

$ZnFe_2O_4$ samples prepared by both low temperature and ceramic method were found to be single phasic in nature from XRD analysis. Magnetisation measurements carried out on these samples shows a magnetisation value contrary to the classical case of normal spinel ferrites, according to which the zinc ferrite is purported to be exhibiting a zero net magnetisation. A detailed analysis of these samples were carried out by using low energy ion scattering, BET surface area measurements and Mössbauer spectroscopy. Initial analysis on the results of zinc ferrite samples using LEIS , BET surface area and Mössbauer spectroscopy suggest that zinc occupies the B-site contrary to the earlier belief that it occupies only A-site. The amount of zinc detected on the surface of high surface area zinc ferrite is higher than that of the low surface area zinc ferrite prepared by ceramic technique. This establishes that zinc substitution increases with decreasing particle size. Mössbauer results shows that the A-B interactions are not long range but only short range.

Dielectric properties of RFCs containing mixed ferrites

5.1. Introduction

Ferrite materials have attracted attention due to their good magneto-dielectric properties at high frequencies. Studying the properties of dielectrics and the dependence of these properties on the composition and various external factors like temperature, humidity, mechanical action and the frequency of the applied field have developed into an extremely important field of science. The study of dielectric properties in relation to their chemical composition and structure will lay the basis for obtaining new materials with pre-determined properties. The evaluation of structural, magnetic and dielectric properties of both the ceramic component and rubber ferrite composites (RFC) are also important, since the interrelationship of the properties of the filler and the matrix will help in the design of devices for applications. The frequency dispersion characteristics of the polymer ferrite composites are important because of their application as electromagnetic wave absorbers and EMI shielding materials [117-118]. The modification of the dielectric properties of the lossy dielectric materials by the addition of magnetic fillers is of interest to various researchers in understanding the fundamental aspects governing the properties of these materials.

Many theories and semi empirical relationships exist, which explain the role of different fillers in various matrixes. Further more, from the dielectric and magnetic measurements it is possible to gather valuable information regarding the matrix-filler interaction, dispersion of filler and percolation threshold, which are important and they play a significant role in determining the gross physical properties of the composites. Elaborate studies have been conducted to evaluate the dielectric properties of ceramic NiZnMg ferrites, LiTi-Co ferrites, Cu-Cr ferrites, Mg-Zn ferrites, NiZn ferrites [119-123]. It is also known that in polycrystalline

materials the dielectric properties are generally dictated by a combination of various factors like method of preparation, cation distribution, grain size, the ratio of $\text{Fe}^{3+}/\text{Fe}^{2+}$ ions, ac conductivity and sintering temperature [124]. So the incorporation of pre-characterised ceramic powders into various matrixes assumes significance. The dependence of these parameters on the dielectric properties of ceramic fillers will also have a profound influence on the overall physical properties of the composites incorporated with the filler. Such a systematic study on the incorporation of pre-characterised powders into various matrixes is rarely found in the literature.

The evaluation of dielectric properties is important in understanding the physical properties of these composites. Pre-characterised Nickel Zinc ferrites ($\text{Ni}_{1-x}\text{Zn}_x\text{Fe}_2\text{O}_4$ where $0 \leq x \leq 1$ in steps of 0.2) prepared by ceramic techniques were incorporated into a butyl rubber matrix according to a specific recipe to yield RFC. The details are cited in chapter 2. The dielectric constant of ceramic $\text{Ni}_{1-x}\text{Zn}_x\text{Fe}_2\text{O}_4$ and the butyl rubber composites incorporated with $\text{Ni}_{1-x}\text{Zn}_x\text{Fe}_2\text{O}_4$ have been studied as a function of frequency, composition, loading and temperature. From the experimentally observed dielectric constant of the filler, the matrix (blank) and the composite, the validity of an appropriate mixture equation, which will govern the dielectric properties of RFC, is established. This is done by using the independently observed value of the respective dielectric constant of filler, matrix and the composite and is fitted theoretically as well as experimentally with the observed value of the dielectric constant of RFCs. The effect of temperature on the dielectric properties of the composite is also studied. These results are discussed in this chapter.

5.2. Dielectric properties of ceramic $\text{Ni}_{1-x}\text{Zn}_x\text{Fe}_2\text{O}_4$

The dielectric constant and dielectric loss of nickel zinc ferrite samples were determined using an experimental setup, described in chapter 2. Impedance Analyzer model: HP 4192 A was employed for the evaluation of the dielectric constant in the frequency range 10KHz to 13MHz. The samples were made in the form of pellets using a hydraulic press by exerting a pressure of 9 ton. These circular disc pellets having a diameter of 10mm was loaded into the dielectric cell. The lead and fringe capacitance was eliminated by a method

described by Ramasastry and Syamasundara Rao [125]. The capacitances at room temperature were measured in the frequency range 10KHz to 13 MHz. This was repeated at different temperatures of 333K, 363K, 393K, 423K, 448K and 473K. The dielectric constant was calculated using the formula

$$C = \epsilon_0 \epsilon_r A/d \dots\dots\dots(5.1)$$

Where A is area of sample piece used, d is the thickness of the sample, ϵ_r is the dielectric constant of the medium and ϵ_0 is the dielectric constant of air and C is the observed capacitance of the sample. Dielectric constant at different temperatures were also determined at different frequencies. Knowledge of dielectric properties at various frequencies and the data on the effect of temperature on various composition was considered a prerequisite since the same ceramic material were to be incorporated in the rubber matrix.

5.2.1. Frequency Dependence

Frequency dependence of the dielectric constant for all ceramic samples (x=0 to 1 in steps of 0.2) are shown in Figure.5.1.

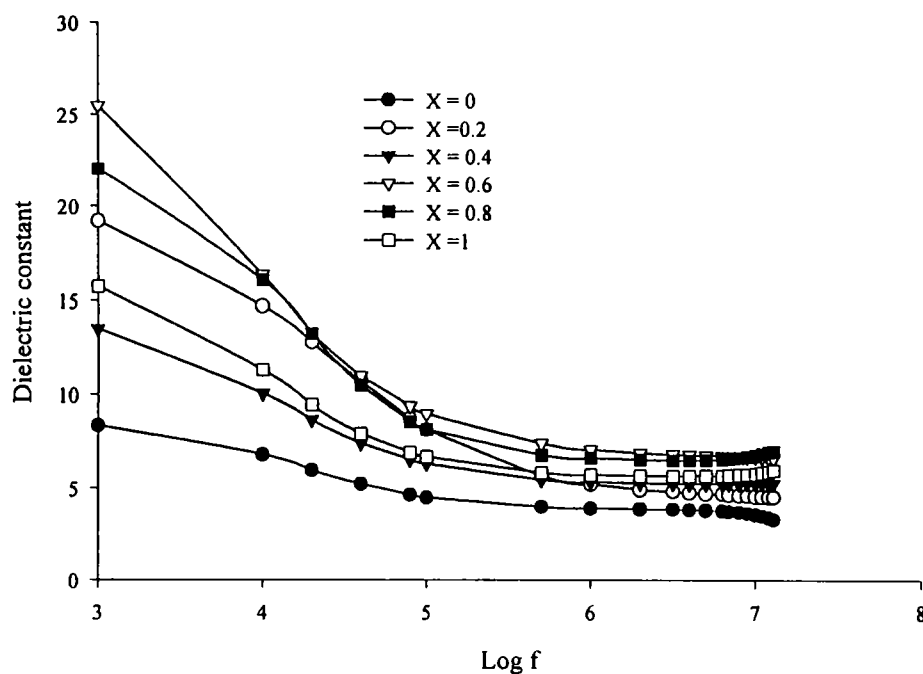


Figure.5.1. Frequency dependence of dielectric constant for $Ni_{1-x}Zn_xFe_2O_4$

A decrease in dielectric constant with increase of frequency was observed. This decrease is rapid at lower frequencies (up to 1MHz) and slower at higher frequencies. A maximum value of dielectric constant was observed at 10KHz and a minimum at around 13MHz. The variation pattern remains the same for all compositions. The dielectric properties of ceramic ferrite samples are influenced by various factors like method of preparation, chemical composition and grain size. When a ferrite is fired at higher temperature it is possible that films of high resistivity over the constituent grains are formed. Such materials in which the individual grains are separated either by air gaps or by low conducting layers behave as an inhomogeneous dielectric material.

The decrease in dielectric constant with increase in frequency can be explained using Koop's phenomenological theory of dispersion [126], which is based on Maxwell Wagner theory of interfacial polarization. In this model the dielectric structure is imagined to be consisting of well conducting grains which are separated by poorly conducting grain boundaries. A general relation of the following form explains the variation of dielectric constant with frequency.

$$\epsilon'' = \frac{\gamma - \gamma^1}{\epsilon^1 \cdot \omega} \dots\dots\dots(5.2)$$

where ϵ' and ϵ'' are the real and imaginary part of the dielectric constant, γ and γ^1 are the a.c and d.c conductivities respectively, and ω is the angular frequency which is equal to $2\pi f$. This dielectric dispersion at higher frequencies is due to the presence of oxygen rich low conducting surface layers on the grains of the ferrites.

5.2.2. Compositional dependence

In this set of experiments conducted for the evaluation of dielectric properties, it was observed that the dielectric constant varies with zinc concentration. The variation of dielectric constant with composition at different frequencies are shown in Figure.5.2. This shows that the dielectric constant initially increases with increase of composition and reaches a maximum at around $x = 0.6$. Thereafter the dielectric constant decreases with increase of zinc concentration. The variation pattern remains the same for all frequencies. Various researchers have tried to correlate dielectric polarization and Vervey type of conduction found in mixed ferrites [127]. In a mixed ferrite the conduction mechanism can be thought of as

electron hopping between $\text{Fe}^{2+} \rightleftharpoons \text{Fe}^{3+}$. It has been established that as porosity decreases resistivity also decreases.

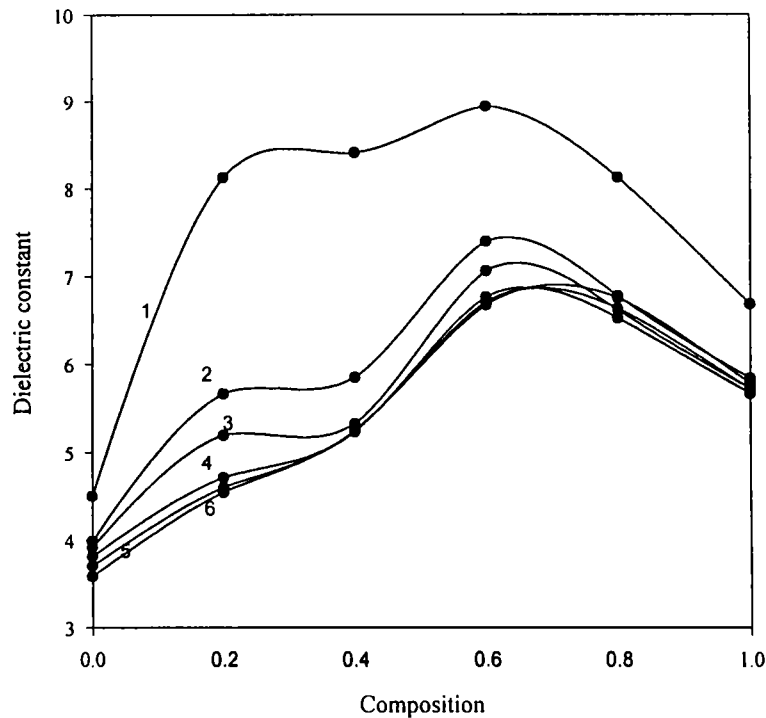


Figure.5.2. Variation of dielectric constant with composition for ceramic $\text{Ni}_{1-x}\text{Zn}_x\text{Fe}_2\text{O}_4$ (1-100KHz, 2-500KHz, 3-1MHz, 4-5MHz, 5-8MHz, 6-10MHz)

In $\text{Ni}_{1-x}\text{Zn}_x\text{Fe}_2\text{O}_4$ the hopping $\text{Fe}^{3+} \rightleftharpoons \text{Fe}^{2+}$ conversion is relatively less up to $x = 0.4$. This can reduce the dc conductivity and this decrease in dc conductivity will result in an increase of dielectric constant of the material. From porosity calculations it was observed that the variation of porosity is linear with particle size [128]. We find from our observations that from $x = 0.4$ to $x = 1$ the particle size as well as the porosity increases (cf Figure 5.3) this will reduce the ac conductivity which in turn decrease the dielectric constant of the material. Similarly at $x = 0.6$ it is known that zinc content is greater than nickel content and hence there is a chance of increase in evaporation rate of zinc at the sintering temperature. Most of the Fe^{2+} ions are formed during the evaporation of zinc. As evaporation rate increases, more $\text{Fe}^{3+} \rightarrow \text{Fe}^{2+}$ ion conversion takes place and hence the ratio $\text{Fe}^{3+}/\text{Fe}^{2+}$ decreases there by increasing dc conductivity. As a result of this, the dielectric constant decreases with increase of composition. This, in conformity with the observations made by various researchers [129-132].

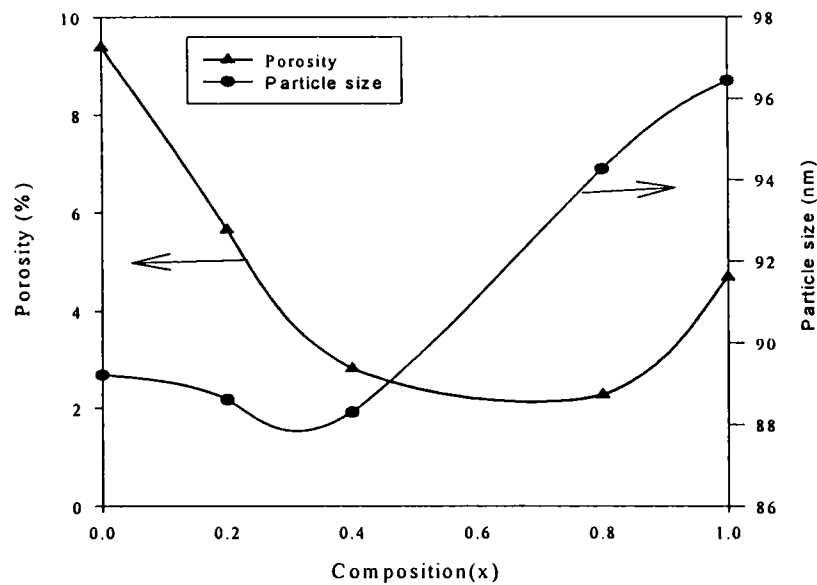


Figure 5.3. Variation of Porosity & Particle size with composition

5.2.3. Temperature dependence

The effect of temperature on the dielectric properties of ceramic nickel zinc ferrites were carried out up to a maximum temperature of 473K. The behaviour of dielectric constant with temperature for different composition at different frequencies are shown in Figure.5.4. It was observed that the dielectric constant of ceramic samples increases with increase of temperature. In dielectrics, ionic polarization increase the dielectric constant with increase in temperature [133]. The atoms or molecules in the samples cannot in most cases orient themselves at low temperature region. When temperature rises the orientation of dipoles is facilitated and this increases dielectric constant. But at very high temperatures the chaotic thermal oscillations of molecules are intensified and the degree of orderliness of their orientation is diminished thus the permittivity passes through a maximum value. It was observed that the variation of dielectric constant with temperature at low frequencies (100KHz) is much more pronounced than at higher frequencies. Variation pattern at lower frequencies seems to be obeying the relation

$$y = y_0 + A \exp(BT) \dots\dots\dots(5.3)$$

For all compositions the same behaviour is observed. At higher frequencies the effect of temperature on dielectric constant is very minimal.

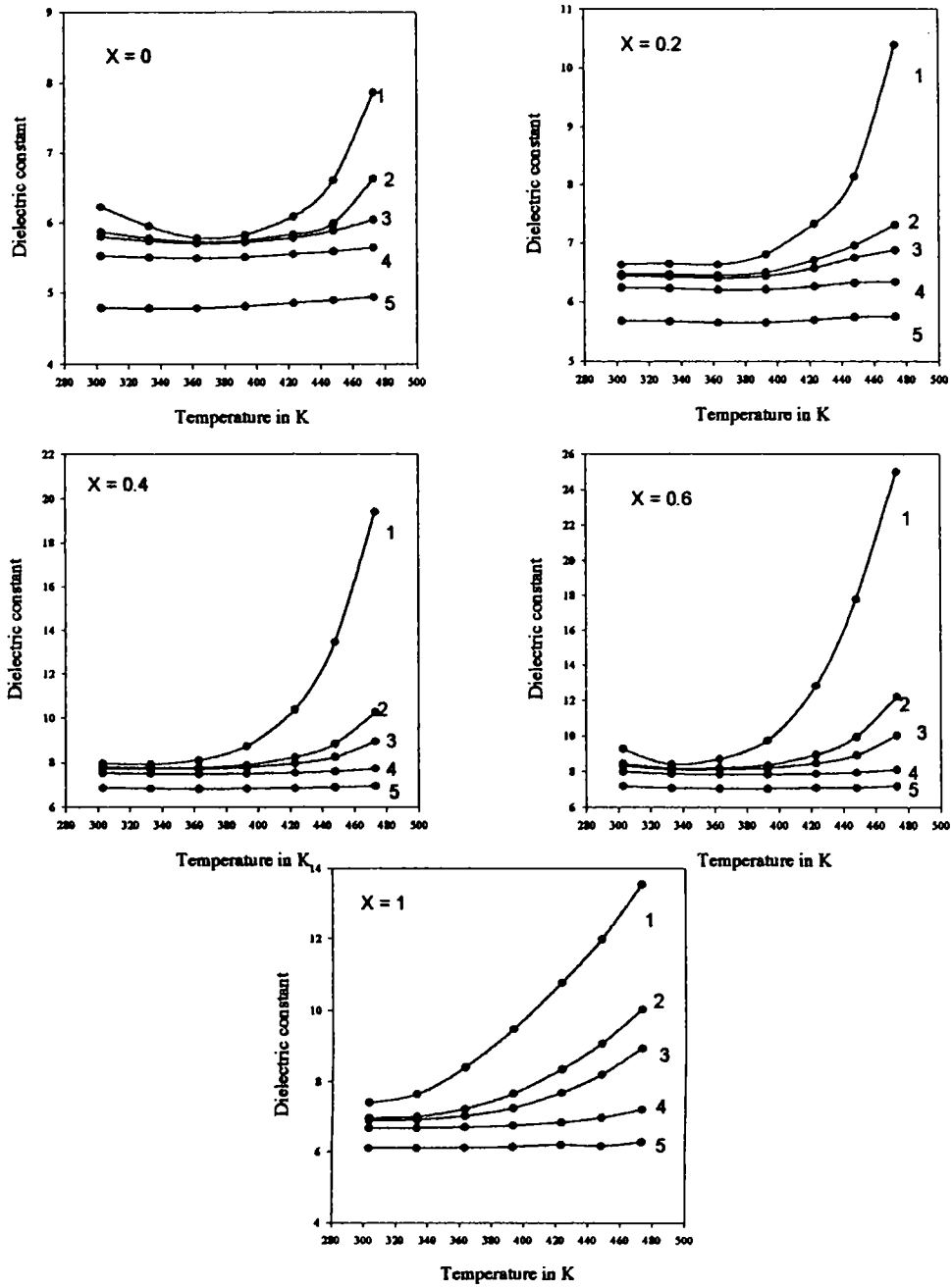


Figure.5.4.Variation of dielectric constant with temperature for ceramic $\text{Ni}_{1-x}\text{Zn}_x\text{Fe}_2\text{O}_4$ (1-100KHz, 2-500KHz, 3-1MHz, 4-5MHz, 5-10MHz)

5.3. Dielectric Properties of blank butyl rubber

The dielectric properties of blank butyl rubber was also evaluated. A dielectric constant of 1.9 was observed blank butyl rubber at low frequencies and it decreases slightly as frequency increases. The temperature dependence of dielectric constant for these butyl rubber matrix was also done. It shows a decrease in dielectric constant with increase in temperature. The variation pattern is shown in Figure 5.5. This is because, as temperature increases the polymer density decreases [134]. The reduction in polymer density will cause a decrease in dielectric constant. In non-polar dielectrics, like butyl rubber, due to thermal expansion of matter the ratio of number of molecules to the effective length of the dielectric diminishes with increase of temperature by this reason dielectric constant also diminishes.

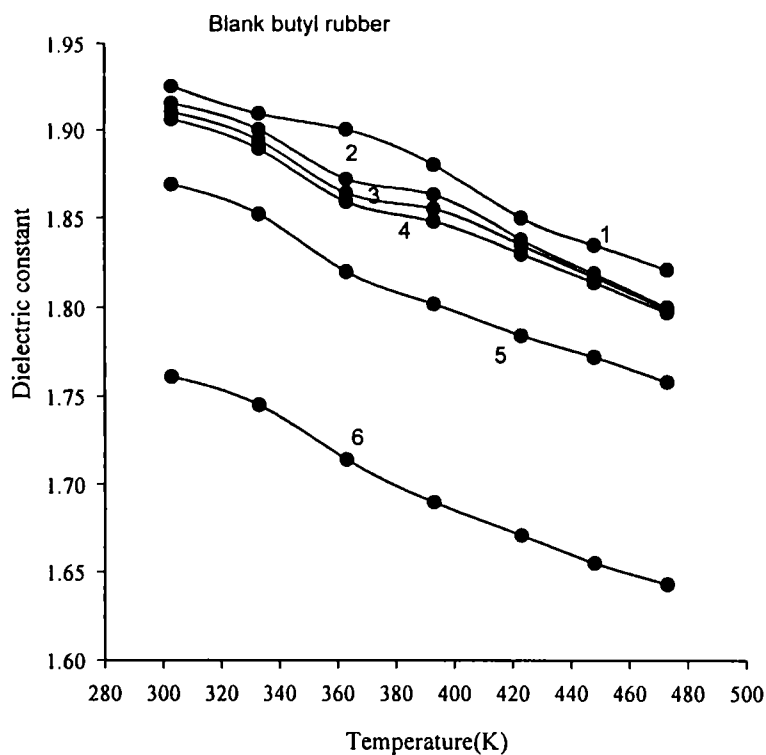


Figure.5.5.Variation of dielectric constant with temperature for Blank butyl rubber (1-100KHz,2-500KHz,3-1Mhz,4-5MHz,5-8MHz,6-10MHz)

5.4. Dielectric studies on rubber ferrite composites

The dielectric properties of RFCs were also carried out at different frequencies and at different temperatures. The dependence of dielectric constant on various factors like frequency, composition, loading and temperature are discussed in the following paragraphs. From the experimentally observed dielectric constant of the filler, matrix (blank) and the composite, the validity of an appropriate mixture equation, which will govern the dielectric properties of the RFCs, will be established. This will be done using the independently observed value of the respective dielectric constant of the filler, matrix and the composites and will be fitted theoretically as well as experimentally with the observed value of the dielectric constants of the RFCs.

5.4.1. Frequency dependence

Like ceramic nickel zinc ferrite rubber ferrite composites also shows a decrease in dielectric constant with increase of frequency. The variation pattern for representative samples is shown in Figure.5.6. However, here in the case of rubber ferrite composites the variation is not so rapid as in the case of ceramic samples at lower frequencies. The value of dielectric constant is small as compared to that of the corresponding ceramic nickel zinc samples in the composites, but it is larger than that of blank butyl rubber. For blank butyl rubber a maximum value of 1.9 was observed at low frequencies. This shows that the dielectric property of the matrix was improved by the addition of the magnetic filler. Maxwell Wagner interfacial polarization is applicable in the case of RFCs for the dependence of dielectric constant with frequency. A maximum value of dielectric constant was obtained for samples with maximum loading of 120phr.

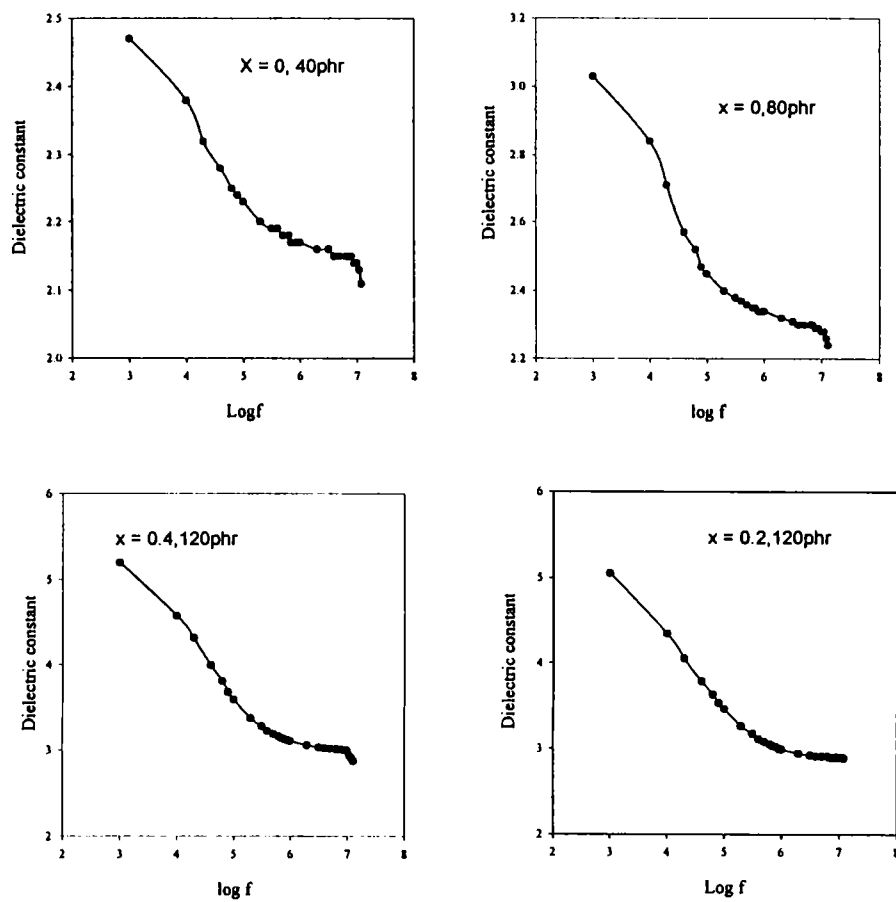


Figure.5.6.Representative graphs showing the variation of dielectric constant with frequency for RFCs

5.4.2 Compositional dependence

The variation pattern of dielectric constant with composition (zinc content) for rubber ferrite samples is shown in Figure 5.7. It was observed that the variation is same as that of the ceramic samples, the pattern remains the same for all loadings. Here it may be noted that for each composition a maximum of 4 samples were evaluated (20phr, 40phr, 80phr, 120phr).

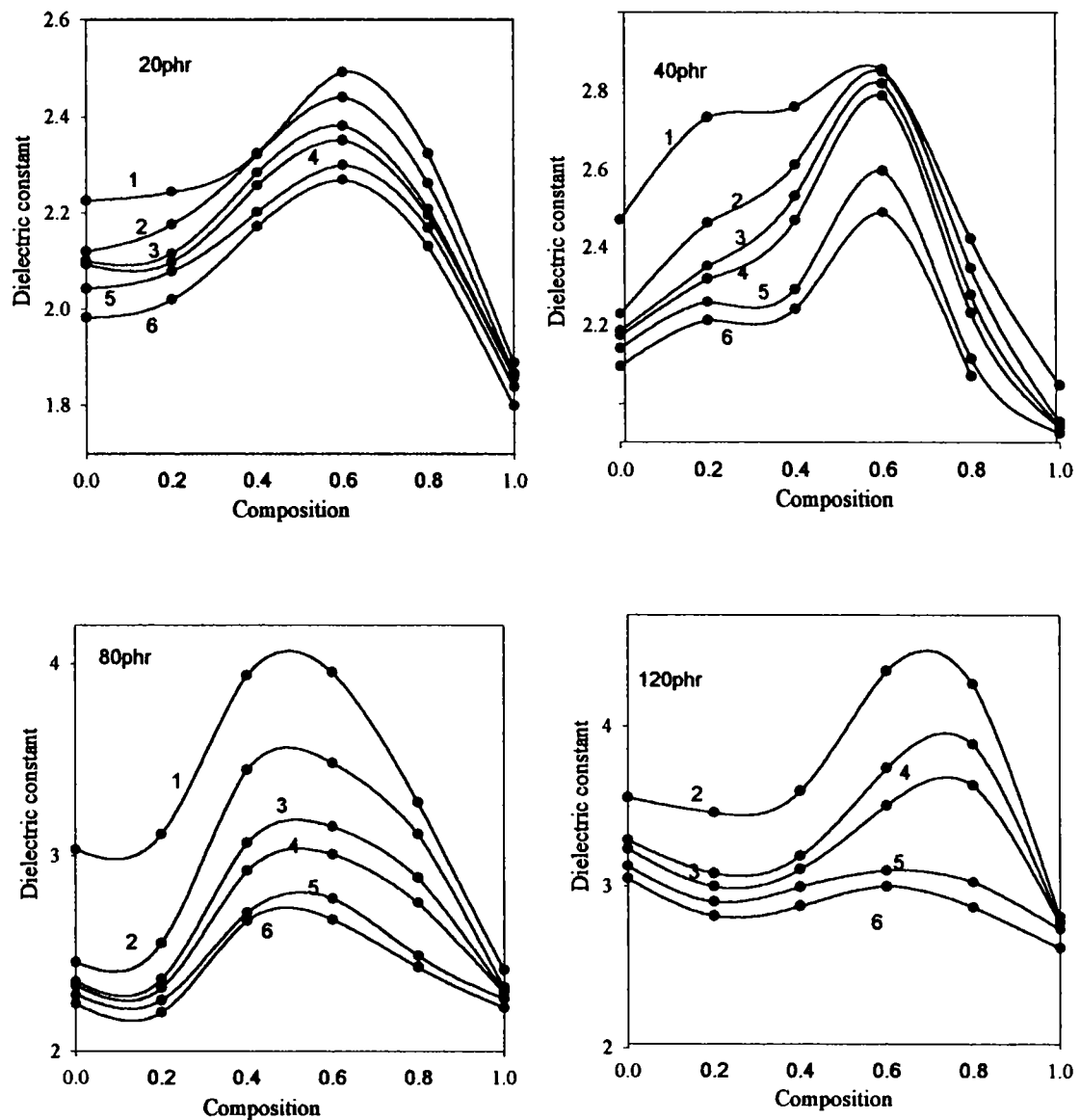


Figure.5.7.Variation of dielectric constant with composition for RFCs (1-100KHz,2-500KHz,3-1MHz,4-5MHz,5-8MHz,6-10MHz)

In rubber ferrite composites also a maximum value of dielectric constant was observed at around $x = 0.6$. The variation pattern is by and large the same for all loadings of the filler. These results suggest that the dielectric properties of the rubber matrix can be suitably modified by an appropriate choice of the composition and with the required loading of the filler.

5.4.3. Loading dependence

Studies on the variation of dielectric constant with the addition of magnetic filler (loading) were also carried out. It was observed that for all compositions the dielectric constant increases with increase of volume fraction of the ferrite material. A maximum value of dielectric constant was observed for a loading of 120phr. The variation is same for all composition(x) at different frequencies. The details of the dependence of dielectric constant on loading are shown in Figure 5.8.

Composite dielectrics can be treated as chaotic or as static mixtures of several components. Researchers [135-136] have suggested many formulae and semi empirical relationships for the evaluation of permitivity of the composites. This is based on various theoretical presumptions.

For example, for a mixture of m components, the dielectric constant ϵ^* is connected by a relation,

$$\text{Log } \epsilon^* = \sum_{i=1}^m Y_i \log \epsilon_i \dots\dots\dots(5.4)$$

Where ϵ^* is the dielectric constant of the mixture and y is the volume fraction of the component. For a two component system the relationship can be written as

$$\log \epsilon^* = y_1 \log \epsilon_1 + y_2 \log \epsilon_2 \dots\dots\dots(5.5)$$

where ϵ^* is the dielectric constant of the composite, ϵ_1, y_1 and ϵ_2, y_2 are the dielectric constant and volume fractions of the matrix and the filler component respectively.

Another mixture equation, which is used to calculate the dielectric constant of the mixture, is given by

$$\epsilon^* = \frac{\epsilon_1}{(1 - y)^3} \dots\dots\dots(5.6)$$

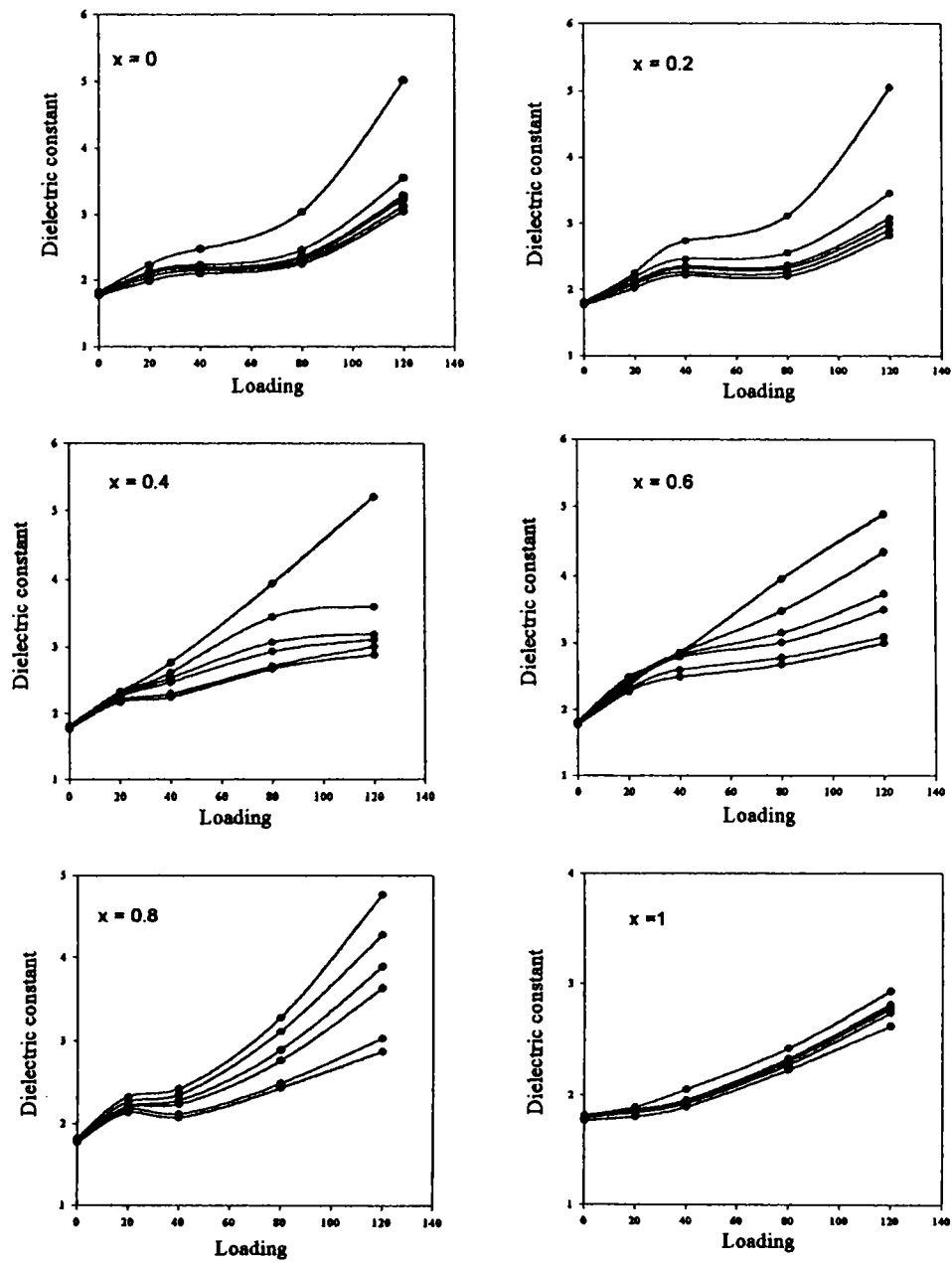


Figure.5.8.Variation of dielectric constant with loading for different compositions(x)

Here ϵ_1 is the permittivity of the matrix and y the volume fraction of the inclusion or filler. Employing equation.5.6 the dielectric constant of the composites were calculated using the experimentally measured permittivity of the matrix. It was found that the calculated value of ϵ^* and experimentally observed ϵ^* do not tally each other. These formulae have their own limitations. Equation 5.6 seems to be satisfying a composite containing conducting fillers and can not be applied to a composite containing an insulating filler. For a two component system consisting of a non-polar matrix and insulating filler of the ferrite type the relationship can be written with the help of an equation of the form

$$\epsilon^* = \epsilon_1 \cdot \left\{ \frac{[2\epsilon_1 + \epsilon_2 + 2y(\epsilon_2 - \epsilon_1)]}{[2\epsilon_1 + \epsilon_2 - y(\epsilon_2 - \epsilon_1)]} \right\} \dots\dots\dots(5.7)$$

Where ϵ_1 is the dielectric constant of the blank matrix, ϵ_2 is the dielectric constant of the uniformly distributed (by volume) spherical inclusions($\text{Ni}_{1-x}\text{Zn}_x\text{Fe}_2\text{O}_4$) and let y be the volume fraction of the inclusion and ϵ^* is the dielectric constant of the matrix mixture or the composite.

A characteristic feature of this equation is that the formula does not require any symmetry with respect to the components of the mixture or composites. The experimentally observed value of ϵ_1 and ϵ_2 were employed to calculate the ϵ^* of the composite. **Since the experimentally observed value of ϵ^* were also available the validity of the above equation (5.7) was checked.** The details are shown in Figure.9. Equation 5.7 generally satisfies the experimentally observed value of dielectric constant(ϵ^*) of the composite. Calculations carried out using equations 5.7 up to a loading of 120phr is generally found to be in conformity with experimentally observed values of ϵ^* . So the most probable relationship, which determines the permittivity of the composite consisting of a two component system

consisting of an insulating filler could be $\epsilon^* = \epsilon_1 \cdot \left\{ \frac{[2\epsilon_1 + \epsilon_2 + 2y(\epsilon_2 - \epsilon_1)]}{[2\epsilon_1 + \epsilon_2 - y(\epsilon_2 - \epsilon_1)]} \right\}$.

This observation implies that the magnetic filler is uniformly distributed in the matrix and the percolation threshold is probably not reached even up to a loading of 120phr.

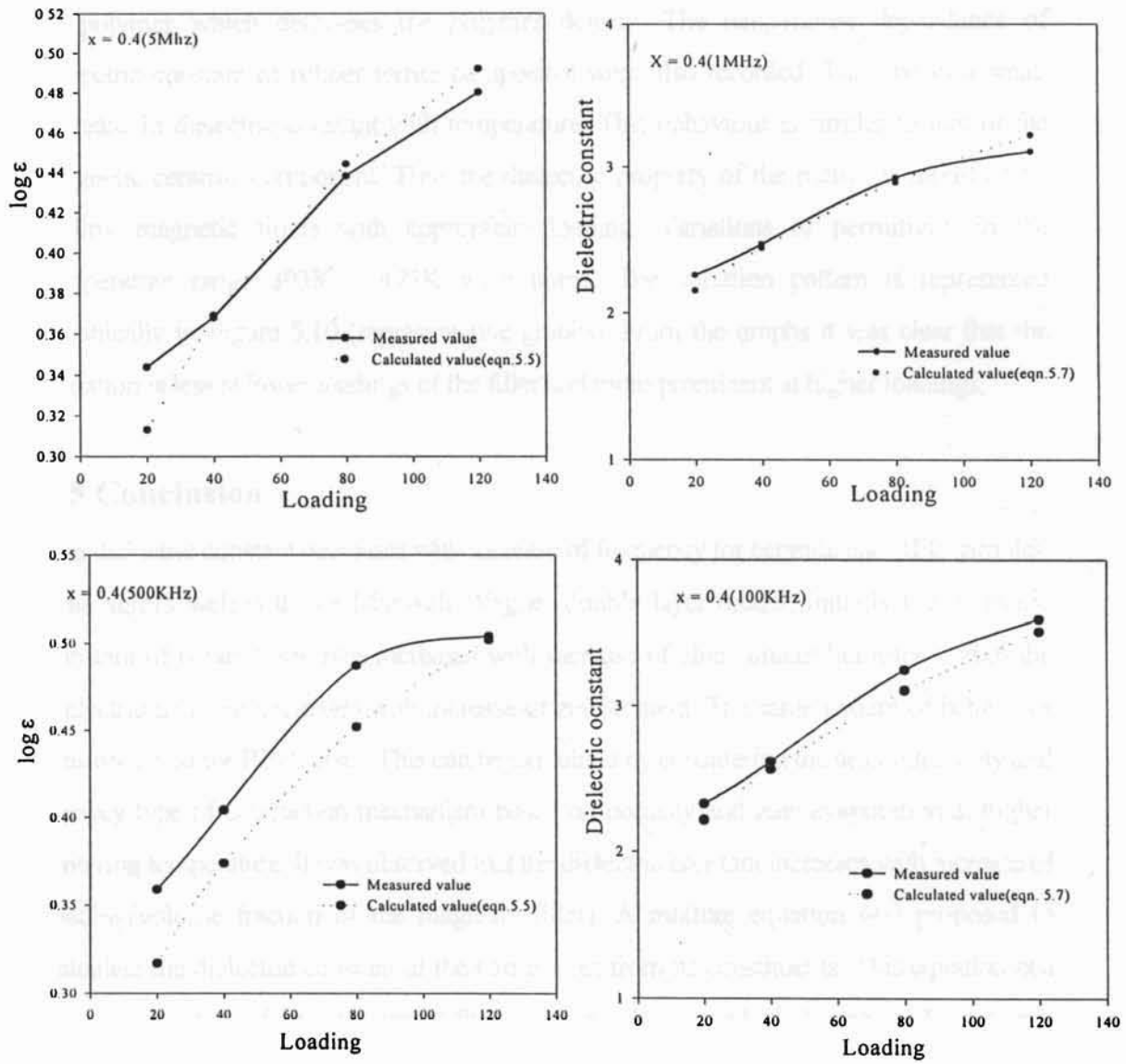


Figure.5.9.Loading dependence of permittivity (calculated and Measured value)

5.4.4 Temperature dependence

The effect of temperature on the dielectric constant for the ceramic samples were discussed and found that the dielectric constant increases with increase of temperature. The dielectric constant at different temperature for blank butyl rubber (without the filler) was also evaluated. It shows a decrease in dielectric constant with temperature due to the expansion of polymer which decreases the polymer density. The temperature dependence of dielectric constant of rubber ferrite composites were also recorded. This shows a small increase in dielectric constant with temperature. This behaviour is similar to that of the magnetic ceramic component. Thus the dielectric property of the matrix is modified by adding magnetic fillers with appropriate loading. Variations of permittivity in the temperature range 303K – 473K were noted. The variation pattern is represented graphically in Figure 5.10 (representative graphs). From the graphs it was clear that the variation is less at lower loadings of the filler and more prominent at higher loadings.

5.5 Conclusion

The dielectric constant decreases with increase of frequency for ceramic and RFC samples. This agrees well with the Maxwell Wagner double layer model. Initially the dielectric constant of ceramic samples increases with increase of zinc content but after $x = 0.6$ the dielectric constant decreases with increase of zinc content. The same pattern of behaviour was observed for RFCs also. This can be explained by considering the ac conductivity and verwey type of conduction mechanism based on porosity and zinc evaporation at higher sintering temperature. It was observed that the dielectric constant increases with increase of loading (volume fraction of the magnetic filler). A mixture equation was proposed to calculate the dielectric constant of the composites from its constituents. This equation can be employed to fabricate composites with predetermined dielectric and magnetic properties. The experimentally observed values of dielectric constant of the composite suggest that the magnetic filler is uniformly distributed and the percolation threshold is not reached up to a loading of 120phr. The dielectric constant of the composite as well as that of filler increases with increase of temperature. For blank butyl rubber the dielectric constant decreases with increase of temperature, because in non-polar dielectrics due to thermal expansion of matter the ratio of number of molecules to the effective length of the dielectrics diminishes with increase of temperature. Thus the dielectric and magnetic properties of RFCs can be appropriately modified by a judicious choice of matrix and filler. This is important in designing microwave absorbers.

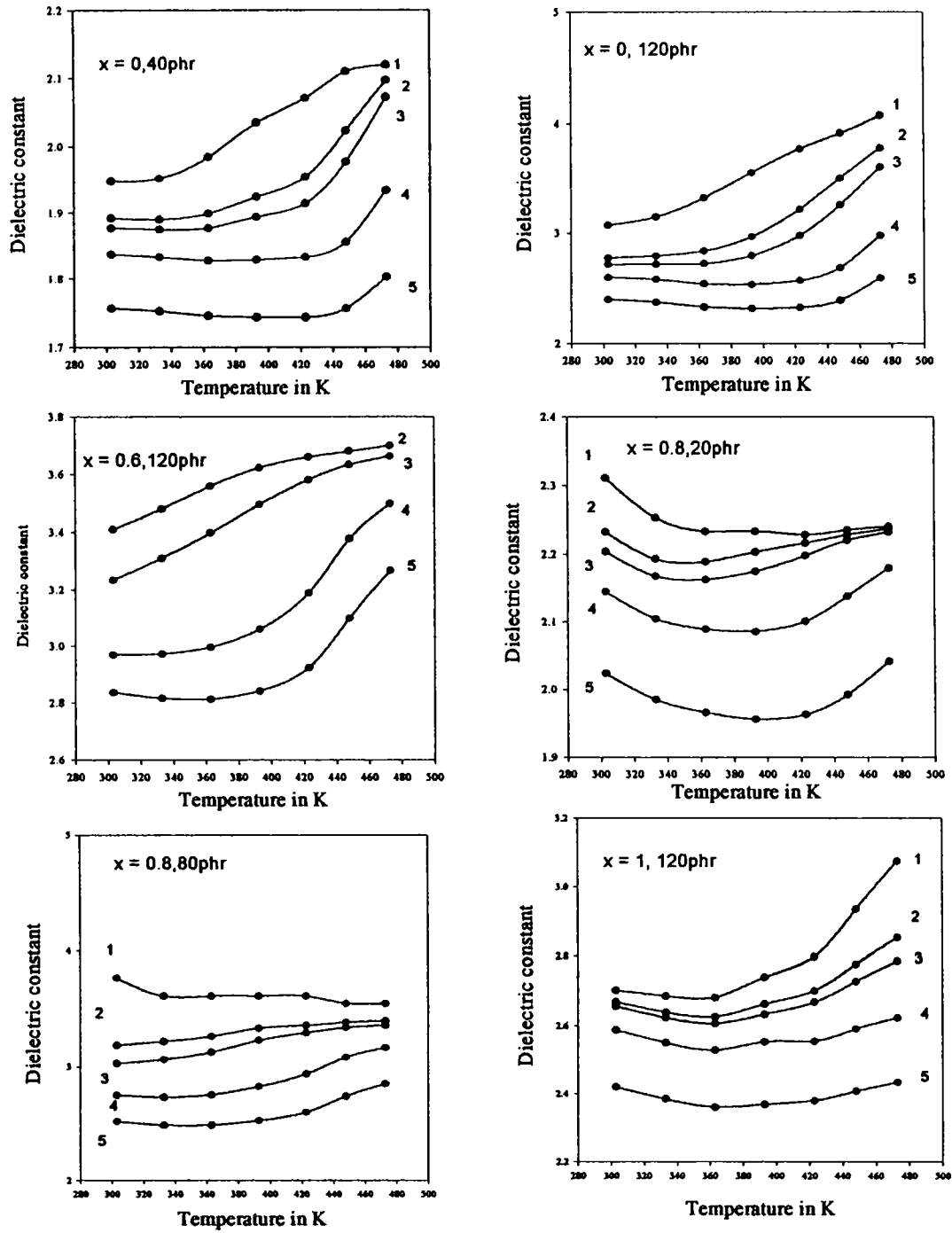


Figure.5.10. Representative graphs showing the temperature dependence of dielectric constant for RfCs(1-100KHz,2-500KHz,3-1MHz,4-5MHz,5-10MHz)

Evaluation of ac conductivity of RFCs from dielectric measurements

6.1. Introduction

The electrical properties are most important for ferrites and composites containing mixed ferrites, not only from the application point of view but also from the fundamental view point [137-143]. Evaluation of ac electrical conductivity reveals a wealth of information as regards the usefulness of these materials for various applications. Moreover, the study of ac electrical conductivity sheds light on the behaviour of charge carriers under an ac field, their mobility and the mechanism of conduction [144-145]. It was reported that the electron hopping between Fe^{2+} and Fe^{3+} ions and the hole hopping between Ni^{2+} and Ni^{3+} on B sites are responsible for conduction in ferrites. The conductivity studies on nickel zinc ferrites were carried out by various researchers on the basis of hole and electron hopping, the site occupation of Ni^{2+} ions and Zn ions were also reported [146-169]. El Hiti et.al carried out the conductivity studies for different mixed ferrite system like Mn-Zn, Ni-Mg, Sb-CoNi, Cu-Cr and also for Mg substituted nickel zinc ferrites [170-178]. The conductivity studies on ferrites carried out by various researchers proved its semiconducting behaviour and also proved the dependence of electrical conductivity on preparation condition, sintering time, temperature and the types of impurities [179-184]. However a survey of literature reveals that the conductivity studies on ferrite incorporated rubber composites are rather scarce or seldom reported. RFCs are essentially dielectric materials and ac conductivity plays an important role. So study of these materials, particularly, in an ac field assumes significance.

The present study includes evaluation of ac electrical conductivity for both ceramic $\text{Ni}_{1-x}\text{Zn}_x\text{Fe}_2\text{O}_4$ as well as the filler incorporated composites. It is also to be noted that the evaluation of ac conductivity for both ceramic and RFCs have been carried

out using the data made available from the dielectric measurements conducted on these samples, in the frequency range 100KHz to 13MHz[185] by employing a simple relationship. The effect of frequency, composition, loading and temperature on the ac electrical conductivity were studied for the ceramic $Ni_{1-x}Zn_xFe_2O_4$ as well as the filler ($Ni_{1-x}Zn_xFe_2O_4$) incorporated rubber ferrite composites (RFCs). The dependence of ac conductivity on the volume fraction of the magnetic filler was also investigated.

6.2. AC electrical conductivity – Principle & Theory

A capacitor when charged under an ac voltage will have some loss current due to ohmic resistance or impedance by heat absorption. If Q be the charge in coulombs due to a potential difference of V volts between two plates of a condenser of area A and interplate distance d then ac conductivity (σ_{ac}) due to ac voltage $v(v_0 e^{j\omega t})$ is given by the relation

$$\sigma_{ac} = \frac{J}{E} \quad (6.1)$$

J is the current density and E is the electric field strength vector.

But we know that the electric field vector $E = \frac{D}{\epsilon}$. D is the displacement vector of the dipole charges and ϵ is the complex permittivity of the material. It is also known that for a parallel plate capacitor the electric field intensity (E) is the ratio of potential difference between the plates of the capacitor to the inter plate distance.

$$\text{That is } E = \frac{V}{d} \quad (6.2)$$

Since the current density $J = \frac{dq}{dt}$ but q is given by $\frac{Q}{A} = \frac{V\epsilon}{d}$

$$J = \frac{dq}{dt} = \frac{d}{dt} \left(\frac{V\epsilon}{d} \right) = \frac{\epsilon}{d} \frac{dV}{dt} \quad (6.3)$$

$$\therefore J = \frac{\epsilon}{d} V j \omega \quad (6.4)$$

substituting for E and J in equation (6.1)

$$\begin{aligned} \sigma_{ac} &= \frac{J}{E} = \epsilon j \omega \text{ since } \epsilon \text{ being a complex quantity} \\ &= (\epsilon^1 - j\epsilon^{11}) j \omega = \epsilon^1 j \omega + \omega \epsilon^{11} \end{aligned} \quad (6.5)$$

in order that ac conductivity may be a real quantity the term containing j has to be neglected hence

$$\sigma_{ac} = \omega \epsilon'' \quad (6.6)$$

In any dielectric material there will be some power loss because of the work done to overcome the frictional damping forces encountered by the dipoles during their rotation. If an ac field is considered, then in an ideal case the charging current I_C will be 90° out of phase with the voltage. But in most of the capacitors due to the absorption of electrical energy some loss current I_L will also be produced, which will be in phase with the voltage. Charging current I_C and loss current I_L will make angles δ and θ respectively with the total current I passing through the capacitor. The loss current is represented by $\sin\delta$ of the total current I . Generally, $\sin\delta$ is called the loss factor but when δ is small then $\sin\delta = \delta = \tan\delta$. The two components ϵ' and ϵ'' of the complex dielectric constant ϵ will be frequency dependent and is given by

$$\epsilon'(\omega) = D_0 \cos\delta / E_0 \quad (6.7)$$

$$\epsilon''(\omega) = D_0 \sin\delta / E_0 \quad (6.8)$$

since the displacement vector in a time varying field will not be in phase with E and hence there will be a phase difference δ between them.

From equation (6.7) and equation(6.8) we have

$$\tan\delta = \frac{\epsilon''(\omega)}{\epsilon'(\omega)} \quad (6.9)$$

Substituting the value of $\epsilon''(\omega)$ from equation (6.9) in equation (6.6) then we have

$$\sigma_{ac} = \omega \tan\delta \epsilon'(\omega) \quad (6.10)$$

Where $\omega = 2\pi f$ and $\epsilon' = \epsilon_0 \epsilon_r$, here ϵ_r is the relative permittivity of the material and ϵ_0 the permittivity of free space.

$$\text{So } \sigma_{ac} = 2\pi f \tan\delta \epsilon_0 \epsilon_r \quad (6.11)$$

This equation is used to calculate the ac conductivity using dielectric constant and $\tan\delta$ at a given frequency. It is to be noted that both $\tan\delta$ and ϵ_r were available from dielectric measurements. The details of dielectric studies of both ceramic and rubber ferrite composites were discussed in chapter 5. The details of these measurements are given in chapter 2.

6.3. Frequency dependence

The ac electrical conductivity of ceramic nickel zinc ferrites and rubber ferrite composites have been computed for different frequencies (100KHz to 10MHz) and also at different temperatures (varying from 303K to 473K). It was observed that the ac electrical conductivity increases with increase of frequency initially and it shows a small dip at higher frequencies that is above 5MHz. This variation is same for samples with different concentration of zinc ions. Frequency dependence of conductivity for blank butyl rubber was also noted. It also shows a small decrease after 5MHz. Figure 6.1. shows the dependence of conductivity with frequency for both ceramic and blank butyl rubber. The hopping of electron between Fe^{2+} and Fe^{3+} ions on the octahedral sites is responsible for conduction mechanism in ferrites. Also various reports show that the hole hopping between Ni^{2+} and Ni^{3+} on B site also contribute to the electric conduction in ferrites. In this $\text{Ni}_{1-x}\text{Zn}_x\text{Fe}_2\text{O}_4$ system the hole conduction depends on the concentration of Zn ions on the A site to the Ni ion concentration on B site. In general the increase in conductivity with increase of frequency can be explained on the basis of Maxwell-Wagner theory [126]. According to this theory dielectric structure was formed by two layers. First layer consists of ferrite grains of fairly well conducting (ferrous ions), which is separated by a thin layer of poorly conducting substances, which forms the grain boundary. The non conducting layer or grain boundary is formed by oxygen ions.

Thus each grain possesses an oxygen rich layer on the surface as boundary. These grain boundaries are more active at lower frequencies, hence the hopping frequency of Fe^{2+} and Fe^{3+} ion is less at lower frequencies. As the frequency of the applied field increases the conductive grains became more active by promoting the hopping between Fe^{2+} and Fe^{3+} ions, there by increasing the hopping frequency. Thus we observe a gradual increase in conductivity with frequency. Also the theoretical equation which we used here to calculate the ac electrical conductivity shows a direct proportionality with frequency. But at higher frequencies the frequency of the hopping ions could not follow the applied field frequency and it lags behind it. This causes a dip in conductivity at higher frequencies. We also observed an increase in conductivity with frequency from 100KHz to 5MHz. But after 5MHz we observed a decrease in conductivity this may be due to the lagging of hopping ions with the applied field frequency. The same variation is observed

Figure 6.1

for ferrite incorporated rubber samples also. Figure.6.2. shows the dependence of ac electrical conductivity with frequency for representative rubber ferrite composites. It was also noted that this remains the same for samples with different volume fractions of the magnetic filler. The frequency dependence is same at different temperatures for both ceramic as well as for rubber ferrite composites.

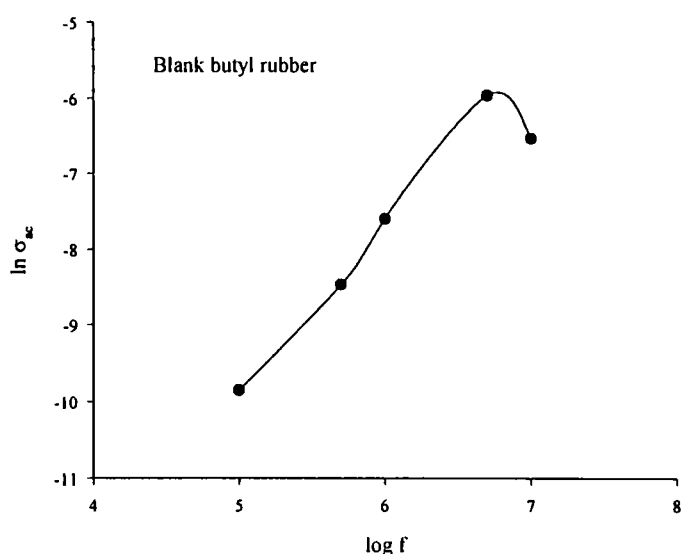
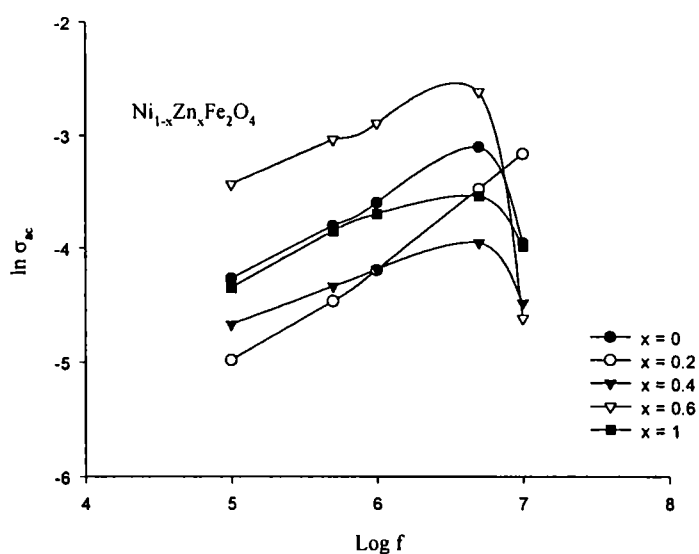


Figure.6.1. Frequency dependence of conductivity for $\text{Ni}_{1-x}\text{Zn}_x\text{Fe}_2\text{O}_4$ blank butyl rubber (room temperature)

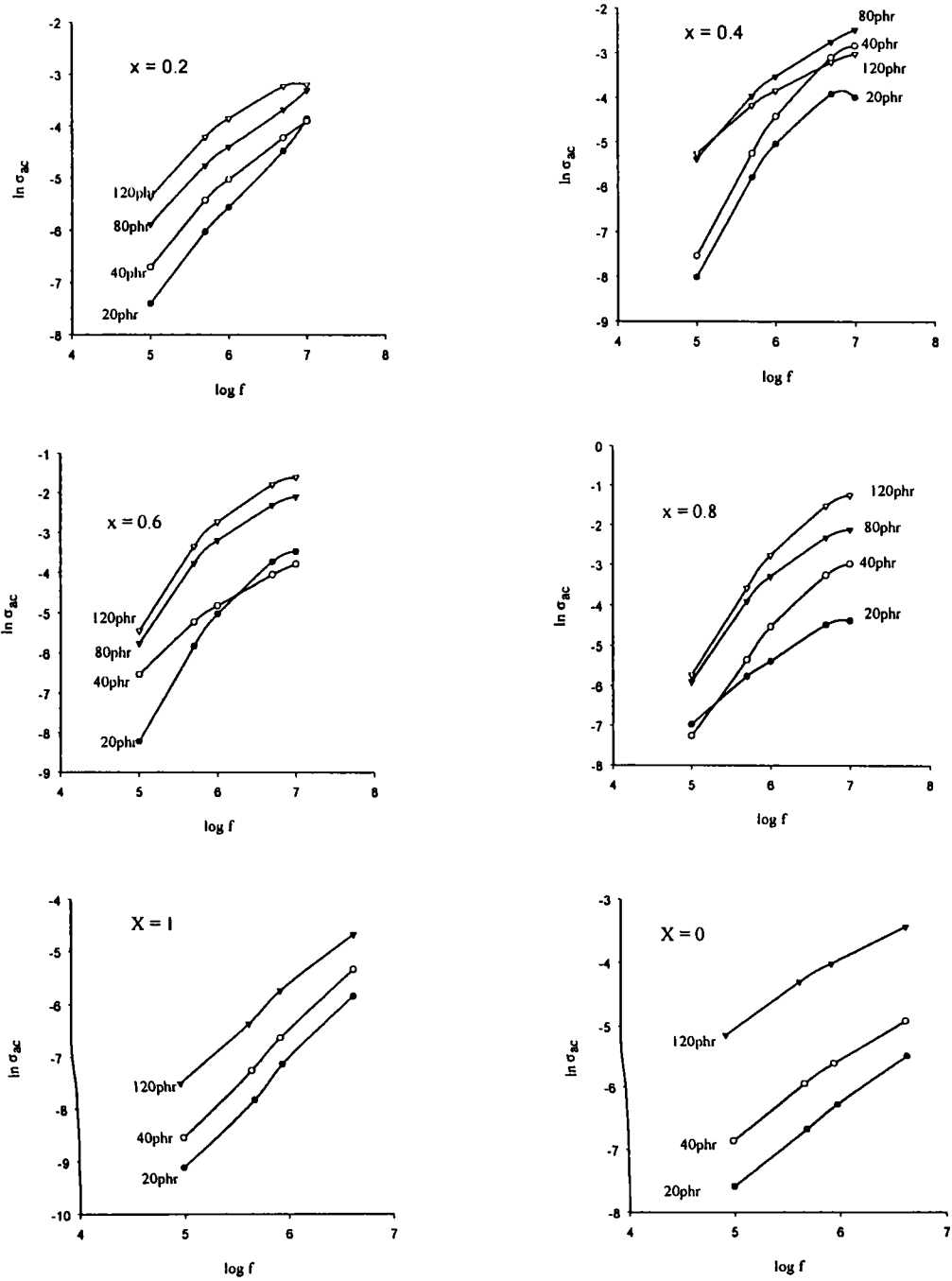


Figure.6.2. Variation of conductivity with frequency for rubber ferrite composites

6.4. Compositional dependence

Compositional dependence of ac electrical conductivity for both ceramic and rubber ferrite composites were studied at different frequencies and also for different temperatures. The variation of conductivity with composition (zinc content) for ceramic nickel zinc ferrites at room temperature was shown in figure.6.3. It is found that the ac electrical conductivity for NiFe_2O_4 (i.e $x = 0$) is greater than that for $\text{Ni}_{0.8}\text{Zn}_{0.2}\text{Fe}_2\text{O}_4$ and $\text{Ni}_{0.6}\text{Zn}_{0.4}\text{Fe}_2\text{O}_4$. As we know the conductivity in ferrites is mainly due to the hole hopping in metallic ions (Ni ions) and electron hopping in ferrous ions on the octahedral sites.

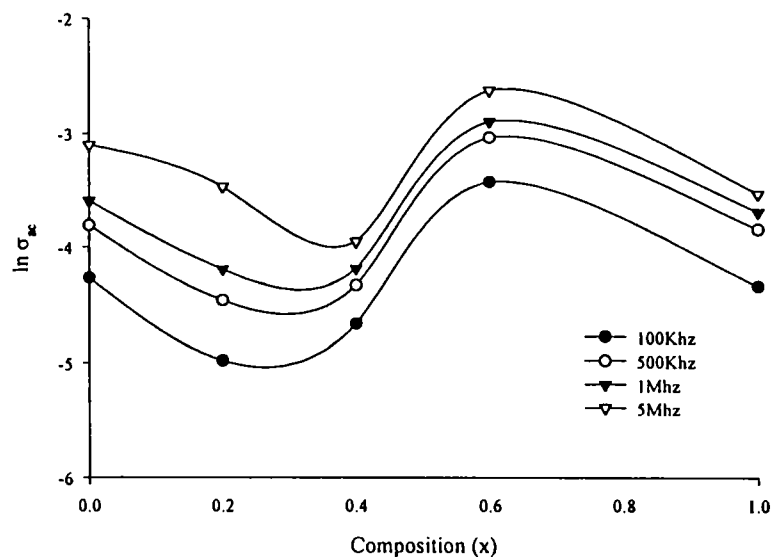


Figure.6.3.Variation of conductivity with composition for ceramic $\text{Ni}_{1-x}\text{Zn}_x\text{Fe}_2\text{O}_4$

In the $\text{Ni}_{1-x}\text{Zn}_x\text{Fe}_2\text{O}_4$ system when $x = 0$ maximum number of Ni^{2+} and Ni^{3+} ions are available for hopping. Hence the main contribution of conductivity may be due to the hole hopping. As the zinc concentration (x) increases the number of Ni^{2+} and Ni^{3+} ions on B sites decreases. In the present work the small decrease in conductivity for composition $x = 0.2$ and $x = 0.4$ was observed, this may be due to the electron hole compensation at the B site. Further increase of zinc concentration diminishes the hole hopping by decreasing the no of Ni^{2+} and Ni^{3+} ions on the B

site. Thus electron hopping become predominant and it increases the conductivity. Thus we observe a maximum conductivity for $\text{Ni}_{0.4}\text{Zn}_{0.6}\text{Fe}_2\text{O}_4$. Again it was observed that for $x = 1$, that is for ZnFe_2O_4 the conductivity decreases. This decrease can be explained by considering the grain size. It is well known that the growth of grain size and the formation of grain boundaries also influences the conductivity. In the present NiZn ferrite system we observed that the grain size first decreases with increase of Zn concentration and attain a minimum for $x = 0.6$, there after it increases with x . Thus a maximum grain size of 96.44nm was observed for $\text{ZnFe}_2\text{O}_4(x = 1)$. As the grain size increases the formation of oxygen rich layers on the surface of the grains are possible. These non conducting layers increases the resistivity there by decreasing the conductivity. This explains the decrease in conductivity at $x = 1$. Porosity variation of ceramic nickel zinc ferrite also support this result. It was found that the porosity initially decreases with increase of zinc content and shows a minimum value for $x=0.6$. There after the porosity increases with increase of zinc content. It was known that when porosity decreases the resistivity also decreases there by increasing the conductivity. Likewise when the porosity increases the resistivity also increases by decreasing the conductivity [186]. This also explains the compositional dependence of ac electrical conductivity in ceramic nickel zinc ferrite system. For rubber ferrite composites also the same variation is observed for all loadings. Variation pattern is shown in figure.6.4. The effect of matrix is minimal in this case.

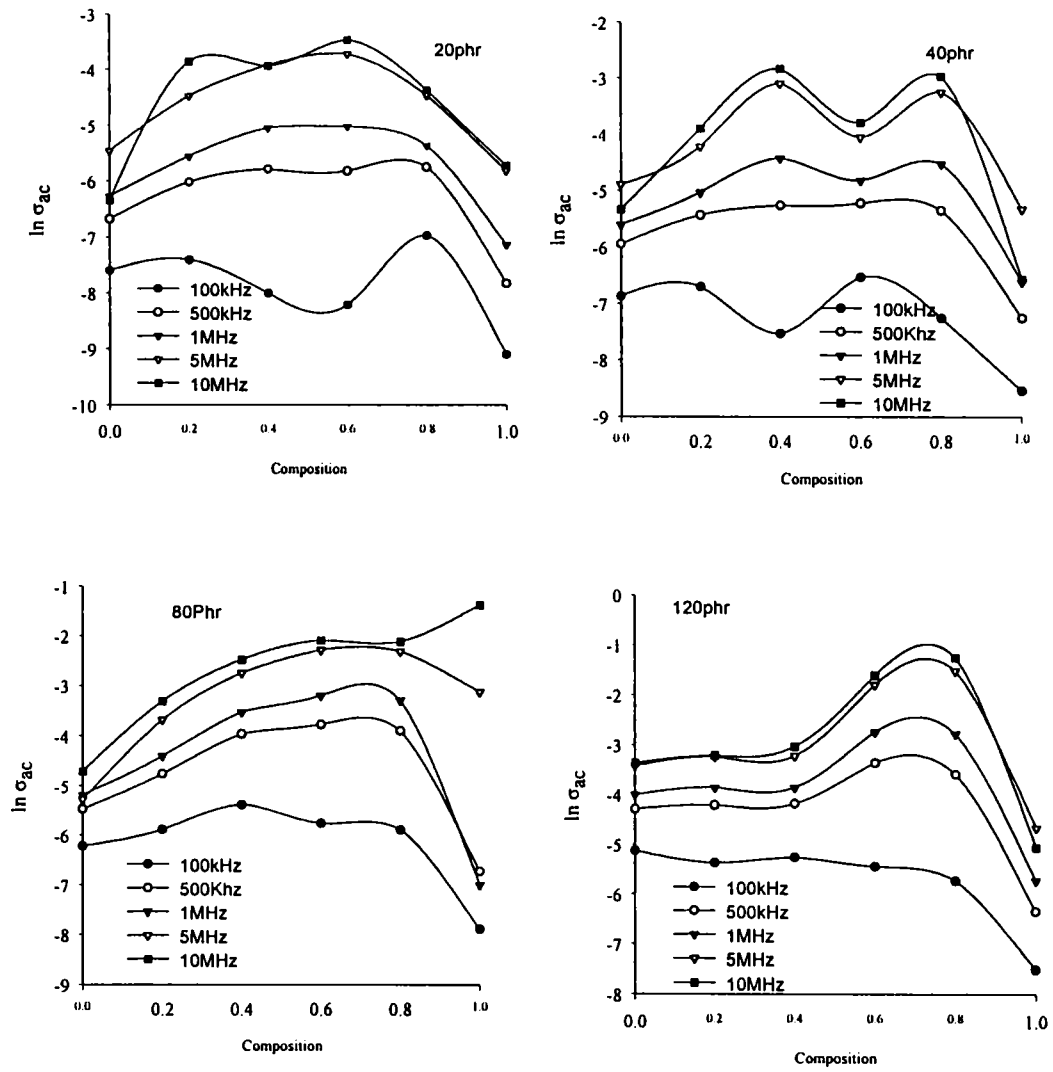


Figure.6.4. Variation of Ac conductivity with composition for RfCs

6.5. Loading dependence

The addition of conductive filler to a rubber or polymer is expected to impart reasonably good bulk conductivity. In the case of butyl rubber containing $\text{Ni}_{1-x}\text{Zn}_x\text{Fe}_2\text{O}_4$ also, increase in conductivity was observed with increase of the volume fraction of the filler. A maximum conductivity is observed for a maximum volume fraction of 120phr. This is same for all compositions (that is for all x values). Graphs showing the variation pattern is depicted in figure.6.5. Conductivity of the matrix at the lowest loading of the filler is affected by three parameters namely, the intrinsic conductivity of the filler, the shape of the filler and also the surface tension of the matrix and the filler [187]. It was expected that fibrous fillers will yield a percolation threshold at lower loadings compared with irregularly shaped particles, since the former will afford many more inter particle contacts. Here the particles are not fibrous but are spherical in nature. So no such tremendous change in conductivity is observed by adding higher volume fraction of the filler. But it was confirmed that the percolation threshold was not yet reached even for a loading of 120phr. From the graphs it is obvious that the conductivity increases with increase of loading of the filler. We have already proved indirectly from the dielectric and magnetic studies that there is no matrix filler interaction in these composites. This itself means that the filler goes in to the matrix uniformly. If the difference in surface tension of the filler and the matrix is large then the filler will tend to aggregate and gives higher conductivity at lower loading. No such effect is observed in this case. This once again confirms that the matrix filler interaction is minimal.



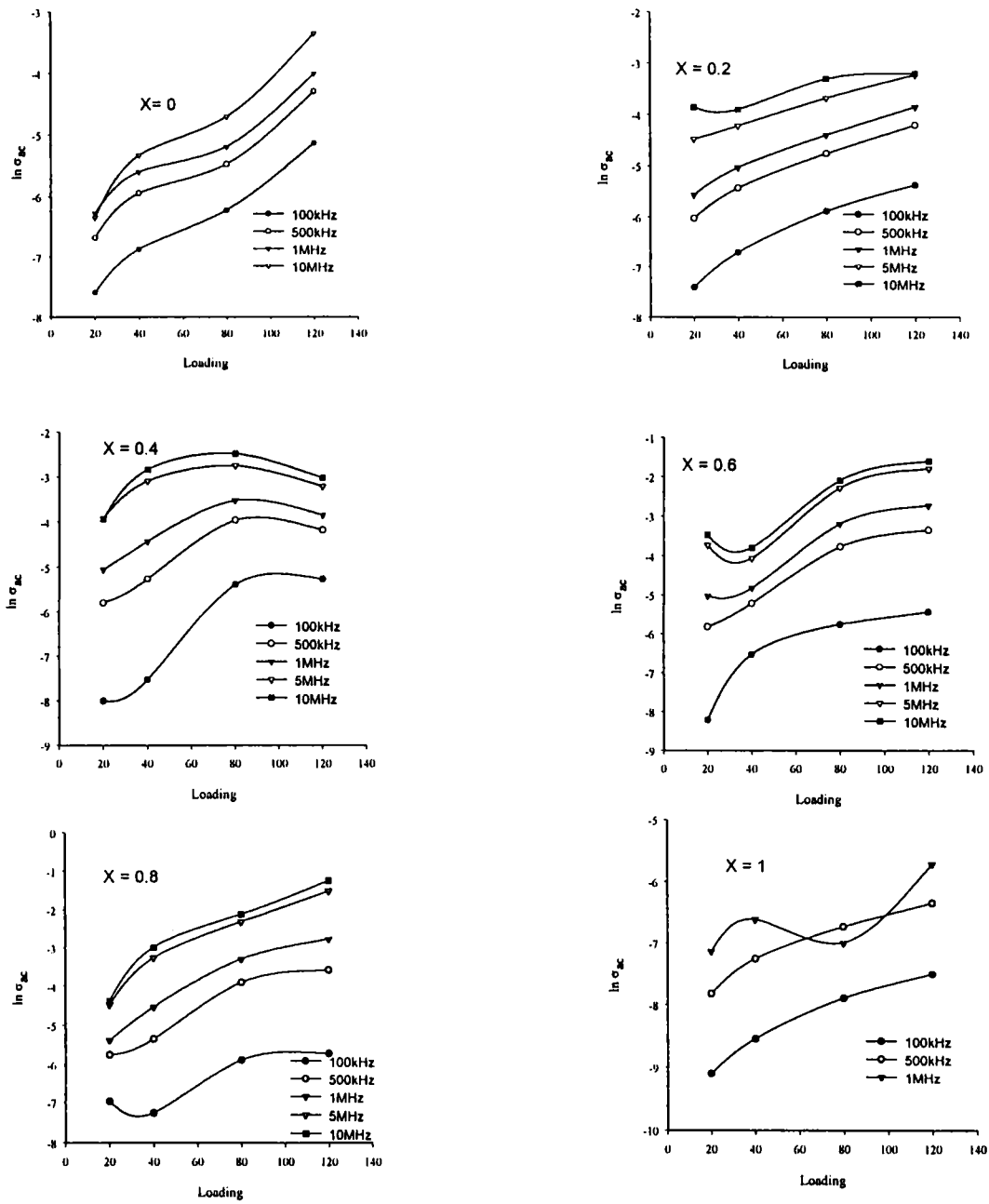


Figure.6.5.Variation of ac conductivity with Loading for different composition at different frequencies

6.6. Temperature dependence

The effect of temperature on the ac electrical conductivity of ceramic nickel zinc ferrite samples as well as the rubber ferrite composites were also studied in the temperature range 303K to 473K. It was observed that the conductivity increases with increase of temperature for all ceramic nickel zinc samples. At low frequencies the variation is very minimal but at higher frequencies the variation is obvious. The variation pattern of conductivity with temperature for different compositions are shown in figure.6.6.

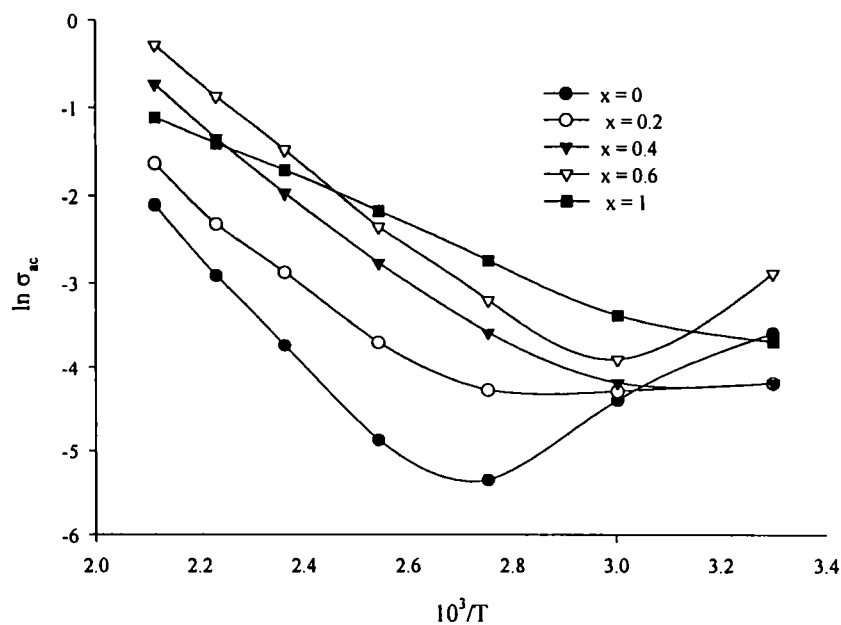


Figure.6.6. $\ln \sigma_{ac}$ Vs $10^3/T$ for ceramic $Ni_{1-x}Zn_xFe_2O_4$ (1MHz)

The influence of temperature on conductivity can be explained by considering the mobility of charge carriers responsible for hopping. As temperature increases the mobility of hopping ions also increases there by increasing conductivity. The electron, which is involved in hopping, is responsible for electronic polarization in these ferrites. The temperature dependence of conductivity for blank butyl rubber was also noted. It shows that the conductivity increases up to a temperature of 393K. Further increase of temperature reduce the conductivity. This decrease in

conductivity at higher temperature is due to the thermal expansion of polymer. At higher temperature the polymer density is reduced by thermal expansion and thus reduces the conductivity. The change is showed graphically in figure.6.7. Like butyl rubber ferrite incorporated rubber composites also shows a small reduction at higher temperature. But the conductivity values are much greater than the blank butyl rubber. Variation pattern is shown in figure.6.8.

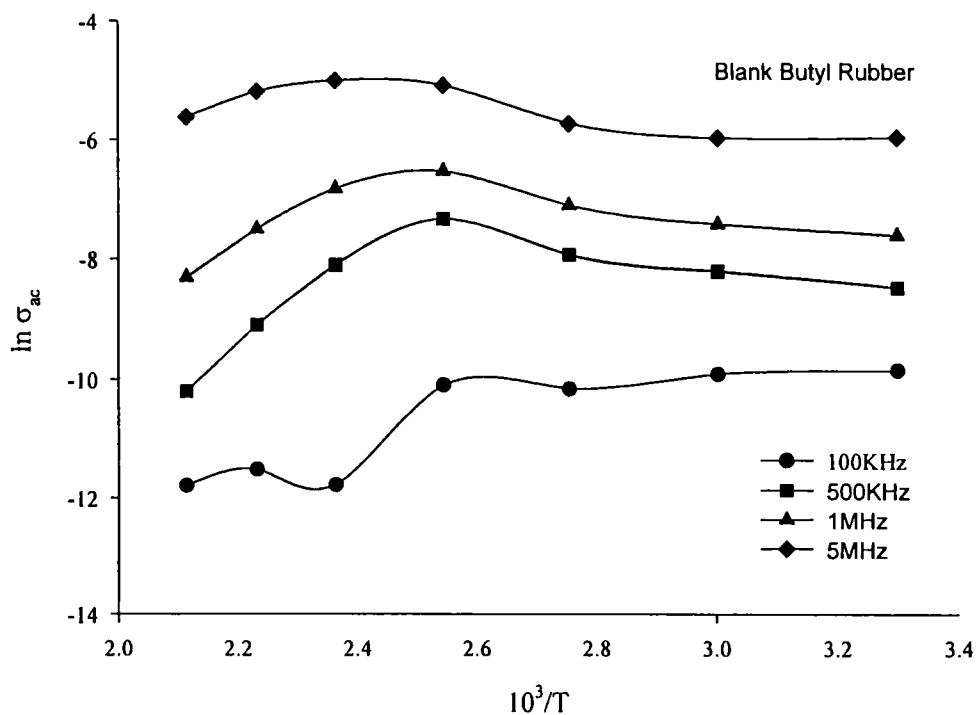


Figure. 6.7. $\ln \sigma_{ac}$ Vs $10^3/T$ for Blank butyl rubber

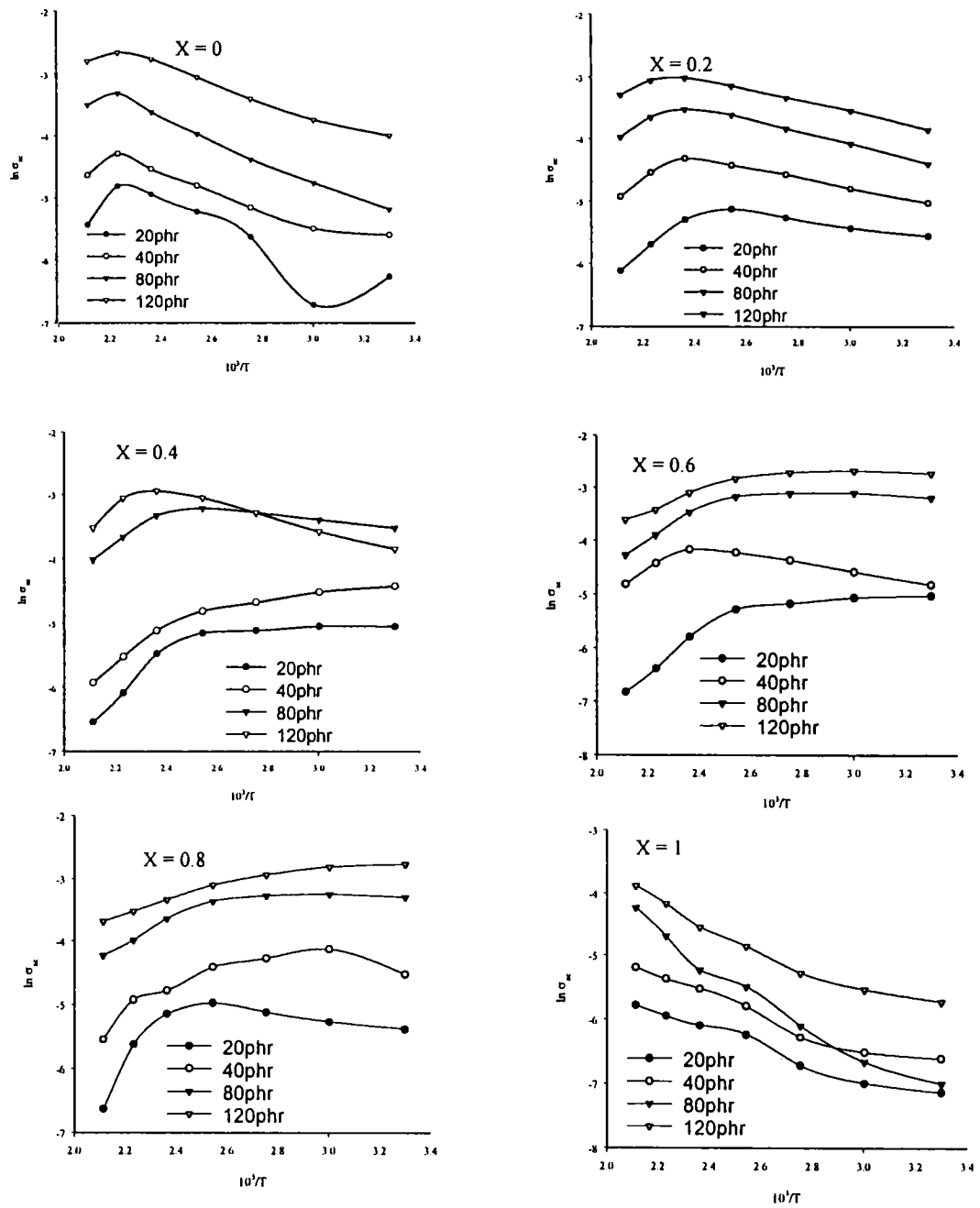


Figure .6.8. Temperature dependence of conductivity for RFCs (1MHz)

6.7. Conclusion

The ac electrical conductivity of ceramic as well as composite samples can be calculated by using a simple relationship of the form $\sigma_{ac} = 2\pi f \tan\delta \epsilon_0\epsilon_r$, with the data available from dielectric measurements. The results suggest that the ac electrical conductivity is directly proportional to the frequency. It shows an increase in conductivity with increase in frequency for both ceramic and rubber ferrite composites. The compositional dependence shows an initial increase of ac electrical conductivity with zinc content and reaches a maximum for $x = 0.6$ thereafter it decreases. This variation can be successfully explained with the help of porosity of the ceramic samples. The variation of conductivity with volume fraction of the magnetic filler shows a continuous increase up to a loading of 120phr. This variation remains the same for all compositions.

Evaluation of hysteresis loss for RFCs & The estimation of magnetostrictive constant λ_s

7.1. Introduction

Magnetostriction is the phenomena exhibited by ferro and ferrimagnetic materials [188-189]. The state of strain of the magnetic sample is dependent on the direction and the extent of magnetization. The strain caused by magnetization from the demagnetized state to the magnetic saturation is denoted by the magnetostriction constant λ . Magnetostriction appears because a crystal is always deformed spontaneously in the direction of magnetization in each domain[190-195]. As the direction of spontaneous magnetization is changed by technical magnetization, the direction of spontaneous strain of the crystal also changes, resulting in a change in the shape of the crystal as a whole. Normally λ is represented by the change in length to the original length and can be written as $\Delta l/l$.

This particular phenomena has important applications in making magnetostrictive transducers, which are used extensively in sonar devices. Currently the phenomena of magnetostriction is used in analog positioning problems. They are also used in acoustic delay lines, sonar devices and oscillators[196].

The theory of magnetostriction is complex and models are generally related to those of magneto crystalline anisotropy since both these phenomena are due to spin orbit coupling[197-198]. The microscopic origin of magnetostriction in spinel ferrites are considered to be due to the strain potential and spin-orbit, intra spin – spin interactions, anisotropy exchange and the strain modulation of the dipolar interaction. The magnetostrictive strains are usually so small that they can only be measured if adequately magnified by mechanical, electrical or optical devices[199].

The precise determination of λ or λ_s the saturation magnetostriction constant is important. This is significant not only from the applications point of view but this also provides information as regard the nature of the domain or the domain dynamics under the application of an external magnetic field. There are several experimental methods available for the determination of λ_s . Of them λ_s evaluation by strain gauge methods, optical dilatometry, capacitance method and X-ray analysis need special mention[200-205]. In most of the cases these experiments are able to predict the magnitude and not the sign.

RFCs are composites containing elastomer matrixes and they are elastic in nature. Under normal circumstances, they cannot be made transparent and hence optical methods can not be employed to determine λ_s . Since they are elastic in nature, employment of strain gauge techniques for the evaluation of λ_s also doesn't give accurate values. This is because the adhesion of strain gauges to the composites, requires a small force and this might already cause a strain to the sample under test even before the application of a magnetic field. So results obtained from these techniques could be erroneous unless appropriate corrections are incorporated. This is often time consuming and not fail proof. This lead us to search for simpler and quicker methods to estimate λ_s .

7.2. Estimation of λ_s from Magnetic measurements

The saturation magnetostriction of a polycrystalline specimen depends on the properties of its individual crystals and the way in which they are arranged. The energy loss is attributed to the creation and annihilation of the domain wall surface during it's displacement. This means that the value of saturation magnetostriction depends on the energy loss. In poly^{cr}crystalline materials the grains are oriented randomly. The saturation magnetostriction obtained here is an average over the orientations.

It is known from first principles that simple relationships exist between λ_s and the total energy loss (W_h) when considering the hysteresis loop of a ferro or ferrimagnetic material. Normally W_h is related to M_s and H_c and they are in turn determined by loop constants. Here the shape of the hysteresis loop plays a very

important role and so do the ratio M_r/M_s . In literature three types of materials are mentioned and they are characterized by loop constants. The equations connecting the hysteresis loss with M_s and H_c is different for different materials and they are the following. For single domain fine particles

$$W_h = 1.98 \cdot M_s \cdot H_c \dots\dots\dots (7.1)$$

For fine particles with multi domain structure

$$W_h = \frac{3.21 \cdot M_s \cdot H_c}{1.3} \dots\dots\dots (7.2)$$

For a cubic magnetic material

$$W_h = \frac{4.3 \times M_s \times H_c}{1.2} \dots\dots\dots (7.3)$$

It is imperative that the exact nature of the loop and the loop constants of the system under investigation is to be determined. For this, the observed W_h from hysteresis loop parameters (VSM measurements) was fitted for various combinations of M_s and H_c (equation 7.1 to 7.3) and it was found that the calculated W_h and the observed W_h obey the equation $W_h = \frac{4.3 \times M_s \times H_c}{1.2}$. This

fact was ascertained by calculating W_h and comparing it with the observed W_h obtained from VSM measurements. These calculations were extended for the $Ni_{1-x}Zn_xFe_2O_4$ ceramic series as well as for the ferrite incorporated composites. Figures 7.1 and 7.2 shows the nature of W_h with x for these samples. It is to be noted that the W_h calculated by using equation 7.3 is in good agreement with the observed W_h from VSM. So it is right to assume that the present mixed ferrite system and the RFCs under investigation also came under the third category as described in literature [72] and they are governed by equation number 7.3.

Relationships connecting the saturation magnetostriction constant λ_s and the energy loss W_h is also possible. In such a case it is to be assumed that all process of magnetisation reversal take place exclusively through the displacement of 180° walls. λ_s is related with W_h by the equation

$$W_h = 4.3 \pi \cdot \lambda_s \sigma_0 \dots\dots\dots (7.4)$$

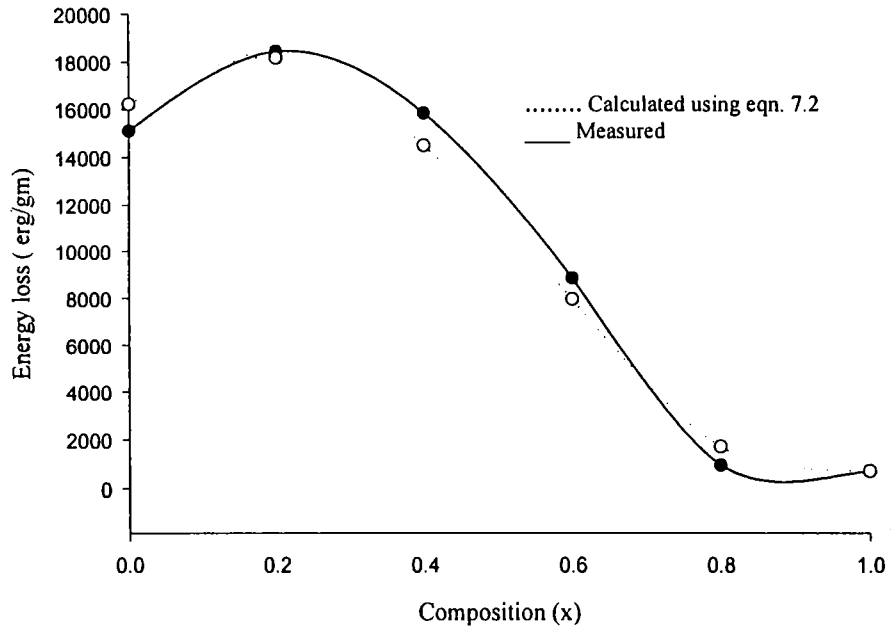


Figure 7.1. Variation of energy loss with composition for $Ni_{1-x}Zn_xFe_2O_4$

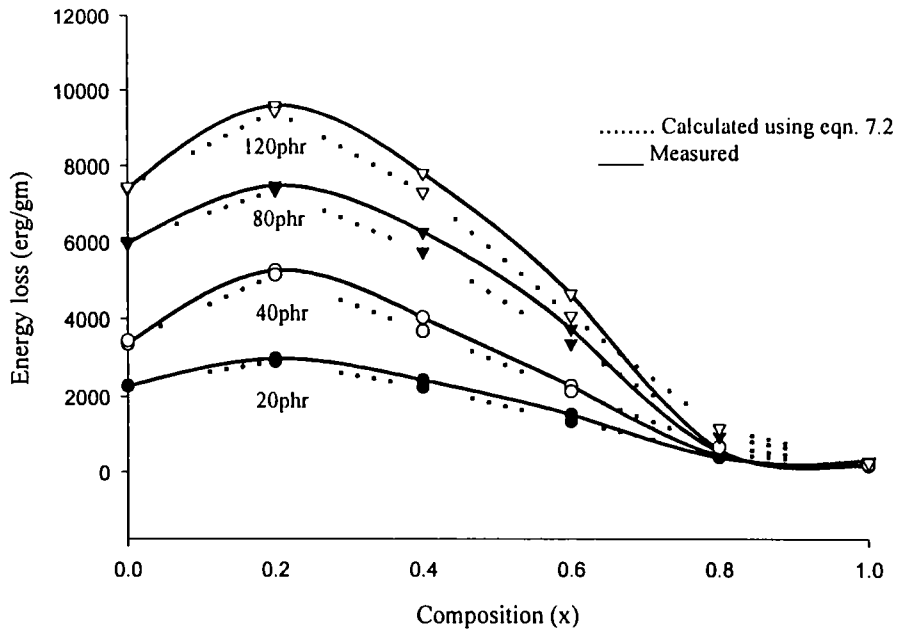


Figure 7.2. Variation of energy loss with composition for rubber ferrite composites

Here hysteresis loss is expressed in terms of magnetostrictive anisotropy because irreversible process of magnetisation is very much affected by the fluctuations of internal stress rather than the magnitude of crystal anisotropy. From equation 7.4 λ_s can be deduced as follows

$$\lambda_s = \frac{W_h}{4.3 \times \pi \times \sigma_0} \dots\dots\dots(7.5)$$

where λ_s is the magnetostrictive constant W_h is the hysteresis loss factor and σ_0 is the internal stress. However this relationship requires a knowledge of σ_0 . One of the two extreme assumptions are possible like stress is uniform throughout but strain varies from grain to grain or strain is uniform and stress varies. It has been reported in the literature that σ_0 is universal in nature, especially, for polycrystals and it is of the order of 10^9 N/m². The origin of σ_0 , is assumed to be a constant which is not clear and dealt very scarcely in literature. This value of σ_0 was employed for the estimation of λ_s .

7.3. Results and discussions

For the purpose of comparison and checking the validity of this simple relationship, data available from literature on similar systems namely, $Ni_{1-x}Zn_xFe_2O_4$ were made use of. λ_s was calculated for $Ni_{1-x}Zn_xFe_2O_4$ with various x for two series of samples fired at different temperatures and they are shown in Figure 7.3. This was done by employing the reported values of M_s and H_c and substituting these values in equation 7.5. λ_s for nickel zinc ferrite series was experimentally found out by J.Smit and H.P.J Wijn [79] and they are compared with the calculated values. Table 7.1 shows a gist of the λ_s values reported by various scientists for various ferrites. λ_s reported for $Ni_{1-x}Zn_xFe_2O_4$ by using experimental techniques was also plotted for different x and is shown in figure 7.3. These were also compared with the calculated λ_s (using the reported M_s and H_c values of $Ni_{1-x}Zn_xFe_2O_4$ ferrite samples by employing equation 7.5). An increase in λ_s was observed with increase in zinc concentration. Etienne du Tremolet de Lacheisserie have found out the magnetostriction coefficients for $Ni_{1-x}Zn_xFe_2O_4$ at 77K and it is found to be lie between 105×10^{-6} and 63×10^{-6} [206]. He also analyzed the x dependence of λ_s for $Ni_{1-x}Zn_xFe_2O_4$. The λ_s for $NiFe_2O_4$ at room temperature was first reported by Smit and Wijn, and it is found to be -26×10^{-6} (cf Table 7.1). But Murthy and Rao reports that for $NiFe_2O_4$ the value of λ_s is -24×10^{-6} [207]. These discrepancies could be because of the influence on the preparative conditions on the value of λ_s . That is as sintering temperature

increases the absolute value of λ_s decreases. This decrease was correlated with the appearance of Fe^{2+} in the nickel ferrite. Since Fe_3O_4 exhibit a positive λ_s value, hence any appearance of Fe^{2+} in the nickel ferrite markedly reduces the absolute value of its λ_s coefficient.[206].

This estimation only provides the magnitude of the magnetostriction and not the sign. This is one of the drawbacks of this method of estimation. However a survey of the literature reveals that except magnetite most of the ferrites exhibit a negative magnetostrictive constant. So intuitively one can indirectly gain an idea about the sign of λ_s . More over a knowledge of anisotropy constants can also give indications about the sign. So going by the vast experimental data available on similar systems sign can be attributed to the λ_s .

Sample ID	$\lambda_s \times 10^6$ By Smit & Wijn
$\text{Ni}_{0.36}\text{Zn}_{0.64}\text{Fe}_2\text{O}_4$	-5
$\text{Ni}_{0.5}\text{Zn}_{0.5}\text{Fe}_2\text{O}_4$	-11
$\text{Ni}_{0.64}\text{Zn}_{0.36}\text{Fe}_2\text{O}_4$	-16
$\text{Ni}_{0.8}\text{Zn}_{0.2}\text{Fe}_2\text{O}_4$	-21
NiFe_2O_4	-26
Fe_3O_4	40
CoFe_2O_4	-110
MnFe_2O_4	-5
MgFe_2O_4	-6
$\text{Li}_{0.5}\text{Fe}_{2.5}\text{O}_4$	-8

Table: 7.1 Linear magnetostriction coefficient for some mixed ferrites(reported by Smit & Wijn)

The graph depicting the variation of λ_s with x for samples fired at higher temperature indicates that λ_s is higher for particles with lower H_c . The variation pattern of λ_s with x is the same for $\text{Ni}_{1-x}\text{Zn}_x\text{Fe}_2\text{O}_4$ for both calculated and measured values (from literature). However barring compositions at $x = 0$ and $x =$

1 (cf.Fig.7.3)the variation pattern for λ_s vs x is almost the same. This could be because no λ_s values were reported earlier for ZnFe_2O_4 and it was assumed to be an antiferromagnetic material. In the present study we observed a net magnetization of 3.118emu/gm for fine particle zinc ferrite and this behaviour has been discussed in detail in chapter 4. It is also possible that at $x = 0$ the Ni^{2+} too will be occupying the tetrahedral sites instead of octahedral sites. This observation is supported by complimentary evidences and is reported by Chinnasamy et al [208]. The estimated λ_s for the samples under investigation is less than that of the reported.

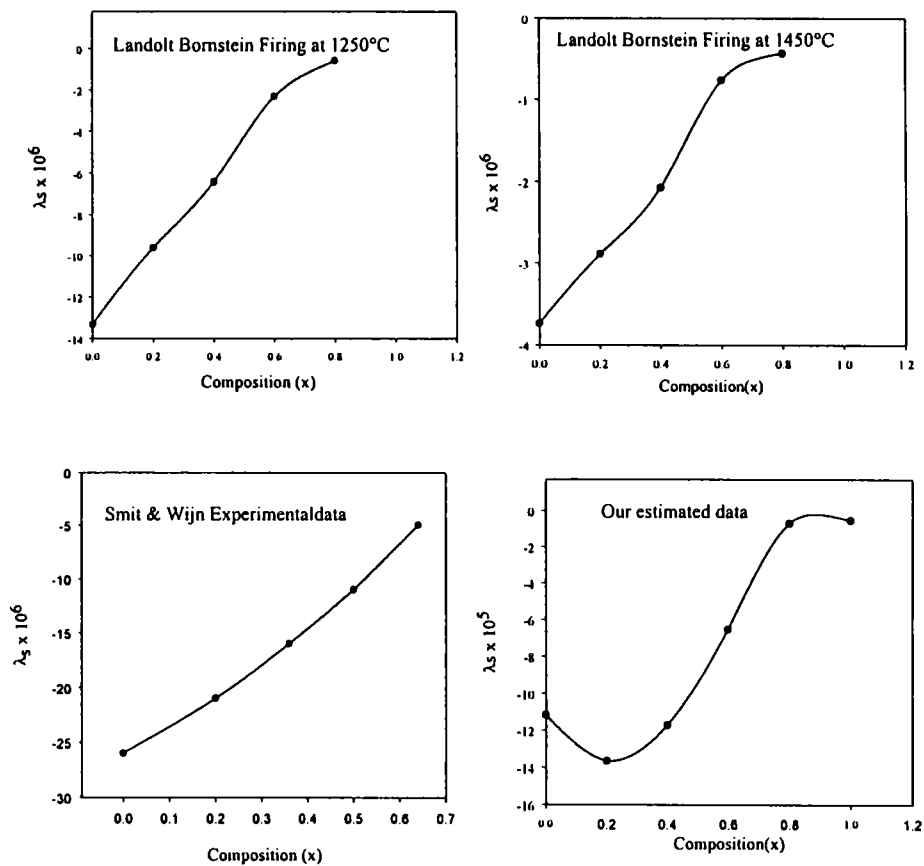


Figure 7.3 λ_s Vs Composition for $\text{Ni}_{1-x}\text{Zn}_x\text{Fe}_2\text{O}_4$

From the graphs it is clear that the λ_s calculated by using equation 7.5 have resulted in values comparable to the experimentally observed values. λ_s is essentially determined by M_s and H_c and hence H_c influences the λ_s value. Here it

is to be noted that the value of H_c was relatively high (for the sample under present study) almost an order difference and this has resulted a λ_s value which is almost an order less than that of the calculated values (from literature).

The same principle was applied to estimate λ_s for RFCs. The λ_s values of rubber ferrite composites are larger compared to that of its ceramic component. The compositional dependence of λ_s for RFCs shows same pattern as that observed for ceramic fillers. Figure 7.4 shows the variation of magnetostriction constant with zinc concentration for RFCs. It is also to be noted that the saturation magnetostriction decreases with increase of weight fraction of the magnetic filler. The details are shown in Figure 7.5. The λ_s of RFCs exhibit a cumulative property of the matrix and the filler. The λ_s of RFCs is characteristics of a dilute system. The values range from 6.98×10^{-5} to 0.1356×10^{-5} . This is because the matrix is nonmagnetic and are assumed that there is no filler matrix interaction. Moreover magnetization measurements carried out on RFCs (chapter 3) show that the H_c of the composites and H_c of the filler are the same. So naturally the λ_s is determined by the amount of the filler or rather the M_s of the filler.

It is to be noted that the employment of equation 7.5 provides only approximate values for λ_s . If λ_s for ceramic as well as the composites can be determined experimentally a comparative study can be carried out. This together with some modeling and simulation can throw light in the origin of σ_0 and thus could even tell us whether there is a large change in σ_0 or this could be assumed as a constant. This estimation does not provide the sign for the estimated λ_s . This is one of the drawbacks of this method of estimation of λ_s .

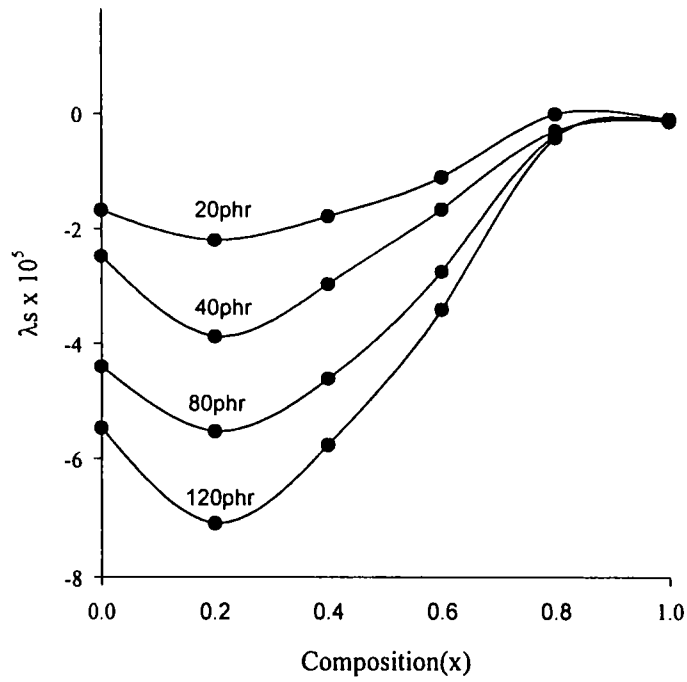


Figure 7.4. Variation of magnetostriction with composition for different loadings

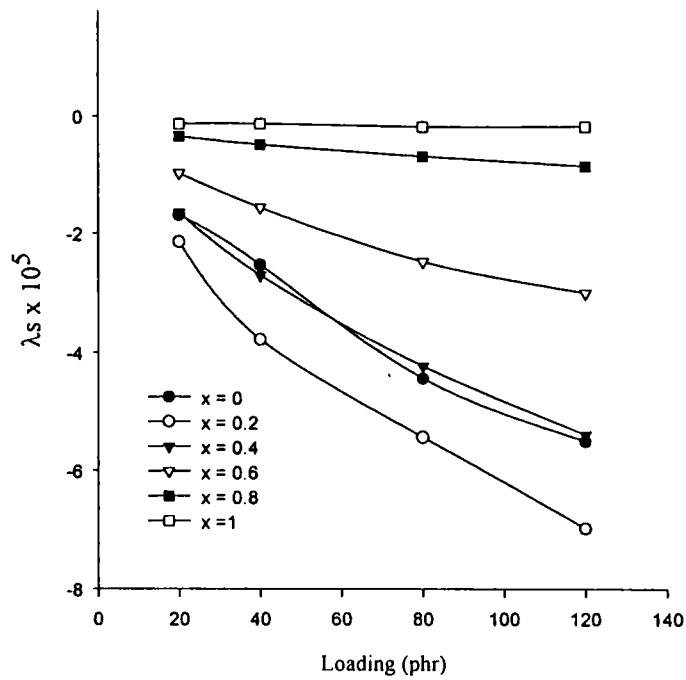


Figure 7.5. Variation of λ_s with loading for different composition

7.4 Conclusion

Estimation of magnetostriction constant λ_s was carried out by utilizing the hysteresis loop parameters and employing a simple relationship. The magnetic parameters obtained from the vibrating sample magnetometer is used to estimate the magnetostriction constant (λ_s). One of the main drawbacks of this estimation is that the sign of λ_s can not be predicted directly. From the literature it can be seen that except magnetite most of the ferrites exhibit a negative magnetostrictive constant. Results on the estimation of λ_s for the ceramic nickel zinc ferrite lies in the range 13.44×10^{-5} to a lower value of 0.51×10^{-5} . The λ_s values of RFCs are found to be less compared with the ceramic ferrite samples.

Summary and Conclusion

Magnetism is one of the oldest phenomena known to the mankind. The area of magnetism and especially the field of ferrimagnetism is the most widely studied phenomenon by engineers and scientists for possible exploitation for commercial applications. Among many ferrimagnetic materials studied ferrites received the utmost attention and still most of the devices based on ferrites are yet to be replaced by other materials. This speaks volumes about the importance of these class of materials. Mouldability and flexibility of ceramic magnetic materials is one of the problem areas as far as applications are concerned. This is where magnetic composites can play a very crucial role. RFCs are magnetic components and can fill these voids where in they can be moulded in to complex shapes. Flexibility with the required mechanical strength is another hallmark of these composites. These composites can be potential microwave absorbers in a wide range of frequencies.

The main focus of the present work was to synthesize ferrite fillers belonging to the series $\text{Ni}_{1-x}\text{Zn}_x\text{Fe}_2\text{O}_4$ in the single phasic form and to incorporate them in a butyl rubber matrix for various loadings. The first chapter presents a general introduction to this area and the second chapter gives a general discussion of the experimental techniques employed for the characterisation at different times. Chapter 3 - 7 gives the details of the findings of the work carried out on the subject of RFCs. The following section provides a glimpse of the conclusions drawn from the present study and the scope for future work.

An inspection of table 3.4 and 3.5 in chapter 3 indicates that the calculated and measured values of the μ_B for the $\text{Ni}_{1-x}\text{Zn}_x\text{Fe}_2\text{O}_4$ do not tally each other. Though this has been explained successfully by invoking canting of spins this needs to be investigated further. This is stated in the light of the observations made in the laboratory on a series of $\text{Ni}_{1-x}\text{Zn}_x\text{Fe}_2\text{O}_4$ samples prepared with different particle

sizes. This indicates that the cation distribution in the fine particle regime could be entirely different and nickel could be occupying A sites also. In order to extract solid evidence one needs to carry out detailed studies by using Mössbauer spectroscopy and low temperature magnetisation measurements. Investigations on fine particle $\text{Ni}_{1-x}\text{Zn}_x\text{Fe}_2\text{O}_4$ and ZnFe_2O_4 may be combined and this will throw light on the magnetic behaviour of spinel ferrite system in the nanoregime.

So far not much attention was devoted to the area of nanoregime, though chemists have devoted a great deal of attention and efforts to this area, most of the work has been on the surface chemistry and surface structure of catalyst materials. These efforts were towards synthesizing high surface area catalysts and understanding the surface chemistry of these materials. The solid state properties of these systems have not been probed in depth. After the discovery of nanomaterials/ nanocomposites and the recent findings, people are devoting much attention to this area in minutest details.

Chapter 4 dealt with the anomalous behaviour of zinc ferrite systems. The anomalous behaviour of ZnFe_2O_4 in the nano regime was successfully explained by conducting a series of experiments by using Mössbauer spectroscopy, Low Energy Ion Scattering (LEIS) and magnetisation measurements using Vibrating Sample Magnetometer (VSM). These studies were of preliminary in nature and scope exists to carry out further studies in a more systematic manner. For example, it has been only concluded tentatively that the occupation of Zn on the B site is dependent on the particle size or rather the surface area. It has not been established whether the amount of inversion is dependent on the size. Similarly the existence of clusters, if any on the surface of fine particle spinel ferrites needs to be investigated separately. It has been reported that the magnetisation of ZnFe_2O_4 is extraordinarily large in small particle forms, compared to the value reported for the bulk. The origin of these magnetisation in these small particles has been interpreted to be the presence of higher concentration of magnetic clusters, which are expected to be formed by A-B interactions of Fe^{3+} ions produced by a small deviation in cation distribution from the normal spinel structure. Clusters are formed by the A-B interactions caused due to the occupancy of small number of Fe^{3+} ions in tetrahedral A-sites with the Fe^{3+} ions at octahedral B sites. In the literature there are also reports suggesting that

surface spins also contribute to the total magnetisation. In the above case the total susceptibility contains a contribution of spins coupled in the clusters and of the free spins of the remaining Fe^{3+} ions in the B-site. It would be appropriate to carry out further studies on fine particle zinc ferrite system by preparing ZnFe_2O_4 of different particle size and study the various properties, like magnetisation and conductivity as a function of size of the particle. In this context it must be mentioned here that these properties are to be studied with respect to the single domain (SD)/superparamagnetic (SP) nature of these magnetic particles and must be correlated. Moreover surface studies also can be conducted to evaluate the surface structure of the spinel system by using Low Energy Ion Scattering (LEIS) and Electron Spectroscopy for Chemical Analysis (ESCA). Scope also exists to evaluate the magnetic structure of ZnFe_2O_4 in the nano regime by employing neutron scattering experiments. From a fundamental point of view more studies on similar spinel systems could also be undertaken in order to establish the magnetic structure of similar compounds. The information thus gathered would enable material scientist to synthesise new magnetic materials with improved magnetic and electrical properties.

Similar systems belonging to the spinel family, not necessarily magnetic, can serve as ideal platforms to test the above hypothesis. It has been established earlier that cations like Zn^{2+} and Cd^{2+} have a strong tetrahedral site preference, and it would be appropriate to delve the energy consideration under which they migrate to the octahedral voids in the nanoregime.

The evaluation of processability parameters indicates that the materials are processable and can be moulded in to different shapes with the required mechanical properties. The processability is not affected and the percolation threshold is also not reached for a maximum loading of 120phr. This means that along with magnetic fillers some reinforcing fillers like carbon black (HAF N330) could be introduced in to the matrix for enhancing the mechanical properties of these composites.

Microwave absorbers are important because of the ever increasing electromagnetic interference (EMI) due to the immense growth in the utilisation of electronic and electrical devices in industrial and other commercial applications. One of the solutions to the problem of EMI is to use shielding or absorbing material to absorb

the corresponding electromagnetic waves. Gadgets based on rubber ferrite composites can play a very crucial role here. Research carried out on these composites by various researchers have shown that rubber ferrite composites are very good microwave absorbers for a wide range of frequencies over intrinsic ceramic ferrites. It is also known from the literature that carbon black enhances the microwave absorbing properties of RFCs. So as a continuation of the present research carried out on RFCs one can undertake a series of studies on the microwave absorption of these composites with carbon black incorporation. The effect of loading of carbon black in increasing or decreasing the bandwidth of microwave absorption of RFCs will be a very good futuristic proposition.

The purpose of studying microwave absorbing characteristics of these RFCs is to bring out a more quantitative relationship between the magnetic and dielectric characteristics of these composites and its microwave absorbing properties. In the literature already relationship for calculating surface impedance exists for the design of microwave absorbers especially for single layer absorbers. For a microwave absorbing layer the normalised input impedance at the absorber surface (Z_{in}) is given by

$$Z_{in} = \sqrt{\frac{\mu^*}{\epsilon^*}} \cdot \tanh \left[j \cdot \frac{2\pi d}{\lambda} \cdot \sqrt{\mu^* \cdot \epsilon^*} \right] \dots \dots \dots (8.1)$$

where λ is the wavelength of microwave in free space and d is the thickness of the absorber material. μ^* ϵ^* are the complex permeability and complex permittivity of the material and is given by $\mu^* = \mu_r^1 - j \mu_r^{11}$ and $\epsilon^* = \epsilon_r^1 - j \epsilon_r^{11}$. The complex permeability and permittivity of the constituent materials of the microwave absorbers play a key role in determining the reflection or attenuation properties. They can be determined from the reflected and transmitted scattering parameters obtained from network analyser. The reflection loss which is a function of Z_{in} is then expressed as

$$\text{Reflection loss (dB)} = 20 \cdot \log \left| \frac{Z_{in} - 1}{Z_{in} + 1} \right| \dots \dots \dots (8.2)$$

The absorbing properties of the sample is calculated at a given λ and d . It is to be noted that the reflection loss is found to depend sensitively on the absorber thickness

wavelength, complex permittivity and complex permeability. The absorption performance can be improved by increasing the filler permeability, filler concentration and material thickness. A control of magnetic permeability is possible by preparing ferrite fillers with different chemical compositions. High permittivity is achievable and is possible by nitrogen sintering of the ferrite fillers. It was also reported that non-spherical magnetic particles exhibit a higher permeability and hence better absorption in the radar band, when compared to spherical magnetic particles. Here it is to be noted that acicular precursors for the synthesis of acicular ferrites can be prepared by the employment of complexing agents/media. Ferrite fillers with needle shaped particles can be synthesized and the same can be incorporated in appropriate matrixes.

The formulation of an empirical relationship for the evaluation of M_s of RFCs will be of use in predetermining the magnetic properties. The same empirical relationship can be applied for a composite containing a mixed ferrite series obeying a Gaussian pattern with respect to the composition versus magnetisation. Experiments also prove that the H_c of the filler and the filler incorporated composites remains the same. If the H_c of the composite is to be modulated impurities like cobalt, which derives its coercivity enhancing property from the magnetocrystalline anisotropy is to be incorporated. So composites with Co modified ferrite fillers can be a good candidates for RFCs with a large H_c . Results obtained from magnetic and dielectric studies (chapter 3 and 5) indicates that the dielectric and magnetic properties can be tailored. These semi empirical equations can be combined with the surface impedance equation. These together will form the basis for the synthesis of RFCs for microwave absorption applications. Emphasis was laid on the evaluation of ϵ and M_s and similar studies can be extended for the evaluation of ϵ and μ in the microwave frequencies by using vector network analysers. Scope also exists to make emulsions and try it as a coating especially for antiradar applications. It will be interesting to disperse these fillers in latex (natural rubber) and study the properties. Gaskets based on RFCs could easily be moulded and this can form part of microwave devices, which will prevent electromagnetic radiations. Polar matrixes like Nitrile can be a suitable matrix for RFC preparation, Nitrile, which has superlative properties, will be suitable for specific applications.

Thermal properties of polymer composites are important because these materials are required to be suitable for applications over a wide range of temperatures, perhaps a few hundred degrees both above and below room temperature. Polymer composites often undergo comparatively large volume changes with respect to temperature during fabrication. Hence they have very large coefficients of thermal expansion than many other structural materials. This will result in a quite mis-match in expansion between polymer system and the filler materials with which they might be in contact. Hence thermal expansion of the composite materials is important. Due to this mis-match in expansion of the filler and the polymer, differential shrinkage is possible during cooling of a composite. Similarly heating can produce significant stress changes, which in turn may have a profound effect on the mechanical properties. These stresses will produce micro cracks at the interface while preparing composite materials.

One of the most important stages in the preparation of polymer composites is the process of distributing the filler in an even manner through out the polymer matrix. Micro structural studies using optical micrographs or SEM can assess the efficiency of a particular mixing and dispersion of the fillers. It has been concluded that there exists no interaction between the filler and matrix. This inference has been arrived at based on the evaluation of bulk properties of the composites namely magnetic and electrical. These conclusions are applicable at the macroscopic level. There exist possibilities of interactions between filler or matrix at the microscopic level. Tools like Electron Paramagnetic Resonance (EPR) can be utilised to probe the possible microscopic interactions taking place during ferrite incorporation. This is beyond the scope of the present work.

In chapter seven the estimation of magnetostriction constant λ_s from the hysteresis loop parameters was attempted. This gives only a rough estimate of the λ_s , and that too evaluated by employing σ_0 , which was assumed to be universal in nature. The theories governing the determination of stress occurring in ferrite filled composites is not clear. Scope also exists to evaluate the magnetostriction constant λ_s by effective experimental tools. This will determine the utility of these composites as possible sensors.

Now that the use of rare earth magnets has come in a big way, there is a huge potential for carrying out research on polymer bonded magnets based on rare earths.

The present work when viewed from a broad viewpoint is minuscule considering the vastness of this subject and magnetism will be always be a fascinating subject for scientists for the years to come. This field will be ever attractive in nature and at the same time reveal more and more about less and less.

References

1. Benjamin Lax, Kenneth J Button, Microwave ferrites and ferrimagnets, McGraw-Hill Book Co. (1962).
2. F.Brailsford, Magnetic materials, Methun's Physical monographs (1948).
3. H.V.Keer, Principles of the solid state, Wiley Eastern Limited (1993) New Delhi.
4. F.Brailsford, Physical principles of magnetism, D Van Nostrand Co. Ltd. (1966).
5. R.S.Tebble, Magnetic domains, Methuen Co. Ltd. (1969).
6. R.Carey, E.D.Isaac, Magnetic domains and techniques for their observations, Academic press (1966) New York.
7. J.C.M.Li Microstructure and properties of materials, world scientific (1996) Singapore.
8. J.H.Nam, H.H.Jung, J.Y.Shin and J.H.Oh, IEEE Trans. Magn. Vol. 31 No.6 (1995) p 3985 –87
9. M.Pal, P.Brahma, D.Chakravorty, J. Magn. Magn. Mater. 152 (1996) p 370-374.
10. C.M.Williams, M.Abe and T.itoh, P.Lubitz, IEEE Trans. Magn. Vol.30 No.6 (1994) p4896-4899.
11. Sung-soo Kim, Dae-Hee Han, Sung –Baeg Cho, IEEE Trans. Magn. Vol.30, No.6 (1994)p4554-4556.
12. Safari Ardi M, Dick W and McQueen D.H, Plastic rubber and composites processing and applications 24 (1995) p 157 – 164
13. C.P.bean and J.D.Livingstone, J. Appl. Phys. 30 (1959) 120.
14. E.M.Chudnovsky and L.Gunther, Phys. Rev. B 37 (1988) p 9455.
15. R.D.Mc Micheal, R.D.Shull, L.J.Swartzondruber, L.H.Bennet and R.E.Watson, J. Magn. Magn. Mater. 111(1992) 29.
16. K.A.Gschneidner Jr. and V.K. Pecharsky, J. Appl. Phys. 85 No.8(1999)p5365

17. Dishovaski N, Petkov A, Nedkov I and Razkazov I, IEEE Trans. Mag. Mag. 30 (1994) 969.
18. Naito Y and Suetake K, IEEE Trans. Micro. Theo. Tech. , 19 (1971) 65.
19. Gruberger W, Spreingman B, Brusberg M, Schmit M and Jahnke R, J. Mag. Mag. Mat. 101 (1991) 173.
20. Nedkov I, Petkov A and Karpov V, IEEE Trans. Mag. Mag. , 26 (1990) 1483.
21. Shin J.Y and Oh T.H IEEE Trans. Mag. Mag. , 29 (1993) 3437.
22. Kim S.S, Jo S.B, Choi K.K, Kim J.M and Churn K.S, IEEE Trns. Mag. 27 (1991) 5462.
23. Mingzhong Wu, Huahui He, Zhensheng Zhao and Xi Yao, J.Phys. D: Appl. Phys. 33 (2000) 2398 – 2401.
24. Stoyan I, Ganchev, Jay Bhattacharya, Sasan Bakhtiari, Nasser Qaddoumi, Deborah Brandenburg and Reza Zoughi, IEEE Trans. Micro. Theo. And Tech. Vol.42, No.1 (1994) 18-24.
25. William B Weir, Proceedings of the IEEE Vol. 62, No.1 (1974) 33-36.
26. Praveen Singh and T.C. Goel, Ind. Journal Pure. Appl. Phys. , 38 (2000) 213 - 219
27. S.A.Mirtaheri, J.Yin, H.Seki, T.Mizumoto and Y.naito, The Trans. The IEICE , Vol. E72 No.12 (1989) p1447-1452.
28. D.Y.Kim, Y.C.Chung, T.W.kang and K.C.Kim, IEEE Trans. Magn. Vol. 32 , No.2 (1996) p555-558.
29. Y.Naito, J.Yin, T.Mizumoto, Elec. Commun. Japan , Part 2 Vol. 71, No.7 (1988) p77-82.
30. Nitendar kumar, Prankishan, J. Mater. Sci. Lett. 10 (1991) p 217-219.
31. H.M.Musal Jr. and H.T.Hahn, IEEE Trans. Magn. Vol. 25 (1989) p3851 – 3853.
32. H.T.Hahn, J. Appl. Phys. Vol. 69 (1991) p 6192 – 6194.
33. H.T.hahn, J. Appl. Phys. Vol. 69 (1991) p 6195-6197.
34. M.Matsumoto and Y.Miyata, IEEE Trans. Magn. 33 (1997)p4459-4464.
35. Olmedo L, Chateau G, Deleuze .C and Forveillei J.L., J. Appl. Phys. 73 (1993) p6992-6994.
36. Rinchao Che, Yong Qing Li, Zhaohin Chen, Hongji Lin, J. Mater. Sci. Lett. 18(1999) p1963-1964.

37. S.A.Mirtaheri, T.Mizumoto, Y.Naito, The Trans. The IEICE Vol. E73 No. 10 (1990) p1746 – 1752.
38. Kyung Ho Lee, Dang Hoe Cho, Seung suk Jeung, J. Mater. Sci. Lett. 16 (1997) p 83-87.
39. D.C.Khan, M.Misra, Bull. Mater. Sci. 7 (1985) p253.
40. K.Ishino, Y.Narumiya, Cerm. Bull. 66 (1987) p1469.
41. B.V.Bhise, M.B.Dangare, S.A.Patil, S.R.Sawant, J. Mater. Sci. Lett. 10 (1991) p 922.
42. Simon Foner, Rev. Sci. Instrum. Vol. 30, No.7 (1959) p548-557.
43. Joseph A. Pesch, Rev. Sci. Instrum, Vol.54, No.4 (1983)p480.
44. R.V.Krishnan and A.Banerjee, Rev. Sci. Instrum., Vol.70 No.1 (1999)p85.
45. H.H.Brongersma, N.Hazewindus, J.M. Van Niewland , A.M.M. Otten, A.J. Smels, Rev. Sci. Instrum. 49 (6) (1978) p 707
46. H.H.Brongersma and P.M.Mul, Chem. Phys. Lett. 14 (1972) 380,
47. H.H.Brongersma and P.M.Mul, Surf. Sci. 35 (1973) 393.
48. M.Manivel Raja, A.Narayanasamy, V.Ravichandran, J. Mag. Mag. Mater. 10607 (1996)xxxC.
49. C.W.Kimball, Water C.Philips, M.V.Nevitt and K.S.Preston, Phys. Rev. Vol. 146 No.2 (1966) p 375-378.
50. V.R.K.Murthy, S.Chitra sankar, K.V.Reddy and J.Sobhanadri, Ind. J. Pure. Appl. Phys. Vol. 16 (1978) p 79- 83.
51. S.K.Date, Ind. J. Chem. Edu. Vol.1 No. 2 (1970)
52. A.Goswami, Thin Film Fundamentals, New age international Publishers Ltd. New Delhi (1996).
53. Jozef Slama, Anna Gruskova, Ludovit Keszesh, Mojmir Kollar, IEEE Trans. Mag. Vol. 30 No.2 (1994) p1101-1103.
54. Z.Osawa, K.Kawaguchi, M.Iwata, H.Harada, J. Mater. Sci. 23 (1988) p 2637- 44
55. T.Nakamura, T.Tsutaoka,K.Hatekeyama, J. Mag. Mag. Mater. 138 (1994) p 319-328.
56. H.Takei, H.Tokumasu, H.Rikukawa and I.Sasaki, IEEE Trans. Mag. Vol MAJ 23 (1987) p3080-3082.
57. A.M.Sankpal, S.S.Suryavanshi, S.V.Kakatbar, G.G.Tengshe, R.S.Patil, N.D.Chaudhari, S.R.Sawant, J. Mag. Magn. Mater. 186 (1998) p349-356.

58. Ferrite materials – Science & Technology, B.Viswanathan and V.R.K.Murthy
59. ASTM 10- 325 (Ni ferrite) Nat. Bur. Stands (U.S) circ. 539 – 1044 (1960).
60. Smit and Wijn, Philips Technical reports – 144 , 1959
61. Materials science, J.C. Anderson , K.D.Leaver – Thomas Nelson and sons Ltd. , 1969, Great Britain.
62. Physics of magnetism , Soshin Chikazumi, John Wiley and sons, Inc. , New York
63. Lattice defects and non stoichiometry, N.N.greenwood, Butterworth and Co Ltd. (1968).
64. M.Andres Verges, C.de Julian, J.M.Genzalez, C.J.Seina, J. Mater. Sci. 28 (1993)p2962-2966.
65. E.J.Verway, P.W.Haayman and F.C.romeijn, J. Chem. Phys. Vol. 15 No. 4 (1947) p181-187.
66. E.J.W.Verwey, F.De Boer and J.H.Van Santen , J. Chem. Phys. Vol. 16 No. 12 (1948) p 1091 – 1092
67. S.Besenicar, M.Drofenik, T.Kosmac, V. Krasevec, IEEE Trans. Magn. Vol. 24 No.2 (1988)p 1838-1840.
68. C.J.Chen, K.Bridger, S.R.Winzer and V.Paiverneker , J. Appl. Phys. 63 No.8 (1988)p 3786 – 3788.
69. T.T.Srinivasan, P.Ravindranathan, L.E. Cross, R.Roy and R.E.Newnhan, S.G.Sankar, K.C.Patil, J. Appl. Phys. 63 No.8 (1988) p 3789 – 3791.
70. Introduction to magnetic materials , B.D.Cullity, Addison Wesley publishing Company.
71. L.K.Leung, B.J.Evans, A.H.Morrish, Phy. Rev. B, 8 No.1 (1973) p29-43.
72. V.C.Wilson and J.S.Kasper, Phys. Rev. 95, 1408 (1954),
73. N.S.Satyamurthy, M.G.Nater, S.I.Yousef, R.J.Begum and C.M.Srivastava, Phys. Rev. 181, 969 (1969),
74. V.I.Goldonskii, V.F.Belov, M.N.Devisheva and V.A.Trukhtanov, Sov. Phys. JETP 22, 1149 (1966),
75. J.M.Daniels and A.Rosencwaig, Can. J. Phys. 48, 381 (1970).
76. Landolt bornstein, Magnetic properties, Springer – Verlag(1962)

77. R.Valenzuela, Magnetic Ceramics, Cambridge University press, Cambridge (1994).
78. B.D.Cullity, Introduction to magnetic Materials, Addison – Wesley, Reading , MA, (1972).
79. J.Smit, and H.P.J. Wijn, Ferrites, Philips Technical Library (1959).
80. V.R.K.Murthy, B.Viswanathan, Ferrite Materials, Science and Technology (Narosa Publishing House) 1990.
81. E.J.W.Verwey and E.L. Heilmann, J. Chem. Phys. 15, 174 (1947) , E.F. Bertaut, J. Phys. Et radium 12, 252 (1951)
82. L.Neel, Ann. Phys. 3, 139 (1948)
83. G.F.Goya, H.R.Rechenberg, M.Chen and W.B. Yelon, J. Appl. Phys. Vol. 87 No.11 (2000) p 80005 – 7.
84. T.Pannaparayil, S.Komarneni, R.Marande and M.Zadarko, J. Appl. Phys. 67 No. 9 (1990) p 5509- 5511.
85. M.Balanda, A.Szytala, Dimitrijevi and J.Todorouic, Phy. Stat. Soli. 32 K91 (1969) K 91- 93.
86. J.M.Hastings and L.M.Corliss, Rev. of Modern Phys., 25 No.1 (1953) pp 114- 121.
87. Tadashi Mizoguchi and Midori Tanaka , J. Phys. Soc. Japan, 18 No. 9 (1963) p 1301 – 1306.
88. D.M.Grimes and Edgar F Westrum , J. Appl. Phys. , 29 No.3 (1958) p 384-85.
89. Y. Yafet and C.Kittel, Phys. Rev. Vol. 87 No. 2 (1952) p 290 – 94.
90. V.G.Volgin, Sov. Phys. Solid State , 29 No. 8 (1987) p 1339 – 1344.
91. Yu.G. Chukalkch and V.R. Shtirts, Sov. Phys. Solid State 30 No. 10 (1988) p 1683 – 86.
92. H.H.Hamdeh, J.C.Ho, S.A. Oliver, R.J Willey, J.Kramer, Y.Y.Chen , S.H. Lin, Y.D.Yao, M.Daturi and G.Busca, IEEE Trans. Mag. Vol. 31 No. 6 (1995) p 3808- 3810.
93. J.C.Ho, H.H.Hamdeh, Y.Y.Chen, S.H.Lin, Y.D.yao, R.J.Willey , S.A.Oliver, Phy. Rev. B Vol. 52, No. 14 (1995) P 10122 – 10126.
94. H.H.Hamdeh, J.C.Ho, S.A.Oliver, R.J.Willey, G.Oliveri, G.Busca, J. Appl. Phys. Vol. 81 No. 4 (1997) p 1851 – 1857.

-
95. V.Sepelak, K.Tkacova, V.V.Boldyrev, S.Wibmann, K.D.Beilier, *Physica B*, (1997) 617-619.
 96. Ted M.Clark and B.J.Evans, *IEEE Trans. On Mag. Vol. 33 No. 5* (1997) p 3745 – 3747.
 97. R.V.Upadhyay, *Pramana – J. Phys. Vol. 49 No.3* (1997) p 309 – 316.
 98. L.Torres, F.Walz , C.De Francissco and J.Iniguez, *Phys. Stat. Solidi. (a)* 163, (1997) p p221-231.
 99. E.F.Westrum, D.M.Grimes, *J. Phys. Chem.*, 61,(1957) 761.
 100. F.K.Lotgering, *J. Phys. Chem. Solids* 27, (1966) 139
 101. B.N.Brockhouse, L.M.Corliss, J.M.Hastings, *Phys. Rev.* 98, (1975) 1721,
 102. T.Kamiyama, K.Haneda, T.Sato, S.Ikeda and H. Asano, *Solid State communications Vol. 81, No.7*, (1992) pp 563 - 566
 103. B.N.Brockhouse, L.M.Corliss, J.M.Hastings, *Phys. Rev.* 98, (1975) 1721
 104. T.Sato, K.Haneda, N.Seki and T.Iijima, *Appl. Phys. A* 50 (1990) 13-16.
 105. Raul Valenzuela, *Magnetic Ceramics*,(Cambridge University Press) 1994
 106. R.H.H.Smits, K.Seshan and J.R.H.Ross, *Cat. Today.* 16 (1993) 513.
 107. J.P.Jacobs, S.Reijne, R.J.M.Eifrink ,S.N.Mikhailov, N.Wuttingand H.H.Brongersma, *J.Vac.Sci.Techn.,A* 12 (1994)2308.
 108. H.Knozinger and P.Ratnasamy , *catl. Rev. Sci. Eng.* 17 (1979) 31
 109. J.Ziolkowski and Y.Barboux, *J.Mol.Cat.*,67(1991)199
 110. M.Shelef, M.A.Z.Wheeler and H.C.Yao, *Surf.Sci.*,47(1975)697
 111. J.P.Bauffils and Y.Barboux, *J. Chem. Phys.* 78 (1981) p 387
 112. J.P.Jacobs,A.Maltha,J.G.H.Reinjes, J.Drimal, V.Ponec and H.H.Brongersma, *J.Catal.*,147 (1994) 294-300
 113. M.R.Anantharaman, S.Reijne, J.P.Jacobs, K.Seshan and H.H.Brongersma, *Journal of Mater. Sci.* 34 (1999) p 4279 - 4283
 114. B.Window, *J. Phys. E. Sci. Instrum.* 4,401 (1971)
 115. B.Jayadevan, K.Tohji and K.Nakatsuka, *J. Appl. Phys.* 76 No.10 (1994) p 6325-6327.

116. W.Schiessel, W.Potzel, H.Karzel, M.Steiner, G.N.Kalvius, A.Martin, N.K.Karause, I.Halevy, J.Gal, W.Schafer, G.Will, M.Hillberg and R.Wappling, *Phys.Rev.B.* Vol.53, No.14 (1996) 9143-9151
117. Z.Gigbi and L.Jilken, *J. Magn. Magn. Mater.* 37 (1983) 267,
118. D.R.Saini, A.V.Sheony and V.M. Nadkarni, *J. Appl. Polym. Sci.* 29 (1983) 4123
119. Kuanr B K, Singh P K, Kishan P, Kumar N, Rao S L N, Prabhat K Singh, Srivastava G P 15 April *J.Appl.Phys.* 63(8) (1988)p3780-3782.,
120. El Hiti M A, *J.Mag. and Mag. Mat.* 164 (1996) p 187-196.,
121. Josyulu O and Sobhanadri J, *Phys.Status Solidi(a)* 59 (1980) p323.,
122. Ahmed M A, El Hiti M A, Mosaad M M and Attia S M, *J. Magn. Magn. Mater.* 146 (1995) p84.,
123. Murthy V R K and Sobhanadri J, *Phys. Status Solidi(a)* 36 (1976) p133.
124. Reddy P V and Rao T S, *J. Less. Common. Met.* 86 (1982) p255
125. Ramasastry C and Syamasundara Rao Y, *J.Phys.E:Sci.Instrum.*12 (1979) p1023-4.
126. C.G.Koops, *Phys. Rev.* 83 (1951) p 121-124.
127. Rezlescu.N and Reslescu. E. *Physica status solidi (a)* 23 (1974) 575
128. Kyung Ho Lee, Dong Hoe Cho and Seung Suk Jeung, *J. Mater. Sci. Letters* 16 (1997) p83-87
129. Van Gitert L.G., *J. Chem. Phys.* 24 (1956) p 306.
130. Chandra Prakash and Baijal J.S, *J. Less. Commn. Metals* 107 (1985) p 51-57.
131. Patil R.S., Kakatkar S.V, Maskar P.K., Patil S.A and Sawant S.R, *Ind. J. Pure Appl. Phys.* 29 (1991) p 589 – 592.
132. Chandraprakash and Baijal J.S., *J. Less Commn. Metals* 106 (1985) p 257 – 261.
133. Tareev B 1979 *Physics of Dielectric Materials* (Mir Publishers) Moscow
134. Frank E Karasz 1972 *Dielectric Properties of Polymers* (Plenum Press) New York
135. Musal Jr. H M, Hahn H T and Bush G G *J.Appl. Phys.*63(8) (1988) p3768-3770.
136. Ki Chulhan, Hyung Do Choi, Tak Jin Moon, Wang Sup Kim and Kyung Yong Kim *J.Mater.Sci.* 30(1995) p3567-3570.

137. Andrej Žnidaršič and Miha Drofenik J. Amer. Ceram. Soc. 82 (1999)
p 359-365.
138. Yootarou Yamazaki and Minuru Satou Jap. J. Appl. Phys. 12 No.7 (1973)
p998-1000.,
139. Ahmed M.A. and Elhiti M.A 1995 Journal de Physique III 5 775- 781.,
140. Shaikh A.M., Bellad S.S. and Chougule B.K J. Mag. Mag. Mater. 195
(1999) p384-390.,
141. Elhiti M.A, Ahmed M.A, Mosaad M.M and Attia S.M , J. Mag. Mag.
Mater. 150 (1995) p399-402.,
142. Ahmed M.A, Elhiti M.A, El Nimr M.K and Amer M.A , J. Mag. Mag.
Mater. 152 (1996) p391-395.,
143. Pal M, Brahma P and Chakravorty D , J. Phys. Soc. Jap. 63 No.9 (1994)
p3356- 3360.
144. Jankowski S , J. Amer. Ceram. Soc. 71 (1988) c- 176.
145. Brockman F.G and White R.P , J. Amer. Ceram. Soc. 54 (1971) p183
146. Abdeen A.M , J. Mag. Mag. Mater. 185 (1998) p199 – 206.,
147. Elhiti M.A , J. Mag. Mag. Mater. 164 (1996) 187 – 196.,
148. Pal M, Brahma P and Chakravorty D , J. Mag. Mag. Mater.152 (1996)
p370- 374.
149. Samokhvalov A.A and Rustamov A.G , Soviet Physics – Solid State 6
No.4 (1964) 749 – 752
150. G.K.Joshi, S.A.Desh Pande, A.Y. Khot, S.R.Sawant, J. Appl. Phys. A 61
(1987) 251
151. R. Satyanaryana, S.R. Murthy, T.S.Rao, J. Less Commn. Met. 90 (1983)
243
152. B.V.Bhise, M.B.Donger, S.A.Patil, S.R.Sawant, J. Metr. Sci. lett. 10C
(1991) 922
153. G.K.Joshi, A.Y.Khot, S.R.Sawant, Solid State Commun. 65 (1988) 1593
154. H.D.Patil, R.V.Upadhyay, N.R.Shamkamar, R.G.Kulkarni, Solid State
Commun. 81 (1992) 1001
155. R.B.Jotamia, R.V.Upadhyay, R.G.Kulkarni, IEEE Trans. Magn. 28 (1992)
1889

-
156. J.S.Bijal, S. Phanjouban, d.Kothari, C.Prakash, P.kishan, Solid State Commun. 83 (1992) 679
 157. P.V.Reddy, T.S.Rao, S.M.D.Rao, J. Less Commn. Met. 79(1981) 1
 158. P.V.Reddy, T.S.Rao, S.M.D. Rao, J. Less Commn. Met. 79 (1981) 191
 159. E. Iguchi, A. Tamenori and N.Kubota, Phys. Rev. B , 45 (1992) 697
 160. E.Iguchi, N. Kubota, T.Nakamori, N. Yamamoto and K.J.Lee, Phys. Rev. B 43 (1991) 8646
 161. N.F.Mott, J. Non. Cryst. Solids 1 (1968) 1
 162. D.Chakravorthy and A.Srivastava, J. Phys. D : Appl. Phys. , 19 (1986) 2185
 163. D.Emin and T.Hostein , Ann. Phys. N.Y. , 53 (1969) 439
 164. W.A.Philips , Phil. Mag. , 34 (1976) 983
 165. S.R. Elliott , Adv. Phys. 36(2) (1978) 135
 166. G.E.Pike , Phys. Rev B 6 (1972) 1572
 167. S.R.Elliot , Phil. Mag. 36 (1977) 1291
 168. A.R. Long , Adv. Phys. 31 (1982) 553
 169. L.G.Austin and N.F. Mott , Adv. Phys. 18 (1969) 41
 170. M.A.El Hiti, J. Phys. D: Appl. Phys. 29(1996) 501
 171. M.A.El Hiti Phase Trans. 54 (1995) 117
 172. M.A.Ahmed, M.A.El Hiti, M.K.El Nimr, M.A.Amer, J. Magn. Magn. Mater. 152 (1996)391
 173. M.A.El Hiti, M.K. El Nimr, M.A. Ahmed, Phase Trans. 54 (1995) 137
 174. M.M.Mosaad, M.A.Ahmed, M.A.Ahmed, J. Magn. Magn. Mater. 150 (1995) 51
 175. M.A.Ahmed, M.A.El Hiti , M.M.Mosaad, S.M.Ahmed, J. Magn . Magn. Mater. 146 (1995) 84
 176. M.A.El Hiti, J.Magn. Magn. Mater. , 164 (1996) 187
 177. M.A.El Hiti, J. Magn. Magn. Mater. 136 (1994) 138
 178. Largeteau, J.M. Reau and J.Raves , Phys. Stat. Sol. (a) 121 (1990) 627
 179. S.Jankowski, J.Amer. Ceram. Soc.,71 (1988) C-176
 180. F. haberey, H.J.P.Wijn, Phys. Stat. Sol. (a) 26 (1968) 231
 181. P.V.Reddy, R.Satyanarayana, T.S.Rao, Phys. Stat. Sol. (a)78 (1983)109
 182. C.Prakash, J.S.Bijal, P.Kishan, J. Less- common Met. 106 (1985) 243
 183. R.Satyanarayana, S.R.Murthy, Crystal Res. Technol. 20 (1985) 701

184. A.B.Naik, J.J.Powar , Ind. J. Pure Appl. Phys. 23 9(1985) 436.
185. Anantharaman M.R, Sindhu S, Jagatheesan S, Malini K.A and Kurian P
1999 J.Phys. D: Appl. Phys. 32 1801-1810.
186. Patil R.S, Kakatkar S.V, Maskar P.K, Patil S.A and Sawant S.R 1991 Ind.
J. Pure Appl. Phys. 29 589- 592.
187. Terje A. Skotheim 1986 Handbook of Conducting Polymers, Vol. I & II,
Marcel Dekker Inc. USA.
188. R.Smoluchowski, Phys. Rev. Vol.59 (1941) p 309-317.
189. E.Callen, J. Appl. Phys. Vol. 36No.3 (1965)p976.
190. N.Buiron,L.Hirsinger, R.Billardien, J. Magn. Magn. Mater. 196-197 (1999)
p868-870.
191. Ce-Wen Nan and Yong Huang, G.J.Weng, J. Appl. Phys. Vol. 88 No.1
(2000) p 339-343.
192. L.Lanotte, G.Ausamo, V.Iannotti, J. Magn. Magn. Mater. , 196-197 (1999)
p 865-867.
193. K.Inomata and Y.Saito, J. Magn. Magn. Mater. , 198-199 (1999) p 18-20
194. Hiroaki samata, Nobuto Fujiwara, Yujiro Nagata, Takayuki Uchida, Ming
Der Lan, J. Magn. Magn. Mater. 195 (1999) p 376-383.
195. H.Morita, S.W.Kim, H.Yoshida, H.Fujimori, J. Magn. Magn. Mater. 177-
181 (1998) p113-114.
196. Vasile Z. Iusan and Aurora Gh. Stanci, IEEE Trans. Magn. Vol. 30 No.2
(1994) p 1104-1106.
197. Wu Mei , Toshimitsu Okane and Takateru Umeda , J. Appl. Phys. Vol. 84,
No.11 (1998) p 6208- 6216.
198. T. Kimura, Y.Tomioka, A.Asamitsu, Y.Tokura, Phys. Rev. Lett. Vol. 81,
No.26 (1998) p 5920-5923.
199. Min Hyoung Kim, Kyung Shik Lee, Sang Ho Lim, J. Magn. Magn. Mater.
191 (1999) p 107-112.
200. George H.Bellessis, Peter S Harilee, Andrew Renema and David N.
Lambeth, IEEE Trans. Magn. Vol. 29 No.6 (1993) p 2989-2991.
201. L.Gates and G.Stroink, Rev. Sci. Instrum. 63 No.3 (1992) p 2017-2025.
202. David Markham and Neil Smith, IEEE Trans. Magn. Vol. 25 No.5 (1989)
p4198 – 4200.

-
203. Hiroshi takahashi, Shigeru Tsunashima , Stoshin Iwata and Susumu Chiyama, *Jpn. J. Appl. Phys.* , Vol. 32 (1993) p L1328 – L1331.
 204. C.Gourdin, L. Hirsinger, G.Barbier, R.Billardon, *J.Magn. Magn. Mater.* 177 – 181 (1998) p 201-202.
 205. C.Sierks, M.Doer, A.Kreyssig, M.Loewenhaupt, Z.Q.Peng. K.Winzer, *J. Magn. Magn. Mater.* 192 (1999) 473-480.
 206. Etienne du Tremolet de Lacheisserie, *Magnetostriction – Theory and applications of mgnetoelasticity*, CRC Press, Boca Raton, Florida,(1993)
 207. .Murthy S.R and Rao T.S. magnetostriction of Ni-Zn and Co-Zn ferrites, *Phys. Status solidi* , a – 90, 631 (1985)
 208. C.N.Chinnasamy, A.Narayanasamy, N.Ponpandian, Justin Joseph (*Phys. Rev. B* in press).